DEPARTMENT OF MECHANICAL ENGINEERING AND MECHANICS
COLLEGE OF ENGINEERING & TECHNOLOGY
OLD DOMINION UNIVERSITY
NORFOLK, VIRGINIA 23508

INTERACTION OF TRANSIENT RADIATION IN NONGRAY GASEOUS SYSTEMS

By

S. N. Tiwari, Principal Investigator

and

D. J. Singh, Graduate Research Assistant

Progress Report
For the period ending December 31, 1986
(A Supplementary Report)

Prepared for the
National Aeronautics and Space Administration
Langley Research Center
Hampton, VA 23665

Under
Research Grant NAG-1-423
A. Kumar and J.P. Drummond, Technical Monitors
HSAD-Computational Methods Brancn

January 1987

DEPARTMENT OF MECHANICAL ENGINEERING AND MECHANICS
COLLEGE OF ENGINEERING & TECHNOLOGY
OLD DOMINION UNIVERSITY
NORFOLK, VIRGINIA 23508

INTERACTION OF TRANSIENT RADIATION IN NONGRAY GASEOUS SYSTEMS

By

S. N. Tiwari, Principal Investigator

and

D. J. Singh, Graduate Research Assistant

Progress Report
For the period ending December 31, 1986
(A Supplementary Report)

Prepared for the
National Aeronautics and Space Administration
Langley Research Center
Hampton, VA 23665

Under
Research Grant NAG-1-423
A. Kumar and J.P. Drummond, Technical Monitors
HSAD-Computational Methods Branch

Submitted by the
Old Dominion University Research Foundation
P.O. Box 6369
Norfolk, VA 23508

January 1987

FOREWORD

This is a progress report on the research project, "Analysis and Computation of Internal Flow Field in a Scramjet Engine," for the period ending December 31, 1986. The work was supported by the NASA Langley Research Center (Computational Methods Branch of the High-Speed Aerodynamics Division) through research grant NAG-1-423. The grant was monitored by Dr. A. Kumar and Mr. J.P Drummond of the High-Speed Aerodynamics Division.

INTERACTION OF TRANSIENT RADIATION IN NONGRAY GASEOUS SYSTEMS

S. N. Tiwari* and D. J. Singh+
Old Dominion University, Norfolk, VA 23508

ABSTRACT

A general formulation is presented to investigate the transient radiative interaction in nongray absorbing-emitting species between two parallel plates. Depending on the desired sophistication and accuracy, any nongray absorption model from the line-by-line models to the wide-band model correlations can be employed in the formulation to investigate the radiative interaction. Special attention is directed to investigate the radiative interaction in a system initially at a uniform reference temperature and suddenly the temperature of the bottom plate is reduced to a lower but constant temperature. The interaction is considered for the case of radiative equilibrium as well as for combined radiation and conduction. General as well as limiting forms of the governing equations are presented and solutions are obtained numerically by employing the method of variation of parameters. Specific results are obtained for CO, CO_2, H_2O, and OH. The information on species H_2O and OH is of special interest for the proposed scramjet engine application. The results demonstrate the relative ability of different species for radiative interactions.

---

*Eminent Professor, Department of Mechanical Engineering and Mechanics. AIAA Associate Fellow.

+Graduate Research Assistant, Department of Mechanical Engineerng and Mechanics. AIAA Student Member.

TABLE OF CONTENTS

LIST OF TABLES

LIST OF TABLES (Concluded)

LIST OF FIGURES

LIST OF FIGURES (Continued)

LIST OF FIGURES (Concluded)

NOMENCLATURE

A	band absorptance = $A(u,\beta)$, cm^{-1}
A_o	band width parameter, cm^{-1}
C_o	correlation parameter, atm^{-1} - cm^{-1}
C_p	specific heat at constant pressure, kJ/kg-K = erg/gm-K
e_ω	Planck's function, $(W\text{-}cm^{-2})/cm^{-1}$
e_{ω_o}	Planck's function evaluated at wave number ω_o
e_1, e_2	emissive power of surfaces with temperatures T_1 and T_2, $W\text{-}cm^{-2}$
H_{1i}, H_1	gas property for the large path length limit, $W/(cm^2\text{-}K)$
k	thermal conductivity, erg/cm-sec-K
K_{1i}, K_1	gas property for the optically thin limit, $W/(atm\text{-}cm^3\text{-}K)$
L	distance between plates, cm
M_{1i}, M_1	large path length parameter, nondimensional
N_{1i}, N_1	optically thin parameter, nondimensional
N	optically thin radiation-conduction parameter = N_1/R, nondimensional
P	pressure, atm
q	conduction plus radiation heat flux = $q_c + q_R$, w/cm^2
q_R	total radiative heat flux, w/cm^2
q_c	conduction heat flux, w/cm^2
$q_{R\omega}$	spectral radiation heat flux, $(w\text{-}cm^{-2})/cm^{-1}$
Q	nondimensional radiative heat flux
$\bar{Q}$	nondimensional conduction plus radiation heat flux
R	nondimensional transient conduction parameter
S	integrated intensity of a wide band, $atm^{-1}\text{-}cm^{-2}$
t	time, sec (also used as t^*)
t_m	characteristic time, sec
t^*	nondimensional time = t/t_m

T	temperature, K
T_1, T_2	wall temperature, K; $T_1 = T_w$
u	nondimensional coordinate = SPy/A_o
u_o	nondimensional path length = SPL/A_o
y	transverse coordinate, cm
θ	nondimensional temperature
κ_ω	spectral absorption coefficient, cm^{-1}
ξ	nondimensional coordinate = $y/L = u/u_o$
ρ	density, kg/m^3
σ	Stefan-Boltzmann constant, $erg/(sec\text{-}cm^2\text{-}K^4)$
ω	wave number, cm^{-1}
ω_o	wave number at the band center, cm^{-1}

1. INTRODUCTION

The field of radiative energy transfer in gaseous systems is getting an ever increasing attention recently because of its applications in the areas of the earth's radiation budget studies and climate modeling, fire and combustion research, entry and reentry phenomena, hypersonic propulsion and defense-oriented research. In most studies involving combined mass, momentum, and energy transfer, however, the radiative transfer formulation has been coupled mainly with the steady processes[1-11] and the interaction of radiation in transient processes has received very little attention. Yet, the transient approach appears to be the logical way of formulating a problem in a general sense for elegant numerical and computational solutions. The steady-state solutions can be obtained as limiting solutions for large times.

A few studies available on radiative ineractions reveal that the transient behavior of a physical system can be influenced significantly in the presence of radiation[12-17]. Lick investigated the transient energy transfer by radiation and conduction through a semi-finite medium[12]. A kernal substitution technique was used to obtain analytic solutions and display the main features and parameters of the problem. Steady and transient heat transfer in conducting and radiating planar and cylindrical mediums were analyzed in Refs. 13 and 14 according to the differential formulation. The analyses based essentially on the gray formulation provide some qualitative insight into the effect of absorption and emission on the transient temperature distribution in the gas. Doornink and Hering[15] studied the transient radiative transfer in a stationary plane layer of a nonconducting medium bounded by black walls. A rectangular Milne-Eddington type relation was used to describe the frequency dependence of the absorption coefficient. It was found that the cooling of the layer initially at a uniform temperature

is strongly dependent on the absorption coefficient model employed. Larson and Viskanta[16] investigated the problem of transient combined laminar free convection and radiation in a rectangular enclosure. It was demonstrated that the radiation dominates the heat transfer in the enclosure and alters the convective flow patterns significantly. The transient heat exchange between a radiating plate and a high-temperature gas flow was investigated by Melnikov and Sukhovich[17]. Only the radiative interaction from the plate was considered; the gas was treated as a non-participating medium. It was proved that the surface temperature is a function of time and of longitudinal coordinate. Some other works on transient radiation and related areas are available in Refs. 18-22.

The goal of this research is to include the nongray radiative formulation in the general unsteady governing equations and provide the step-by-step analysis and solution procedure for several realistic problems. The specific objective of the present study is to investigate the interaction of nongray radiation in transient transfer processes in a general sense. Attention, however, will be directed first to a simple problem of the transient radiative exchange between two parallel plates. In subsequent studies, the present analysis and numerical techniques will be extended to include the flow of homogeneous, nonhomogeneous, and chemically reacting species in one- and multi-dimensional systems.

2. BASIC THEORETICAL FORMULATION

The physical model considered for the present study is the transient energy transfer by radiation in absorbing-emitting gases bounded by two parallel gray plates (Fig. 2.1). In general, T_1 and T_2 can be a function of time and position and there may exist an initial temperature distribution in the gas. It is assumed that the radiative energy transfer in the axial direction is negligible in comparison to that in the normal direction.

For radiation participating medium, the equations expressing conservation of mass and momentum remain unaltered, while the conservation of energy, in general, is expressed as[1]

$$\rho\, c_p \frac{DT}{Dt} = \text{div}\,(k\ \text{grad}\ T) + \beta T \frac{DP}{Dt} + \mu\,\phi - \text{div}\ q_R \qquad (2.1)$$

where μ is dynamic viscosity, β is the coefficient of thermal expansion of the fluid and ϕ is the Rayleigh dissipation function. For a semi-infinite medium capable of transferring energy only by radiation and conduction, Eq. (1) reduces to

$$\rho\, c_p \frac{\partial T}{\partial t} = -\frac{\partial q}{\partial y} \qquad (2.2)$$

where q is the sum of the conductive heat flux $q_c = -k\,(\partial T/\partial y)$ and the radiative flux q_R. For the physical model where radiation is the only mode of energy transfer, the energy equation can be written as

$$\rho\, c_p \frac{\partial T}{\partial t} = -\frac{\partial q_R}{\partial y} \qquad (2.3)$$

Use of this simplified equation is made to investigate the transient behavior of a radiation participating medium.

For many engineering and astrophysical applications, the radiative transfer equations are formulated for one-dimensional planar systems. For

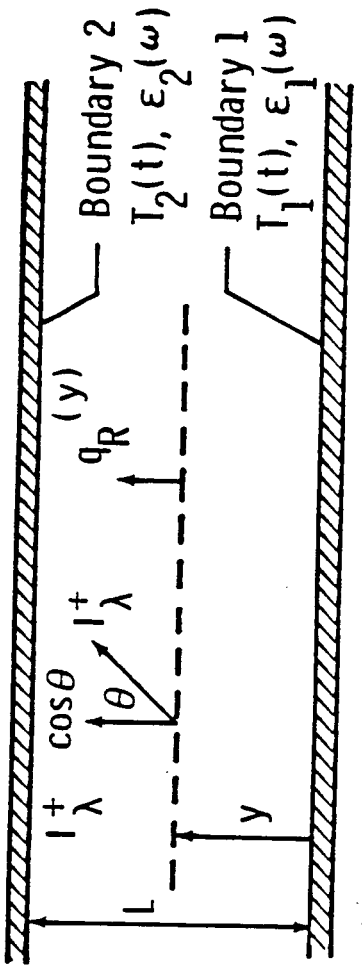

Fig. 2.1 Physical model and coordinate system.

diffuse nonreflecting boundaries and in the absence of scattering, the expression for the total radiative flux is given, for a n-band gaseous system, by[1,8,23]

$$q_R(y) = e_1 - e_2 + \frac{3}{2}\sum_{i=1}^{n}\int_{\Delta\omega_i}\{\int_o^y F_{1\omega_i}(z)\,\kappa_{\omega_i}\exp[-\frac{3}{2}\kappa_{\omega_i}(y-z)]dz - \int_y^L F_{2\omega_i}(z)\,\kappa_{\omega_i}\exp[-\frac{3}{2}\kappa_{\omega_i}(z-y)]dz\}d\omega_i \qquad (2.4)$$

where

$$F_{1\omega_i}(z) = e_{\omega_i}(z) - e_{1\omega_i};\ F_{2\omega_i}(z) = e_{\omega_i}(z) - e_{2\omega_i}$$

Equation (2.4) is in proper form for obtaining the nongray solutions of molecular species. In fact, this is an ideal equation for the line-by-line and narrow-band model formulations. However, in order to be able to use the wide band models and correlations, Eq. (2.4) is transformed in terms of the correlation quantities as[1,7-11,23]

$$q_R(\xi) = e_1 - e_2 + \frac{3}{2}\sum_{i=1}^{n} A_{oi}\,u_{oi}\{\int_o^\xi F_{1\omega_i}(\xi')\,\bar{A}_i'[\frac{3}{2}u_{oi}(\xi-\xi')]d\xi' - \int_\xi^1 F_{2\omega_i}(\xi')\,\bar{A}_i'[\frac{3}{2}u_{oi}(\xi'-\xi)]d\xi'\} \qquad (2.5)$$

where

$$\xi = u/u_o = y/L;\ \xi' = u'/u_o = z/L;\ \bar{A} = A/A_o;$$

$$u = (S/A_o)\,Py;\ u_o = (S/A_o)\,PL;\ PS = \int_{\Delta\omega}\kappa_\omega\,d\omega$$

It should be noted that $F_{1\omega_i}$ and $F_{2\omega_i}$ in Eq. (2.5) represent the values at the center of the ith band and $\bar{A}'(u)$ denotes the derivative of $\bar{A}(u)$ with respect to u. Upon performing the integration by parts, Eq. (2.5) can be

expressed in an alternate form as[23]

$$q_R(\xi) = e_1 - e_2 + \sum_{i=1}^{n} A_{oi} \{\int_o^{\xi} [de_{\omega_i}(\xi')/d\xi'] \bar{A}_i [\tfrac{3}{2} u_{oi}(\xi-\xi')]d\xi'$$

$$+ \int_{\xi}^{1} [de_{\omega_i}(\xi')/d\xi'] \bar{A}_i [\tfrac{3}{2} u_{oi} (\xi'-\xi)]d\xi'\} \qquad (2.6)$$

A direct differentiation of Eq. (2.6) provides the expression for the divergence of radiative flux as

$$\frac{dq_R(\xi)}{d\xi} = \frac{3}{2} \sum_{i=1}^{n} A_{oi} u_{oi} \{\int_o^{\xi} [de_{\omega_i}(\xi')/d\xi'] x$$

$$\bar{A}_i' [\tfrac{3}{2} u_{oi}(\xi-\xi')]d\xi' - \int_{\xi}^{1} [de_{\omega_i}(\xi')/d\xi'] x$$

$$\bar{A}_i' [\tfrac{3}{2} u_{oi}(\xi'-\xi)]d\xi'\} \qquad (2.7)$$

Equations (2.5) through (2.7) are the most convenient equations to use when employing the band-model correlations in radiative transfer analyses.

By defining $\phi(\xi,t) = T(\xi,t)/T_o$ with T_o representing some constant reference temperature, Eqs. (2.2) and (2.7) can be combined to yield the energy equation (for the general case of simultaneous conduction and radiation) in nondimensional form as

$$\partial\phi(\xi,t)/\partial t = R \frac{\partial^2\phi}{\partial\xi^2} - \frac{3}{2} \sum_{i=1}^{n} \{\int_o^{\xi} \psi_{\omega i}(\xi',t) x$$

$$\bar{A}_i' [\tfrac{3}{2} u_{oi} (\xi-\xi')]d\xi' - \int_{\xi}^{1} \psi_{\omega i} (\xi',t) x$$

$$\bar{A}_i' [\tfrac{3}{2} u_{oi} (\xi'-\xi)]d\xi'\} \qquad (2.8)$$

where

$$R = k\, t_m/(\rho\, C_p\, L^2)$$

$$\phi_{\omega i}(\xi,t) = \{PS_i(T)[\partial\, e_{\omega i}(\xi,t)/\partial\xi]/(\rho\, C_p\, T_o/t_m)\}$$

The time t in Eq. (2.8) is defined as $t^* = t/t_m$ with t_m representing some characteristic time scale of the physical problem; however, for the sake of convenience, the asterisk is left out here as well as in further developments. From the definitions of $\phi(\xi,t)$ and $\phi_{\omega i}(\xi,t)$, it should be noted that Eq. (2.8) is a nonlinear equation in $T(\xi,t)$. Equation (2.8), therefore, represents a general case of the transient energy transfer by radiation and conduction between two semi-infinite parallel plates. The nondimensional parameter R in Eq. (2.8) is analogous to the Fourier number. For R = 0, Eq. (2.8) reduces to the case of pure transient radiative energy transfer. The initial and boundary conditions for Eq. (2.8) will depend on the conditions of the specific physical problem.

2.1 Specific Application

As a special case, it is assumed that the entire system initially is at the fixed (reference) temperature T_o. For all time, the temperature of the upper plate is maintained at the constant temperature equal to the reference temperature, i.e., $T_2 = T_o$. The temperature of the lower plate is suddenly decreased to a lower but constant value, i.e., $T_1 < T_2$. The problem, therefore, is to investigate the transient cooling rate of the gas for a step change in temperature of the lower plate.

In many radiative transfer analyses, it is often convenient (although not essential) to employ the relation for the linearized radiation as

$$e_{\omega_i}(T) - e_{\omega_i}(T_w) \simeq (d\, e_{\omega_i}/dT)_{T_w}\, (T-T_w) \qquad (2.9)$$

where again the subscript i refers to the ith band such that ω_i is the wave number location of the band and T_w represents the temperature of the reference wall which could be either T_1 or T_2. For the special case considered, since we are interested in investigating the transient behavior of the gas because of a step change in temperature of the lower plate, T_w is taken to be equal to T_1. It should be pointed out that for a single-band gas, the linearization is not required because the temperature distribution can be obtained from Eq. (2.8) and the radiative heat flux can be calculated from Eqs. (2.5) and (2.6). However, for the case of multiband gases and for systems involving mixtures of gases, it is convenient to employ the linearization procedure in order to use the information on band model correlations. The following definitions are useful in expressing the governing equations in linearized forms:

$$\theta = (T-T_1)/(T_2-T_1) \tag{2.10a}$$

$$N_{1i} = (Pt_m/\rho\, c_p)\, K_{1i}\ ,\ K_{1i} = S_i(T)\ (d\, e_{\omega i}/dT)_{T_1} \tag{2.10b}$$

$$N_1 = (P\ t_m/\rho\, c_p)\, K_1\ ,\ K_1 = \sum_{i=1}^{n} K_{1i} \tag{2.10c}$$

$$M_{1i} = (t_m/L\ \rho\, c_p)\, H_{1i}\ ,\ H_{1i} = A_{oi}(T)(d\, e_{\omega i}/dT)_{T_1} \tag{2.10d}$$

$$M_1 = (t_m/L\ \rho\, c_p)\, H_1\ ,\ H_1 = \sum_{i=1}^{n} H_{1i} \tag{2.10e}$$

$$M_{1i}\, u_{oi} = N_{1i}\ ,\ u_{oi}\, H_{1i} = PL\, K_{1i} \tag{2.10f}$$

where H_1, K_1, N_1 and M_1 represent the values of H, K, N and M evaluated at the temperature T_1. As explained in Refs. 1 and 8, these quantities represent the properties of the gaseous medium.

The initial and boundary conditions for the physical problem considered are

$$\theta(\xi,0) = 1;\ \theta(0,t) = 0;\ \theta(1,t) = 1 \tag{2.11}$$

It is important to note that the boundary conditions given in Eq. (2.11) are applicable only to the case of simultaneous conduction and radiation energy transfer. The cases of transient radiation and radiation with conduction are treated separately in the following sections.

2.2 Transient Radiation

By employing the definitions of Eqs. (2.9) and (2.10), Eq. (2.8) is transformed to obtain a convenient form of the energy equation for the transient radiation case as[23]

$$-\frac{\partial\theta(\xi,t)}{\partial t} = \frac{3}{2}\sum_{i=1}^{n} N_{1i}\left\{\int_{o}^{\xi}\frac{\partial\theta(\xi',t)}{\partial\xi'}\,x\right.$$

$$\bar{A}_i'\left[\frac{3}{2}u_{oi}(\xi-\xi')\right]d\xi' - \int_{\xi}^{1}\frac{\partial\theta(\xi',t)}{\partial\xi'}\,x$$

$$\left.\bar{A}_i'\left[\frac{3}{2}u_{oi}(\xi'-\xi)\right]d\xi'\right\} \tag{2.12}$$

The parameters in Eq. (2.12) are N_1 and u_o. For a given gas, the parameters are the gas pressure and the temperature of the lower wall. As pointed out earlier, the boundary conditions given in Eq. (2.11) are not applicable to Eq. (2.12) because this equation does not require a boundary condition. Thus, in this case, the temperature of the medium adjacent to a surface differs from the surface temperature. This is because the temperature of the medium adjacent to a surface is affected not only by the surface but also by all other volume elements and surfaces. The radiation slip method is a means of accounting for such temperature jumps and this is discussed in Ref. 1.

For the case of transient radiative interaction, the nondimensional radiative heat flux is defined by

$$Q(\xi,t) = q_R(\xi,t)/[e_1(t) - e_2(t)] \tag{2.13}$$

By employing the definitions of Eqs. (2.9), (2.10), and (2.13), relations for the radiative flux, as given by Eqs. (2.5) and (2.6), are expressed as

$$Q(\xi,t) = 1- (3/8\ \sigma\ T_1^3) \sum_{i=1}^{n} u_{oi}\ H_{1i} \{\int_o^{\xi} \theta(\xi',t)\ x$$

$$\bar{A}_i' [\tfrac{3}{2} u_{oi}(\xi-\xi')]d\xi' + \int_{\xi}^{1} [1 - \theta(\xi',t)]\ x$$

$$\bar{A}_i'[\tfrac{3}{2} u_{oi}(\xi'-\xi)]d\xi'\} \tag{2.14a}$$

and

$$Q(\xi,t) = 1 - (1/4\ \sigma\ T_1^3) \sum_{i=1}^{n} H_{1i}\{\int_o^{\xi} \frac{\partial\theta(\xi',t)}{\partial\xi'}\ x$$

$$\bar{A}_{i2}'^{3} u_{oi}(\xi-\xi')]d\xi' - \int_{\xi}^{1} \frac{\partial\theta(\xi',t)}{\partial\xi'}\ x$$

$$\bar{A}_i[\tfrac{3}{2} u_{oi}(\xi'-\xi)]d\xi'\} \tag{2.14b}$$

It should be pointed out that Eq. (2.14a) is a convenient form for the optically thin and general solutions while Eq. (2.14b) is useful for solutions in the large path length limit. Once the solutions for $\theta(\xi,t)$ are known from the energy equation, the appropriate relations for the heat flux can be obtained from Eqs. (2.14). It should be noted that the quantity $H_1/(\sigma T_1^3)$ in Eqs. (2.14) is nondimensional.

2.3 Radiation and Conduction

For this case where conduction heat transfer takes place simultaneously with radiative transfer, the energy equation is given by Eq. (2.8). Thus, a combination of Eqs. (2.8)-(2.10) results in

$$\frac{\partial\theta}{\partial t} = R\frac{\partial^2\theta}{\partial\xi^2} - \frac{3}{2}\sum_{i=1}^{n} N_{1i}\{\int_0^{\xi}\frac{\partial\theta(\xi',t)}{\partial\xi'}\times$$

$$\bar{A}_i\,[\tfrac{3}{2}u_{oi}(\xi-\xi')]d\xi' - \int_{\xi}^{1}\frac{\partial\theta(\xi',t)}{\partial\xi'}\times$$

$$\bar{A}_i'\,[\tfrac{3}{2}u_{oi}(\xi'-\xi)]d\xi'\} \qquad (2.15)$$

Since the presence of conduction implies continuity of temperatures at the boundaries, the boundary conditions for Eq. (2.15) are those given in Eq. (2.11). The quantity N_1/R can be expressed as $N = N_1/R = (PL^2/k)K_1$. The nondimensional parameter N denotes the relative importance of radiation versus conduction in the gas. For particular values of P and L, it is actually the dimensional gas property $N_1/(RPL^2) = K_1/k$ that represents the relative importance of radiation versus conduction.

For the case of no radiation, Eq. (2.15) becomes

$$\frac{\partial\theta}{\partial t} = R\frac{\partial^2\theta}{\partial\xi^2} \qquad (2.16)$$

The separation of variables results in a general solution of Eq. (2.16) as

$$\theta = \exp(-\lambda^2 Rt)\,(B_1\sin\lambda\xi + B_2\cos\lambda\xi) \qquad (2.17)$$

where λ^2 is the separation parameter. The particular solution of Eq. (2.17) can be obtained by satisfying the boundary conditions. Alternately, by defining a similarity variable $\eta = \xi/\sqrt{4Rt}$, Eq. (2.16) can be written as

$$\frac{d^2\theta}{d\eta^2} + 2\eta \frac{d\theta}{d\eta} = 0 \qquad (2.18)$$

The solution of Eq. (2.18), with initial and boundary conditions given by Eq. (2.11), is found to be

$$\theta(\xi,t) = (2/\sqrt{\pi}) \text{ erf } \eta \qquad (2.19)$$

This solution is applicable for relatively large separations between the plates.

In the case of simultaneous conduction and radiation heat transfer, the nondimensional heat flux is defined as

$$\bar{Q} = [q_c(\xi,t) + q_R(\xi,t)]/[e_1(t) - e_2(t)] \qquad (2.20)$$

Alternately, this can be expressed as

$$\bar{Q} = C(\partial\theta/\partial\xi) + Q \qquad (2.21)$$

where

$$C = k(T_1 - T_2)/\{L[e_1(t) - e_2(t)]\}$$

The expression for Q in Eq. (2.21) is obtained either from Eq. (2.14a) or from Eq. (2.14b). It should be noted that the relation for θ needed in Eq. (2.21) comes from the solution of Eq. (2.15).

3. METHOD OF SOLUTIONS

The solution procedures for the transient radiation and radiation with conduction cases are presented in this section. The procedure for the case of transient radiative energy transfer is given first and this is followed by the procedure for combined radiation and conduction.

3.1 Transient Radiative Equilibrium

For the general case of transient radiative equilibrium, the temperature distribution is obtained from the solution of the energy equation, Eq. (2.12). Once $\theta(\xi,t)$ is known, the radiative heat flux is calculated by using the appropriate form of Eq. (2.14). Before discussing the solution procedure for the general case, however, it is desirable to obtain the limiting forms of Eqs. (2.12) and (2.14) in the optically thin and large path length limits and investigate the solutions of resulting equations.

3.1.1 Optically Thin Limit

In the optically thin limit $\bar{A}(u) = u$ and $\bar{A}'(u) = 1$, and therefore, Eq. (2.12) reduces to[1,8,23]

$$\frac{\partial\theta(\xi,t)}{\partial t} + 3\,N_1\,\theta(\xi,t) - \frac{3}{2}\,N_1 = 0 \qquad (3.1a)$$

From an examination of Eq. (3.1a) along with the definitions given in Eq. (2.10), it is evidient that in the optically thin limit the temperature distribution in the medium is independent of the ξ- coordinate for the case of pure radiative exchange. This is a charateristic of the optically thin radiation in the absence of other modes of energy transfer. Thus, Eq. (3.1a) can be written as

$$\frac{d\theta(t)}{dt} + 3\,N_1\,\theta(t) - \frac{3}{2}\,N_1 = 0;\ \theta(\xi,0) = 1 \qquad (3.1b)$$

Since gas properties are evaluated at known reference conditions, N_1 is essentially constant, and solution of Eq. (3.1b) is found to be

$$\theta(t) = \frac{1}{2}[1 + \exp(-3 N_1 t)] \tag{3.2}$$

In the optically thin limit both forms of Eq. (2.14) yield the same final relation for the radiative flux as[23]

$$Q(\xi,t) = 1 - [3/(8\sigma T_1^3)]\ (PLK_1)\ [(1-\xi) + (2\xi - 1)\ \theta(t)] \tag{3.3}$$

It should be pointed out that in Eq. (3.3) the quantity $(PLK_1/\sigma T_1^3)$ is nondimensional. The relation for $\theta(t)$ in Eq. (3.3) is obtained from Eq. (3.2). Thus, evaluation of the temperature distribution and radiative heat flux in the optically thin limit does not require numerical solutions.

3.1.2 Large Path Length Limit

In the large path length limit (i.e., for $u_{oi} >> 1$ for each band), one has $\bar{A}(u) = = \ell n(u)$, $\bar{A}'(u) = 1/u$, and $\bar{A}''(u) = -1/u^2$. Thus, in this limit, Eq. (2.12) reduces to[1,8,23]

$$\frac{\partial\theta(\xi,t)}{\partial t} = -M_1 \int_0^1 \frac{\partial\theta(\xi',t)}{\partial\xi'} \frac{d\xi'}{(\xi-\xi')} \tag{3.4}$$

An analytical solution of Eq. (3.4) may be possible, but numerical solution can be obtained quite easily.

In the large path length limit, Eqs. (2.14a) and (2.14b) reduce respectively to

$$Q(\xi,t) = 1 - (1/\sigma 4T_1^3)\, H_1[\int_0^1 \theta(\xi',t)\, \frac{d\xi'}{(\xi-\xi')} - \int_\xi^1 \frac{d\xi'}{(\xi-\xi')}] \qquad (3.5a)$$

and

$$Q(\xi,t) = 1 - (1/4\sigma T_1^3) \sum_{i=1}^{n} H_{1i}\{\int_0^\xi \frac{\partial\theta(\xi',t)}{\partial\xi'}\, x\, \ell n[\tfrac{3}{2} u_{oi}(\xi-\xi')]d\xi' + \int_\xi^1 \frac{\partial\theta(\xi',t)}{\partial\xi'}\, x\, \ell n[\tfrac{3}{2} u_{oi}(\xi'-\xi)]d\xi'\} \qquad (3.5b)$$

The expressions for dimensionless radiative heat flux from or to the wall are obtained by setting $\xi = 0$ in Eqs. (3.5).

3.1.3 Numerical Solutions of Governing Equations

The general solutions of Eqs. (2.12) and (3.4) are obtained numerically by employing the method of variation of parameters. For this, a polynomial form for $\theta(\xi,t)$ is assumed in powers of ξ with time dependent coefficients as

$$\theta(\xi,t) = \sum_{m=o}^{n} c_m(t)\, \xi^m \qquad (3.6)$$

By considering only the quadratic solution in ξ, and satisfying the boundary conditions of Eq. (2.11), one finds

$$\theta(\xi,t) = \xi^2 + g(t)\, (\xi-\xi^2) \qquad (3.7)$$

where $g(t)$ represents the time dependent coefficient. At $t = 0$, a combination of Eqs. (2.11) and (3.7) yields the result

$$g(0) = (1-\xi^2)/(\xi-\xi^2) \qquad (3.8)$$

Equations (3.7) and (3.8) are used to obtain specific solutions of Eqs. (2.12) and (3.4). Once the temperature distribution is known, the expressions for heat flux are obtained by numerically integrating the corresponding equations. The entire numerical procedure is described in detail in Ref. 23. The numerical procedure is similar for higher order solutions in ξ of Eq. (3.6), but computational resources required are considerably higher.

3.2 Radiation with Conduction

Equations (2.15), (2.20) and (2.21) are the appropriate equations to describe the combined process of conduction and radiation energy transfer. The energy equation, Eq. (2.15), reduces in the optically thin limit to

$$\frac{\partial\theta}{\partial t} + 3N_1\,\theta - \frac{3}{2}\,N_1 = R\,\frac{\partial^2\theta}{\partial\xi^2} \tag{3.9}$$

A closed form solution of this equation may be possible but a numerical solution can be obtained easily. In the large path length limit, Eq. (2.15) reduces to

$$\frac{\partial\theta}{\partial t} = R\,\frac{\partial^2\theta}{\partial\xi^2} - M_1\int_0^1 \frac{\partial\theta}{\partial\xi'}\,\frac{d\xi'}{(\xi-\xi')} \tag{3.10}$$

The solution of this equation is obtained numerically.

The general solution of Eq. (2.15) is obtained by using the method of variation of parameters as discussed in Sec. 3.1 and Ref. 23. For a quadratic solution in ξ, a combination of Eqs. (2.15) and (3.7) results in

$$g'(t) + J_1(\xi)\,g(t) = J_2(\xi) \tag{3.11a}$$

where

$$J_1(\xi) = 2\,R\,C(\xi) + \frac{3}{2}\,C(\xi)\sum_{i=1}^{n} N_{1i}\left\{\int_0^{\xi}(1-2\xi')\,\bar{A}_i'\,[b_i(\xi-\xi')]d\xi' - \int_{\xi}^{1}(1-2\xi')\,\bar{A}_i'\,[b_i(\xi'-\xi)]d\xi'\right\} \tag{3.11b}$$

$$J_2(\xi) = 2\,R\,C(\xi) - 3\,C(\xi)\sum_{i=1}^{n} N_{1i}\left\{\int_0^{\xi}\xi'\,\bar{A}_i'\,[b_i(\xi-\xi')]d\xi' - \int_{\xi}^{1}\xi'\,\bar{A}_i'\,[b_i(\xi'-\xi)]d\xi'\right\} \tag{3.11c}$$

$$b_i = 3\,u_{oi}/2 \quad ; \quad C(\xi) = 1/(\xi-\xi^2) \tag{3.11d}$$

and n represents the number of vibration-rotation bands. The solution of Eq. (3.11a) is found to be[23]

$$g(t) = [g(0) - J_2(\xi)/J_1(\xi)]\exp[-J_1(\xi)t] + J_2(\xi)/J_1(\xi) \tag{3.12}$$

where g(0) is given by Eq. (3.8). The integrals in J_1 and J_2 are evaluated numerically by following the procedure discussed in Ref. 23. With g(t) known from Eq. (3.12), Eq. (3.7) provides the solution for the temperature distribution. Once $\theta(\xi,t)$ is known, the heat transfer is calculated by using either Eq. (2.20) or Eq. (2.21).

In the optically thin limit, the expression for J_1 and J_2, as defined by Eqs. (3.11b) and (3.11c), reduce to

$$J_1(\xi) = 2\,R\,C(\xi) + 3\,N_1 \tag{3.13a}$$

$$J_2(\xi) = C(\xi)\,[2\,R - 3(\xi^2 - 1/2)N_1] \tag{3.13b}$$

In the large path length limit, the expressions for J_1 and J_2 are obtained as

$$J_1(\xi) = C(\xi) \{2 R + \frac{3}{2} M_1 \int_0^1 [(1-2\xi')/(\xi-\xi')]d\xi'\} \qquad (3.14a)$$

$$J_2(\xi) = C(\xi) \{2 R - 3 M_1 \int_0^1 [\xi'/(\xi-\xi')]d\xi'\} \qquad (3.14b)$$

Equations (3.13) and (3.14) are useful in obtaining numerical solutions for the limiting cases.

4. PHYSICAL CONDITIONS AND DATA SOURCE

For the physical problem considered (Fig. 2.1) four specific absorbing-emitting species were selected for an extensive study; these are CO, CO_2, OH and H_2O. The species CO was selected because it contains only one fundamental vibration-rotation (VR) band and all spectral information are easily available in the literature. It is a very convenient gas to test the numerical procedure without requiring excessive computational resources. Species OH and H_2O are the primary radiation participating species for the pressure and temperature range anticipated in the combustor of the scramjet engine. Species CO_2, and combinations of CO_2 and H_2O are important absorbing-emitting species in many other combustion processes.

In radiative transfer analyses, it is essential to employ a suitable model to represent the absorption-emission characteristics of specific species under investigation. Several line-by-line, narrow-band, and wide-band models are available to model the absorption of a VR band (Refs. 7-11). However, it is often desirable to use a simple correlation to represent the total absorption of a wide band. Several such correlations are available in the literature (Refs. 7-11). The relative merits of these correlations are discussed in Ref. 11. In this study, the correlation proposed by Tien and Lowder[7] is employed and this is given by

$$\bar{A}(u) = \ln \{uf(\beta) [\frac{u + 2}{u + 2f(\beta)}] + 1\} \qquad (4.1)$$

where

$$f(\beta) = 2.94[1 - \exp(- 2.60\ \beta)]$$

and β represents the line structure parameter.

The spectral information and correlation quantities needed for CO, CO_2 and H_2O were obtained from Refs. 7-9. The spectral data for OH were obtained from Refs. 24 and 25, and correlation quantities are developed in Appendix A. The specific VR bands considered for each species are: CO (4.7μ fundamental), OH (2.8μ fundamental), CO_2 (15μ, 4.3μ and 2.7μ), and H_2O (20μ, 6.3μ, 2.7μ, 1.87μ, and 1.38μ). The radiative properties of important species are provided in Appendix A.

It is important to consider the variation of thermodynamic and transport properties with temperature and pressure. This information is available for important species in Refs. 26-28 and essential information for the present study is provided in Appendix B.

For the specific problem considered, the dependent variables are θ, Q, and $\bar{Q}$, and independent variables are ξ and t. The parameters for general solutions are T_1, T_2/T_1, u_o, and t_m. For the radiative equilibrium case, θ and Q depend only on t and N_1 in the optically thin limit and on ξ, t, and M_1 in the large path length limit. For the case of combined radiation and conduction, θ and $\bar{Q}$ depend on ξ, t, and $N = N_1/R$ in the optically thin limit and on ξ, t, and $M = M_1/R$ in the large path length limit. Information on radiative ability of various species in the optically thin and large path length limits is available in Ref. 8 and Appendix C. The parameters for specific solutions for different species are T_1, T_2/T_1, P, L, and t_m. Extensive results, therefore, can be obtained by varying these parameters. For parametric studies, however, only certain values of pressure, temperature, and plate spacing were selected and results were obtained for the general as well as limiting cases. Unless stated otherwise, specific results were obtained for $T_2 = 2\ T_1$.

5. RESULTS AND DISCUSSION

Results have been obtained for different radiation participating species for both cases, the radiative equilibrium and radiation with conduction. The computer program used for numerical solutions is provided in Appendix D. It should be realized at the outset that, according to the physics of the problem, the gas initially is at a high temperature $T_1 = T_2$. At $t = 0$, the temperature T_1 is lowered to a constant value. The energy exchange then occurs and the gas cools down in time until a steady-state conditon is reached. At this time, a certain temperature profile is established and a fixed amount of energy exchange occurs irrespective of the time. The rate of cooling of the gas layer, therefore, is dependent on the nature of the participating species and on the physical parameters of the problem.

Some limiting solutions that are independent of any participating species are presented first in Figs. 5.1 and 5.2 for the radiative equilibrium case. In Fig. 5.1, the temperature distribution in the channel is plotted as a function of the optically thin parameter N_1 for different times. Similar results are illustrated in Fig. 5.2 (with solid lines) for even higher values of N_1. These results show an exponential decay with time reaching the steady-state value of $\theta=1/2$ for $t\to\infty$. The temperature distribution for the large path length limit is shown in Fig. 5.2 (with broken lines) as a function of the large path length parameter M_1 and for different times. Although the numerical values are entirely different, these results also show the exponential decay with time and reach the limiting value of $\theta = 1/2$ for $t \to \infty$. It should be noted that while the optically thin solutions are independent of the ξ-coordinate, the large path length solutions do depend on ξ and they have been obtained for $\xi = 0.5$. In the case of simultaneous radiation and conduction, both optically thin and large path length solutions

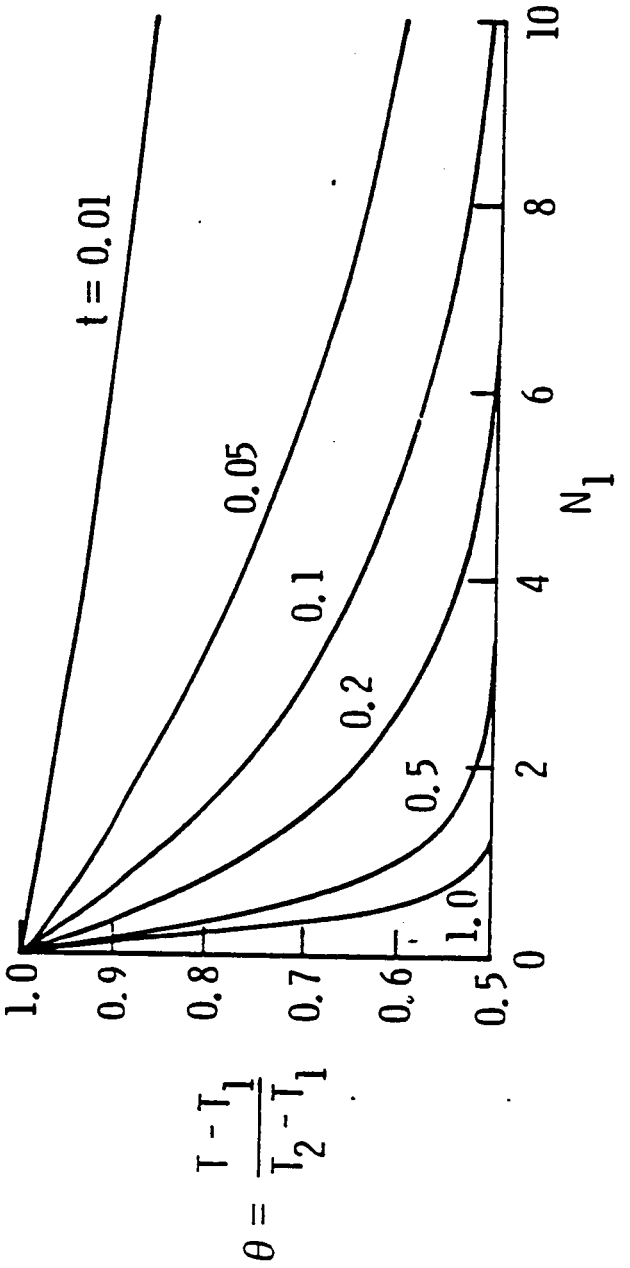

Fig. 5.1 Temperature variation with the optically thin parameter N_1 .

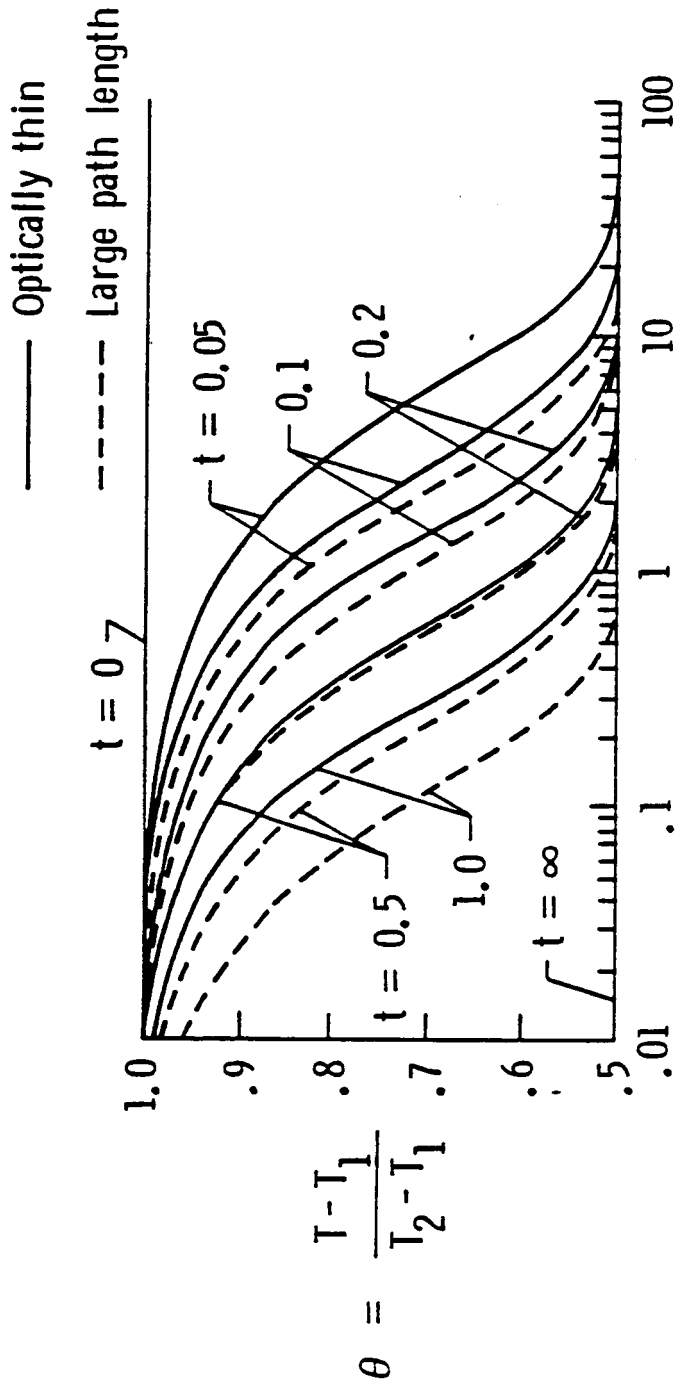

Fig. 5.2 Limiting solutions for the radiative equilibrium case.

for temperature distribution depend on ξ. These results, however, can be expressed in terms of the radiation-conduction parameter $N=N_1/R$ in the optically thin limit and $M = M_1/R$ in the large path length limit.

The radiative equilibrium temperature distribution for CO are shown in Fig. 5.3 for three different characteristic times and for P = 1 atm, L = 10 cm, and T_w = 500 K. For small t_m, $t^* = t/t_m$ becomes large and, therefore, θ varies slowly with t^*; the reverse is true for large t_m values. This trend is evident clearly from the simplest case of the optically thin solution given by Eq. (3.2). Similar trends in results were observed also for other species for different values of P, T_w and L. Thus, to demonstrate typical transient trends, other results presented in this study were obtained for an intermediate value of the characteristic time t_m = 0.00001 sec.

The centerline temperature variations with time are illustrated in Fig. 5.4a for CO and in Fig. 5.4b for OH. General and limiting solutions are shown for pure conduction, radiation, and radiation with conduction for P = 1 atm, T_w = 500 K, and L = 10 cm. It is noted that for both gases the optically thin solutions approach the steady-state conditions faster than the large path length and general solutions. For the physical conditions considered, the energy is transferred faster by conduction than by radiation, and the steady-state conditions are reached earlier by the combined radiation and conduction process. Although OH is a relatively better heat conducting gas, CO is seen to be more effective in the radiative transfer. For the same physical conditions as in Figs. 5.4, the radiation and radiation with conduction results are compared for CO, OH, H_2O, and CO_2 in Fig. 5.5. It is seen that H_2O is most effective and OH is least effective in transferring the radiative energy. The ability of a gas to transfer radiative energy depends on the molecular structure of the gas, band intensities and physical conditions of

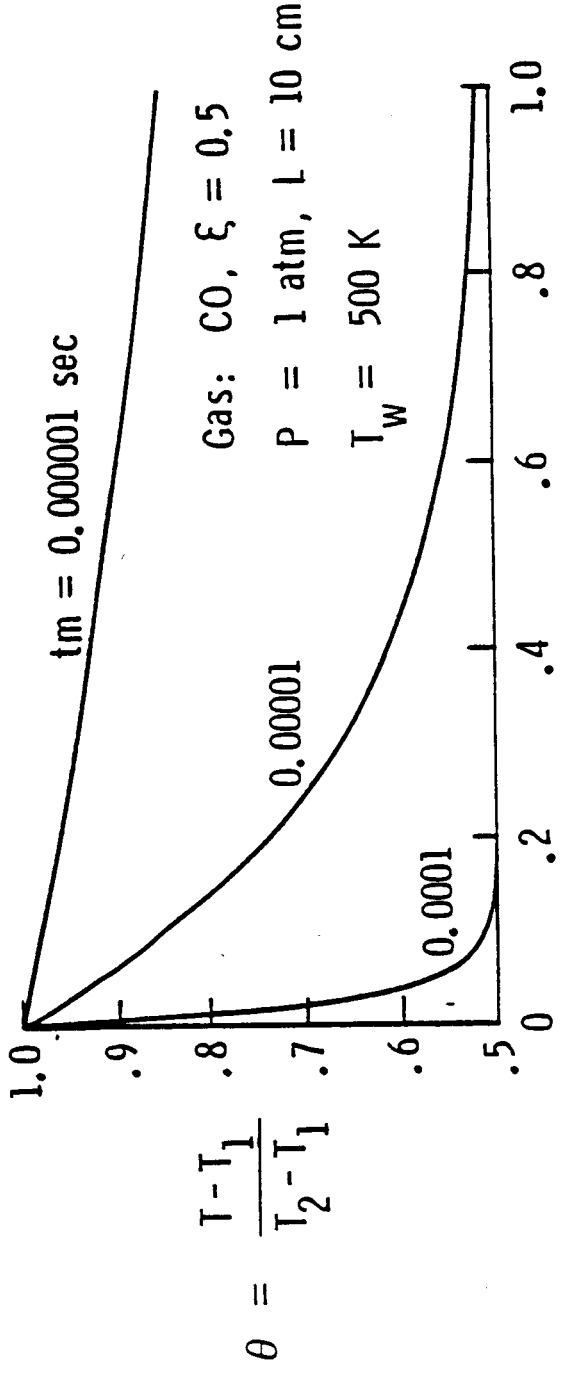

Fig. 5.3 Temperature variation for transient radiation for different characteristic times (CO, P = 1 atm, T_w = 500 K, L = 10 cm and ξ = 0.5).

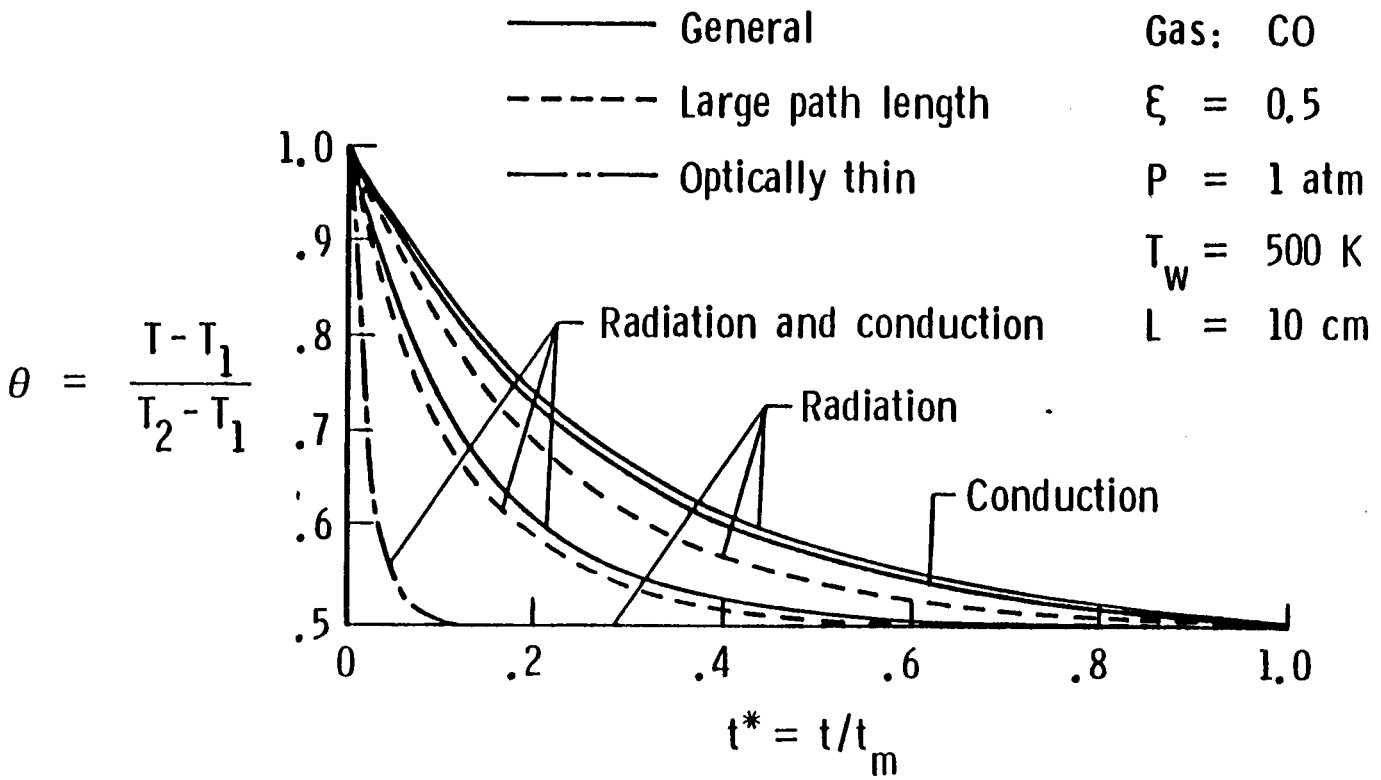

Fig. 5.4a Centerline temperature variation with time for CO with P = 1 atm, T_w = 500 K, and L = 10 cm.

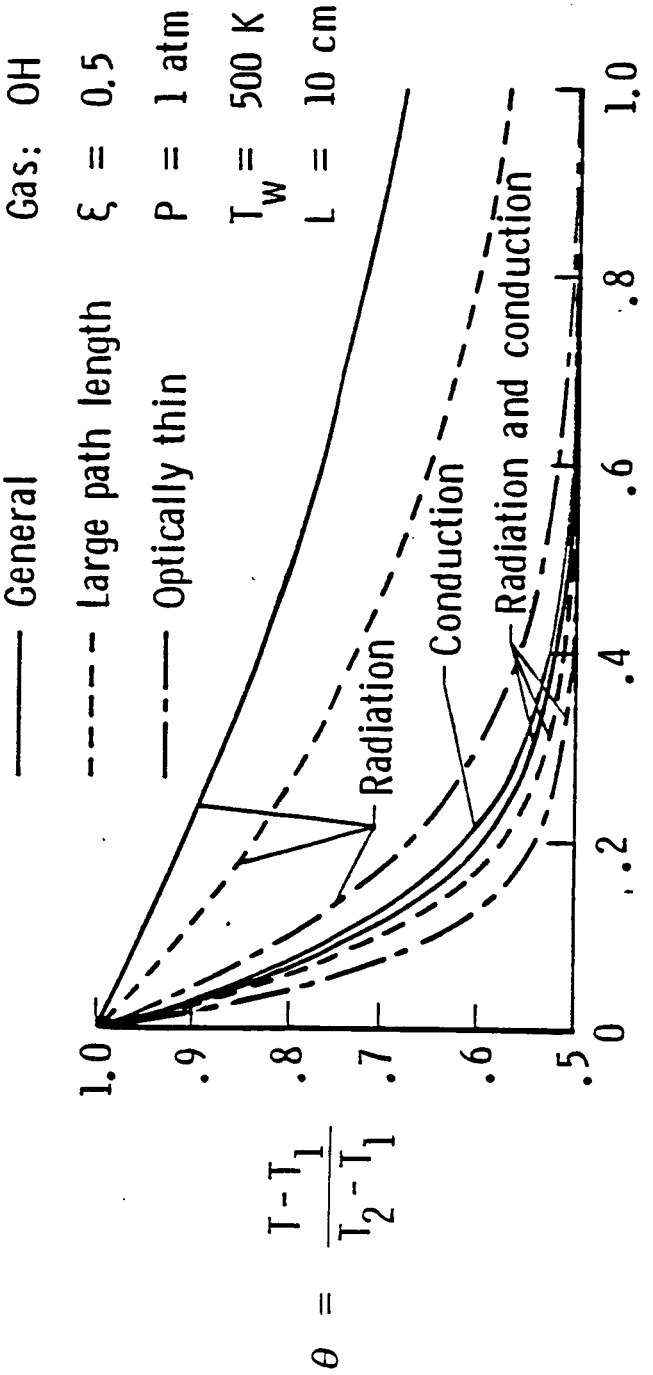

Fig. 5.4b Centerline temperature variation with time for OH with P = 1 atm, T_w = 500 K, and L = 10 cm.

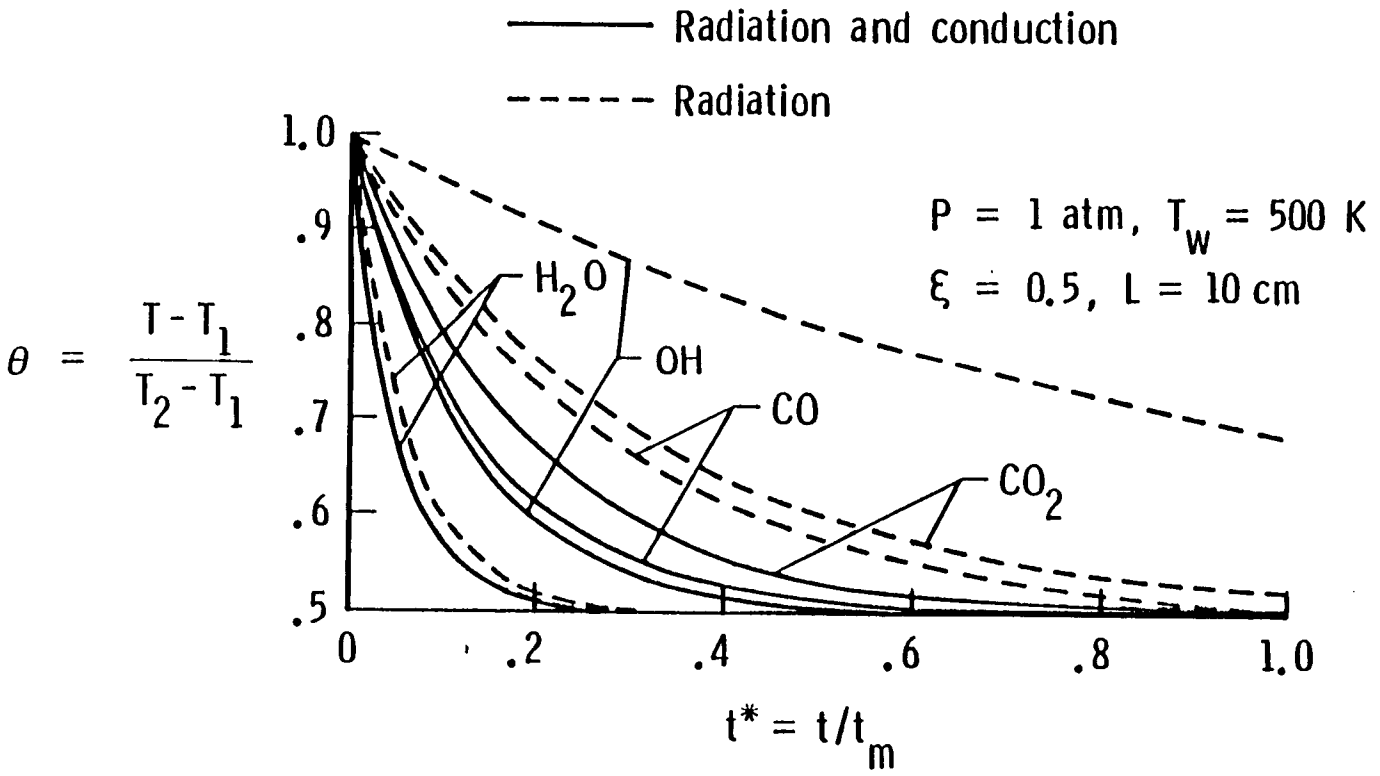

Fig. 5.5 Comparison of centerline temperature variation with time for P = 1 atm, T_w = 500 K and L = 10 cm.

the problem. Thus, H_2O with five strong VR bands is a highly radiation participating species and the steady-state conditions are reached quickly for H_2O than for other species. However, CO with one fundamental band is seen to be a better radiating gas than CO_2 with three VR bands. This is because for the given physical conditions, the optical thickness of CO_2 is sufficiently large and in the large path length limit CO_2 is relatively less effective in transferring the radiative energy (Ref. 8 and Appendix C). Further results for CO and OH are illustrated in Figs. 5.6 for different wall temperatures. It is seen that while radiation is less effective than conduction at T_w = 500 K, it is highly effective at T_w = 1,000 K. This, however, would be expected because radiation becomes considerably important at higher temperatures. The steady-state condition is reached quicker for T_w = 1,000 K than for T_w = 500 K. In fact for the characteristic time considered (t_m = 0.00001 sec.), the steady-state condition is reached quickly for all species for temperatures higher than T_w = 1,000 K. Results for the pure radiation case are illustrated in Figs. 5.7 for CO and OH for L = 1 cm and 10 cm. It is seen that while the general and large path length solutions depend on the plate spacing the optically thin solutions are independent of the spacing. This fact was pointed out earlier in the method of solution. In the presence of other modes of energy transfer, the optically thin solutions also depend on the plate spacings. As would be expected, for the same physical conditions, the steady-state condition is reached quicker for the lower plate spacing.

The temperature variations within the plates are shown in Figs. 5.8-5.11 for different species and for P = 1 atm and L = 5 cm. In the absence of molecular conduction, temperature jumps (radiation slips) occur at the boundaries and, therefore, the general solutions for the case of radiative equilibrium are not presented. However, general as well as limiting solutions

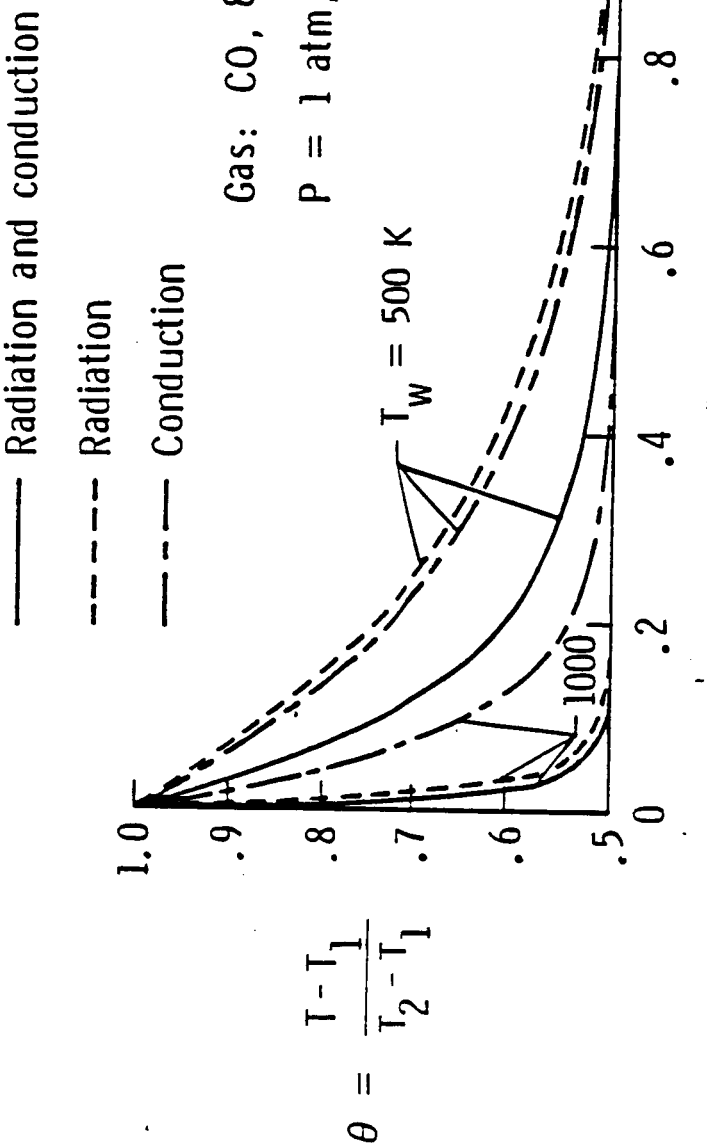

Fig. 5.6a Centerline temperature variation with time for CO with P = 1 atm, and L = 10 cm.

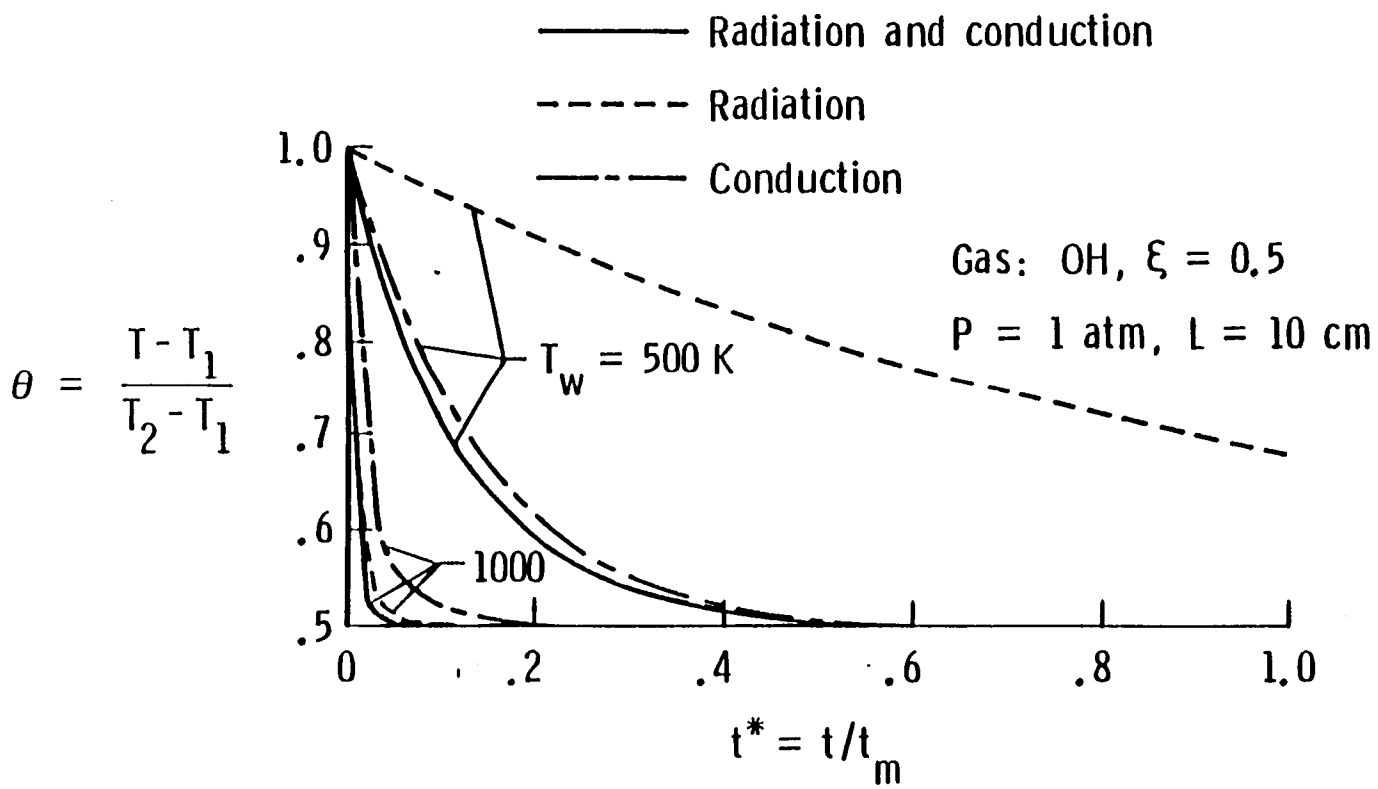

Fig. 5.6b Centerline temperature variation with time for OH with P = 1 atm, and L = 10 cm.

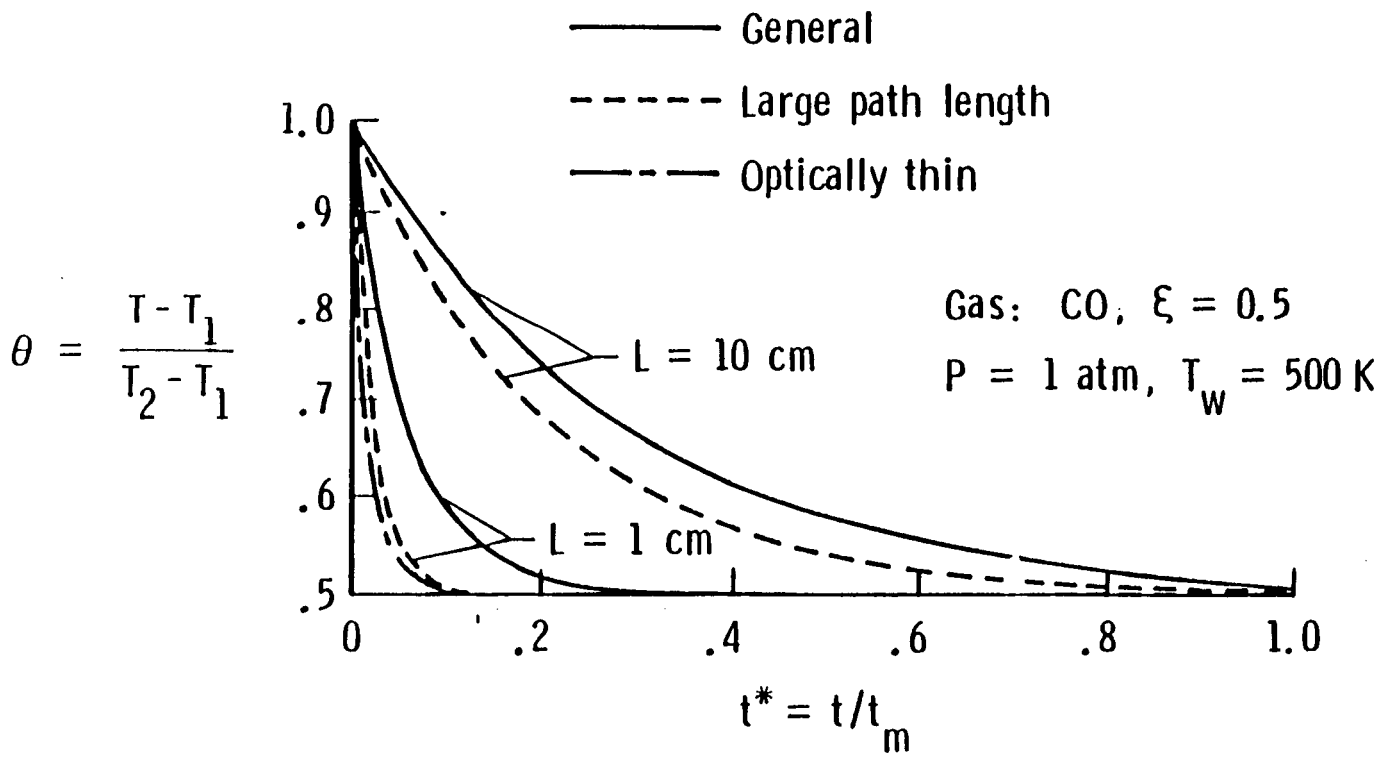

Fig. 5.7a Centerline temperature results for pure radiation (CO, P = 1 atm, and T_w = 500 K).

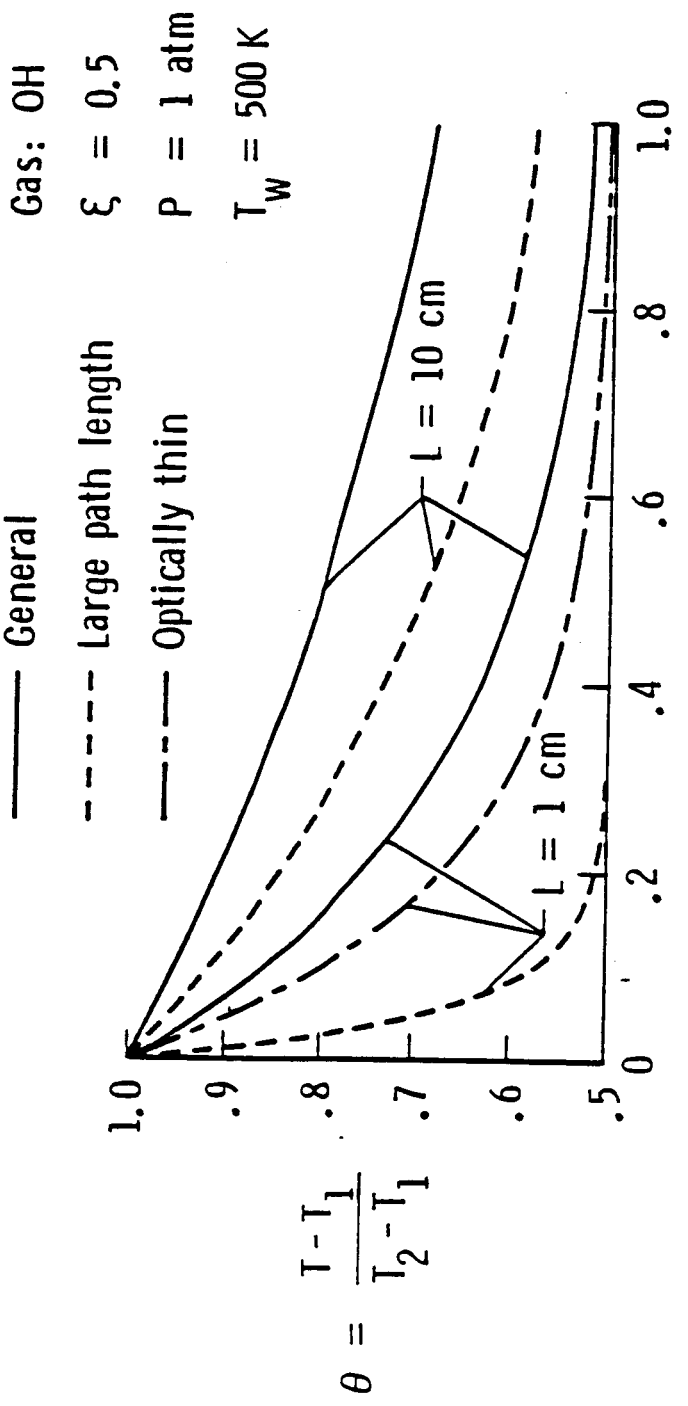

Fig. 5.7b Centerline temperature results for pure radiation (OH, P = 1 atm, and T_W = 500 K).

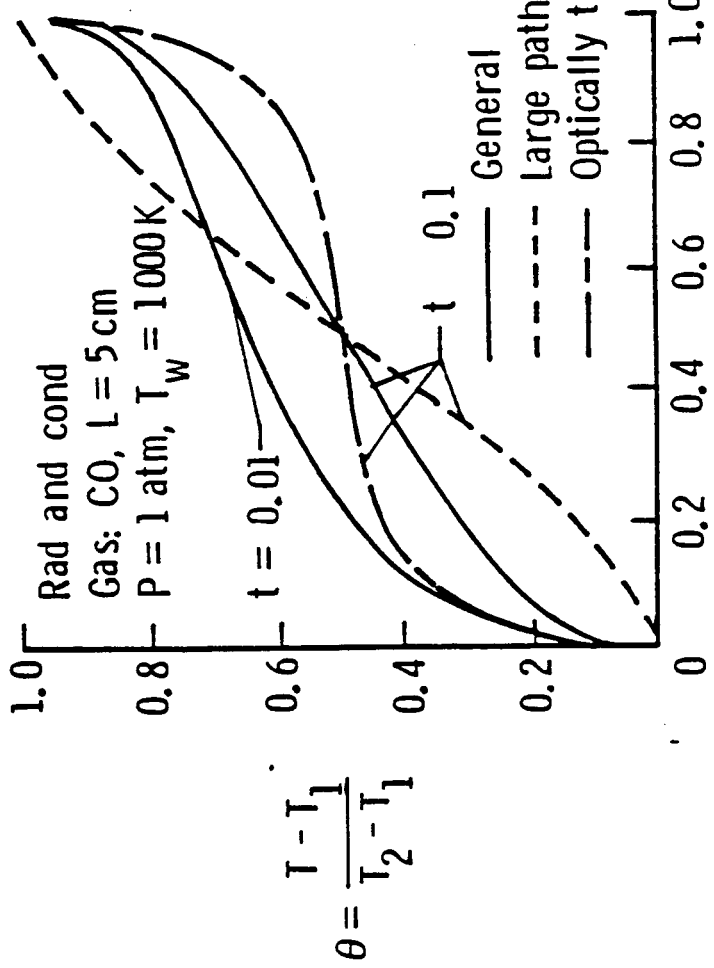

Fig. 5.8a Temperature variation for combined radiation and conduction for CO with P = 1 atm, T_w = 1000 K, and L = 5 cm.

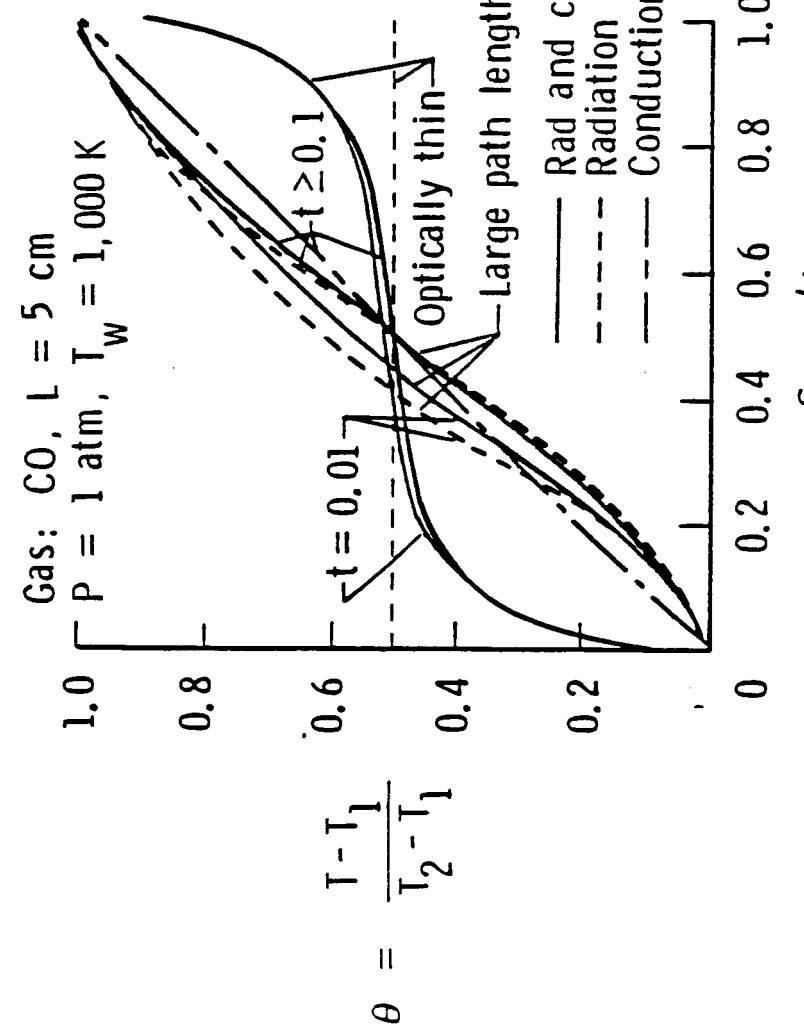

Fig. 5.8b Temperature variation for CO with P = 1 atm, T_w =1000 K, and L = 5 cm.

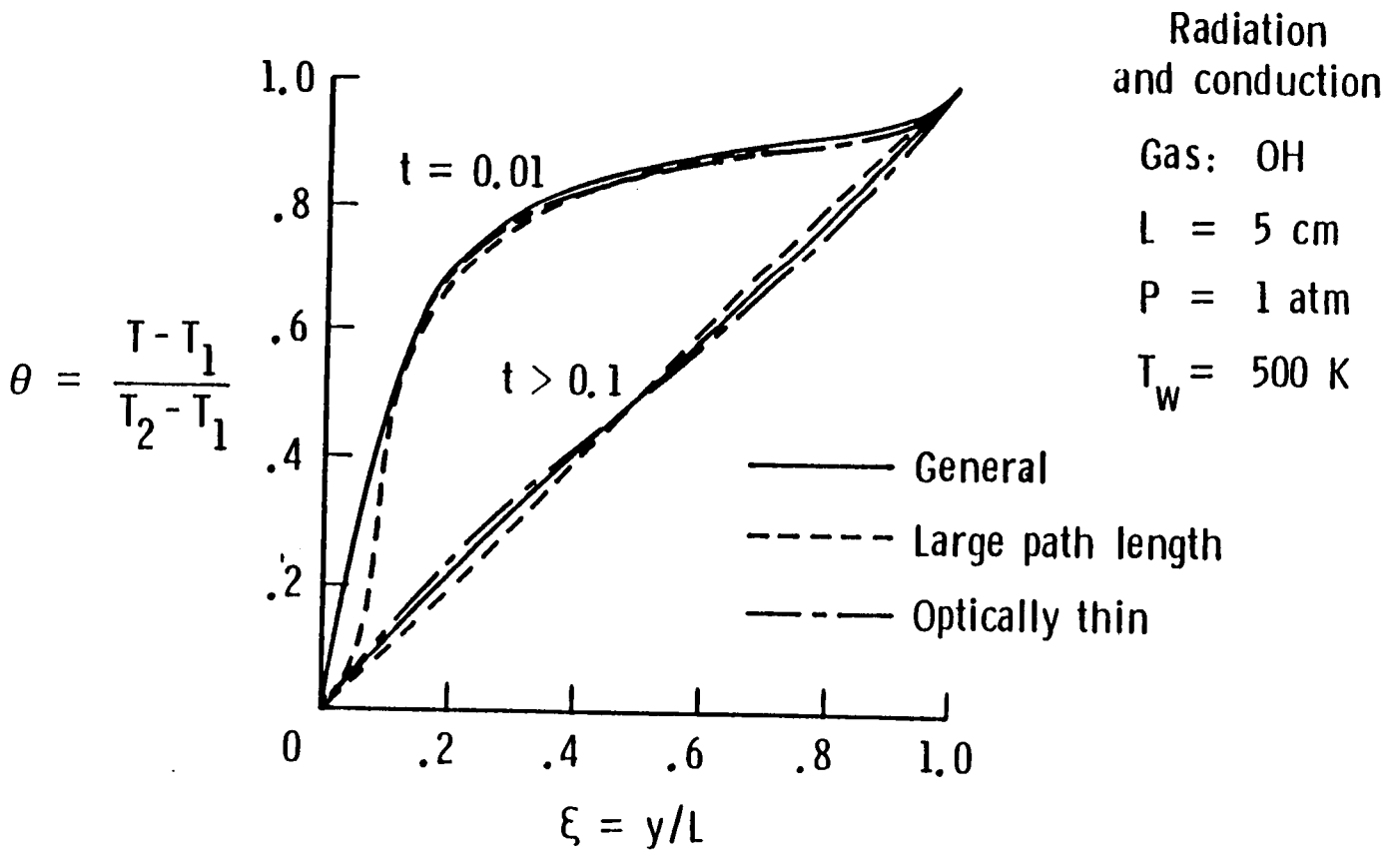

Fig. 5.9a Temperature variation for combined radiation and conduction for OH with P = 1 atm, T_w = 500 K, and L = 5 cm.

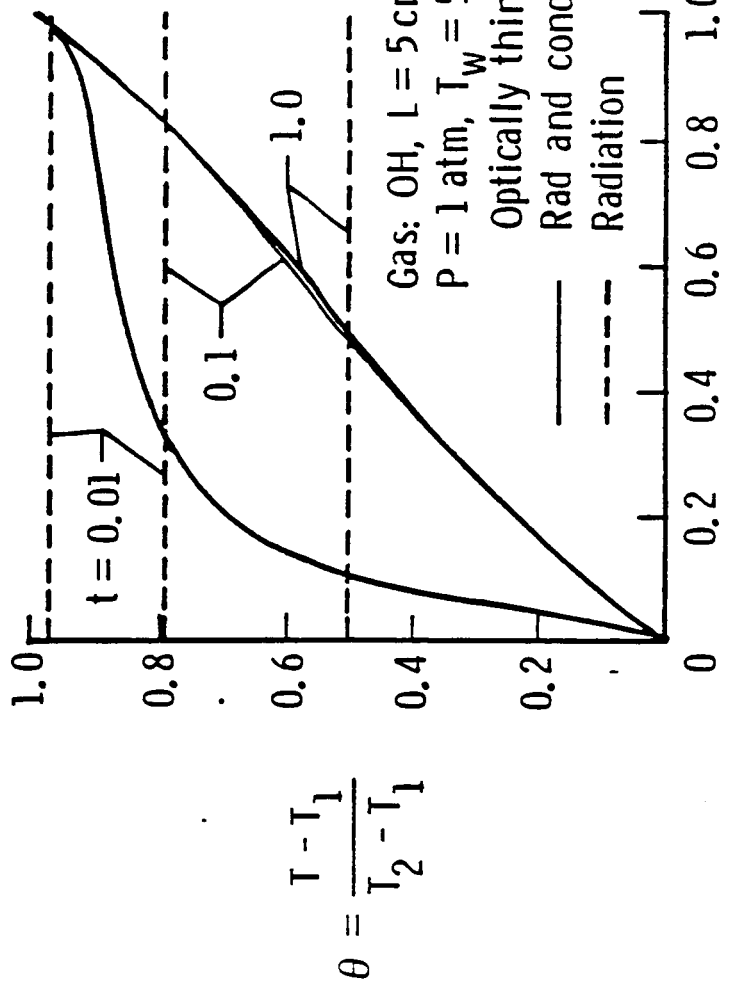

Fig. 5.9b Temperature variation in optically thin limit for OH with P = 1 atm, T_w = 500 K, and L = 5 cm.

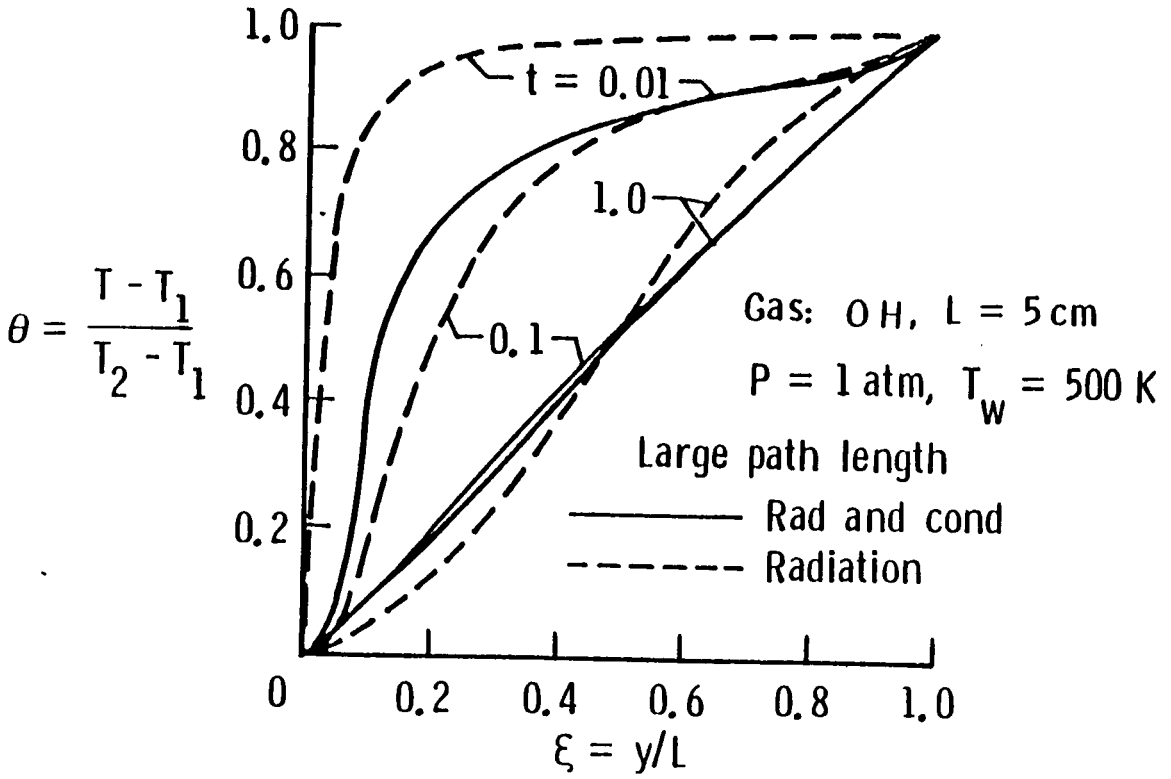

Fig. 5.9c Temperature variation in large path length limit for OH with P = 1 atm, T_w = 500 K, and L = 5 cm.

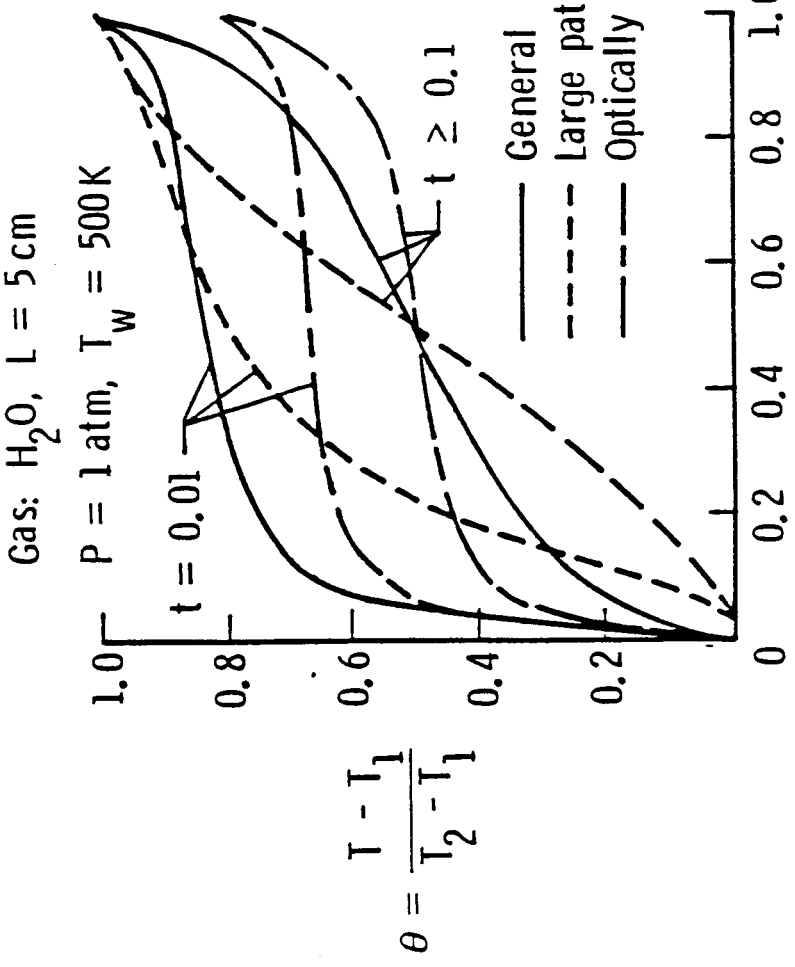

Fig. 5.10a Temperature variation for combined radiation and conduction for H_2O with P = 1 atm, T_w =500 K, and L = 5 cm.

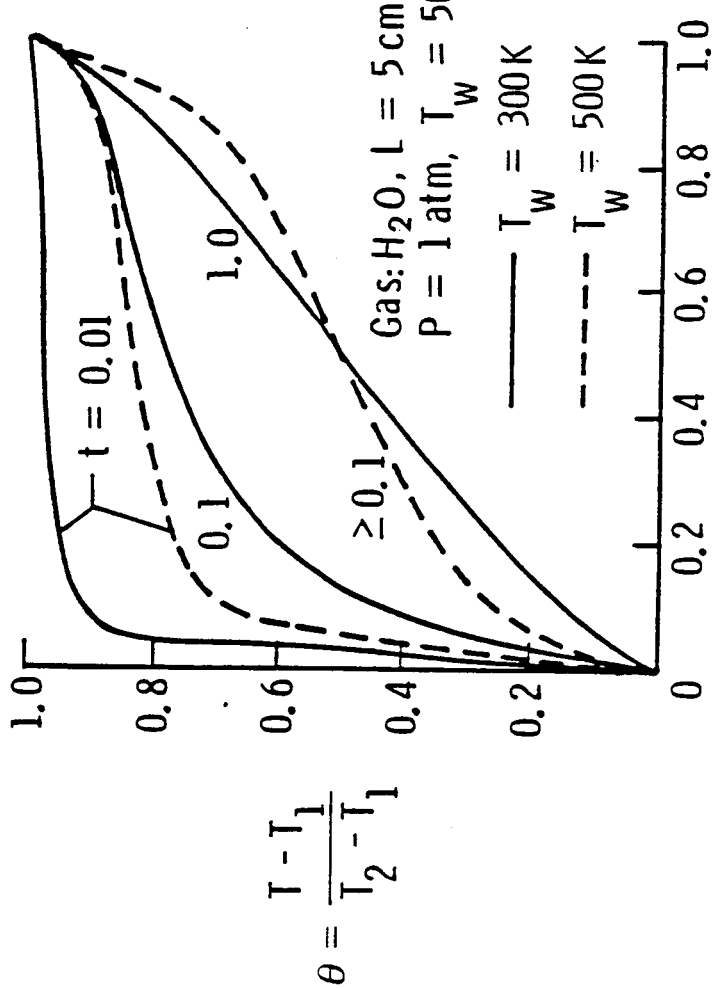

Fig. 5.10b Temperature variation for combined radiation and conduction for H_2O with P = 1 atm, and L = 5 cm.

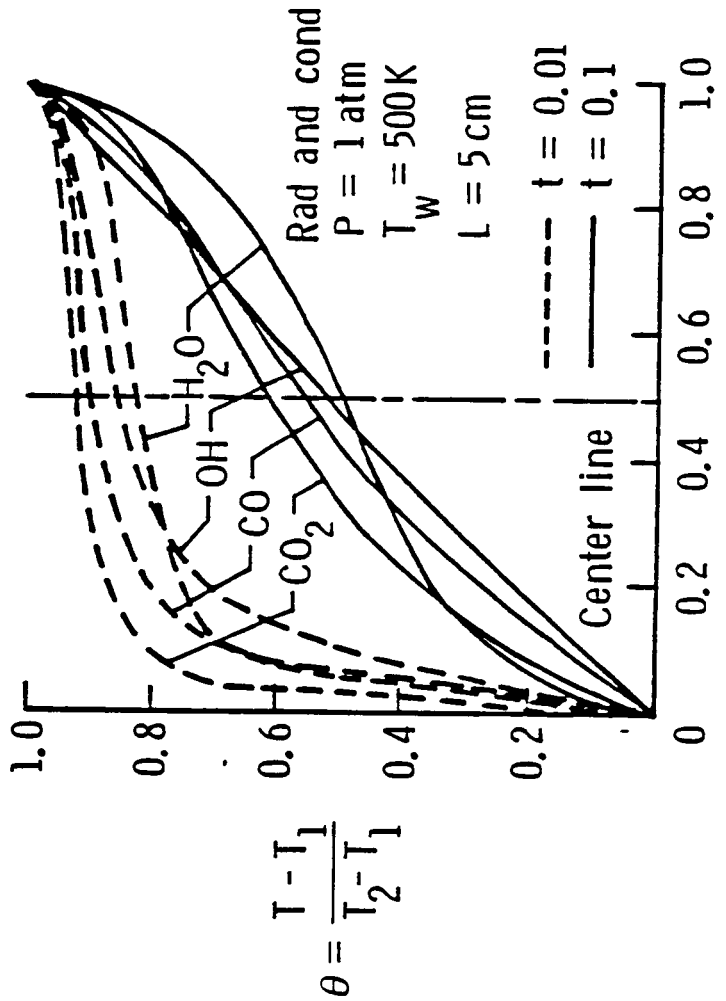

Fig. 5.11 Comparison of temperature variation for combined radiation and conduction for P = 1 atm, T_w = 500 K, and L = 5 cm.

are presented for the case of radiation with conduction. It is noted, in general, that for the case of radiation with conduction, the steady-state conditions are reached for all species at $t \geq 0.1$ and for $T_w \geq 500$ K. For the case of pure radiation, the steady-state conditions are reached at relatively longer times. The optically thin results are seen to be independent of the ξ-coordinate for the case of radiative equilibrium and are seen to vary slowly in the central portion of the plates for the case of radiation with conduction. This is because, in this limit, the gas interacts directly with the boundaries and conduction is predominant near the walls. Specific results for CO are illustrated in Figs. 5.8 for T_w = 1,000 K. For the case of radiation with conduction, general and limiting solutions are compared in Fig. 5.8a; and for both cases, the radiative equilibrium and radiation with conduction, limiting solutions are compared in Fig. 5.8b. The steady-state results for pure conduction are also shown in Fig. 5.8b for comparative purposes. The results demonstrate the typical trends for limiting and general solutions, i.e., a lower temperature gradient implies a higher rate of energy transfer. Specific results for OH are illustrated in Figs. 5.9 for T_w = 500 K. General and limiting solutions are shown in Fig. 5.9a; and limiting solutions are compared in Figs. 5.9b and 5.9c. For the case of radiation with conduction, the limiting and general solutions are seen to be in good agreement for all times (Fig. 5.9a). This is because for the conditions of the illustrated results, conduction dominates the energy transfer process in OH. The typical trends in results for the optically thin and large path length limits are shown in Figs. 5.9b and 5.9c, respectively. Figure 5.9b clearly shows that for all times the radiative equilibrium results are independent of the ξ-coordinate in the optically thin limit. Figure 5.9 shows that at earlier times the rate of energy transfer is higher in the

presence of conduction. Specific results for H_2O are illustrated in Figs. 5.10 for the case of radiation with conduction. It is seen clearly that the rate of cooling is signficantly higher in the large path length limit (Fig. 5.10a), and the steady-state conditions are reached at relatively longer times for lower T_w values (Fig. 5.10b). For the case of combined radiation and conduction, a comparison of results for different species is shown in Fig. 5.11 for t = 0.01 and 0.1. The results for t = 0.1 essentially correspond to the steady-state conditions. For t = 0.01, the variation in temperature is seen to be relatively small between ξ=0.2 and 0.9. The centerline temperature is found to be the lowest for H_2O, and this is followed by OH, CO, and CO_2. However, it is noted that OH is very effective in transferring the net energy in comparison to the other species. As discussed earlier, this is mainly due to relatively higher conductive ability of OH at T_w = 500 K.

The centerline temperature distributions are shown in Figs. 5.12-5.15 for different gases as a function of the spacing between the plates. In most figures, results are presented for both cases, the radiative equilibrium and radiation with conduction. In selected figures, results for the case of pure conduction are included also for comparative purposes. For a particular gas, specific results are presented for various times to demonstrate the radiative nature of the gas under different pressure and temperature conditions.

The results for CO are presented in Figs. 5.12 for different cases. For P = 1 and T_w = 500 K, the results illustrated in Fig. 5.12a show that the time required to reach the steady-state condition increases with increasing plate spacings. For a particular plate spacing, the centerline temperature is lower for the case of radiation with conduction than for pure radiation for all times. For P = 1 atm and T_w = 1,000 K, results presented in Fig. 5.12b show that the large path length solutions are closer to the general solutions for L

> 20 cm; and the results for pure radiation and radiation with conduction are identical for $t \geq 0.5$. The centerline temperature variations are shown in Fig. 5.12c for $t = 0.5$ $T_w = 500$ K, and different pressures. It is noted that while the heat transfer by conduction is insensitive to the change in pressure, the radiative heat transfer is strongly dependent on it. The rate of radiative interaction increases with increasing pressure until the large path length limit is reached for sufficiently large values of L. For the case of pure radiation, the results for P = 0.1 atm differ considerably from other results. This is due to use of the Tien and Lowder's correlation which is suitable only at relatively higher pressures (Ref. 11). The centerline temperature variations are shown in Fig. 5.12d for $t = 0.5$, P = 1 atm, and different values of T_w. As would be expected, both conductive and radiative interactions increase with increasing temperatures, although the increase in radiative transfer is comparatively higher. It should be noted that for T_w = 300 K, $T_2 = 2\ T_w = 600$ K, for $T_w = 500$ K, $T_2 = 1{,}000$ K, and so on. Thus, for a higher value of $T_w = T_1$, the energy interactions occur at a sufficiently large temperature difference between the upper and lower plates. At these temperatures, if the plate spacing is small, the energy is transferred quickly and the steady-state condition is reached at relatively shorter times. This fact was pointed out also in the discussion of results of Figs. 5.7.

The centerline temperature variations for OH are illustrated in Figs. 5.13 for different conditions. The results presented in Fig. 5.13a for P = 1 atm and $T_w = 500$ K show the similar trend as CO in Fig. 5.12a, although the extent of energy transfer by simultaneous radiation and conduction is relatively higher. This is because at $T_w = 500$ the energy transfer in OH is dominated by the conduction heat transfer. General and limiting solutions for radiative equilibrium are shown in Fig. 5.13b and for radiation with

conduction in Fig. 5.13c. These results clearly demonstrate the typical radiative interaction trends for different times. The results show that the optically thin solutions are independent of the plate spacing in the case of pure radiation but depend on the spacing when molecular conduction is included. The large path length results are seen to be valid only for large values of L for the case of pure radiation (Fig. 5.13b), but they appear to be valid in the entire range for the case of radiation with conduction (Fig. 5.13c). The results for pure conduction, pure radiation, and conduction with radiation are illustrated in Fig. 13d for P = 1 atm and T_w = 1,000 K. For this temperature, the results for pure radiation and radiation wih conduction are found to be identical. This indicates that at higher temperatures, OH becomes a highly radiation participating gas. The results for variation of the centerline temperature for OH with pressure and temperature are given in Figs. 5.13e and 5.13f and they show the same general trend as the results for CO shown in Figs. 5.12c and 5.12d.

Extensive results of $\theta(\xi = 0.5)$ versus L have been obtained for H_2O and CO_2 for different conditions and some of these are illustrated in Figs. 5.14. In general, these results show similar trends as exhibited by the results for CO and OH but the extent of radiative interactions is entirely different. For example, a comparison of results presented in Fig. 5.14a for H_2O with the results of Fig. 5.12a for CO and Fig. 5.13a for OH for identical conditions reveals that H_2O is a highly radiation participating gas even for shorter times. For H_2O, results presented in Fig. 5.14b demonstrate that the large path length solutions are closer to the general solutions for both cases, the radiative equilibrium and radiation with conduction. The centerline temperature variation with L is shown for H_2O in Figs. 5.14c and 5.14d for different pressure and temperature. As epxected, radiative effects are seen to be higher at higher pressure and temperature.

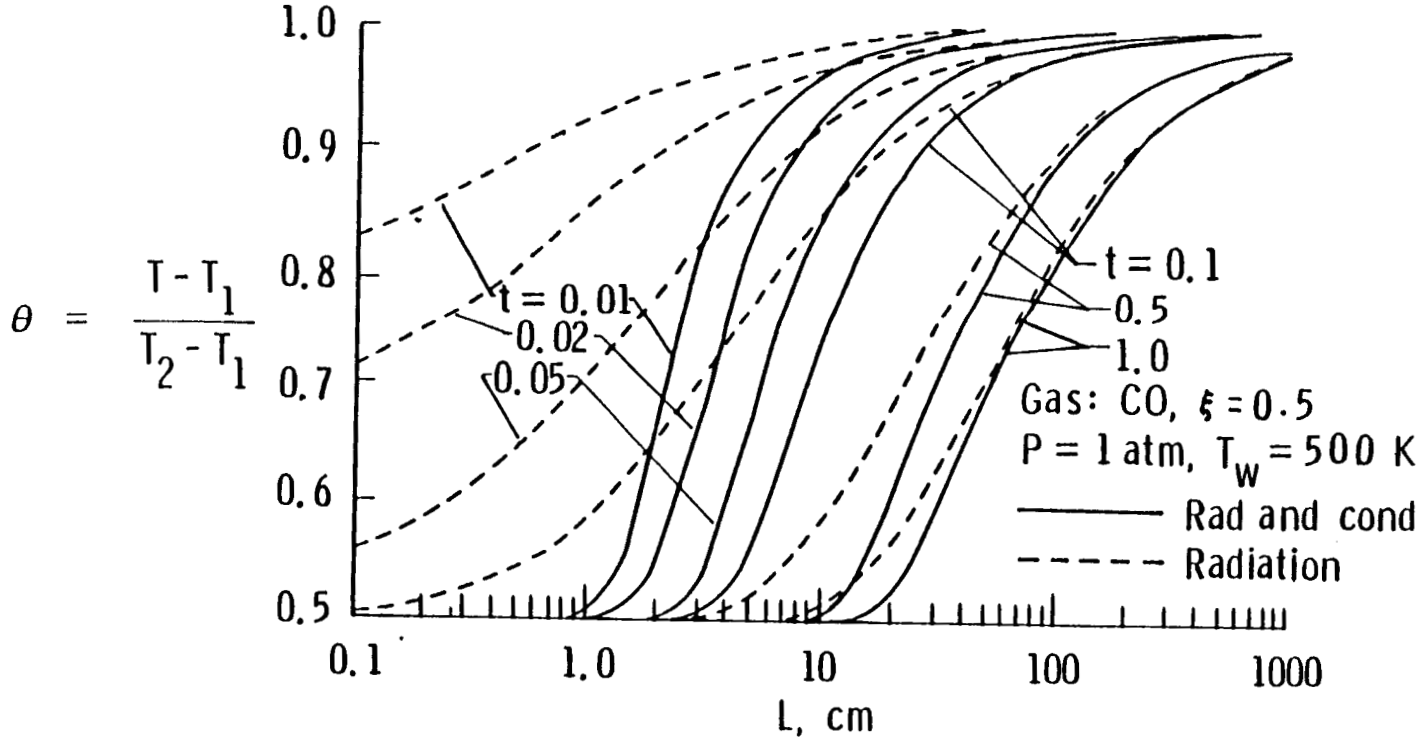

Fig. 12a Centerline temperature variation with L for CO (P = 1 atm, and T_w = 500 K).

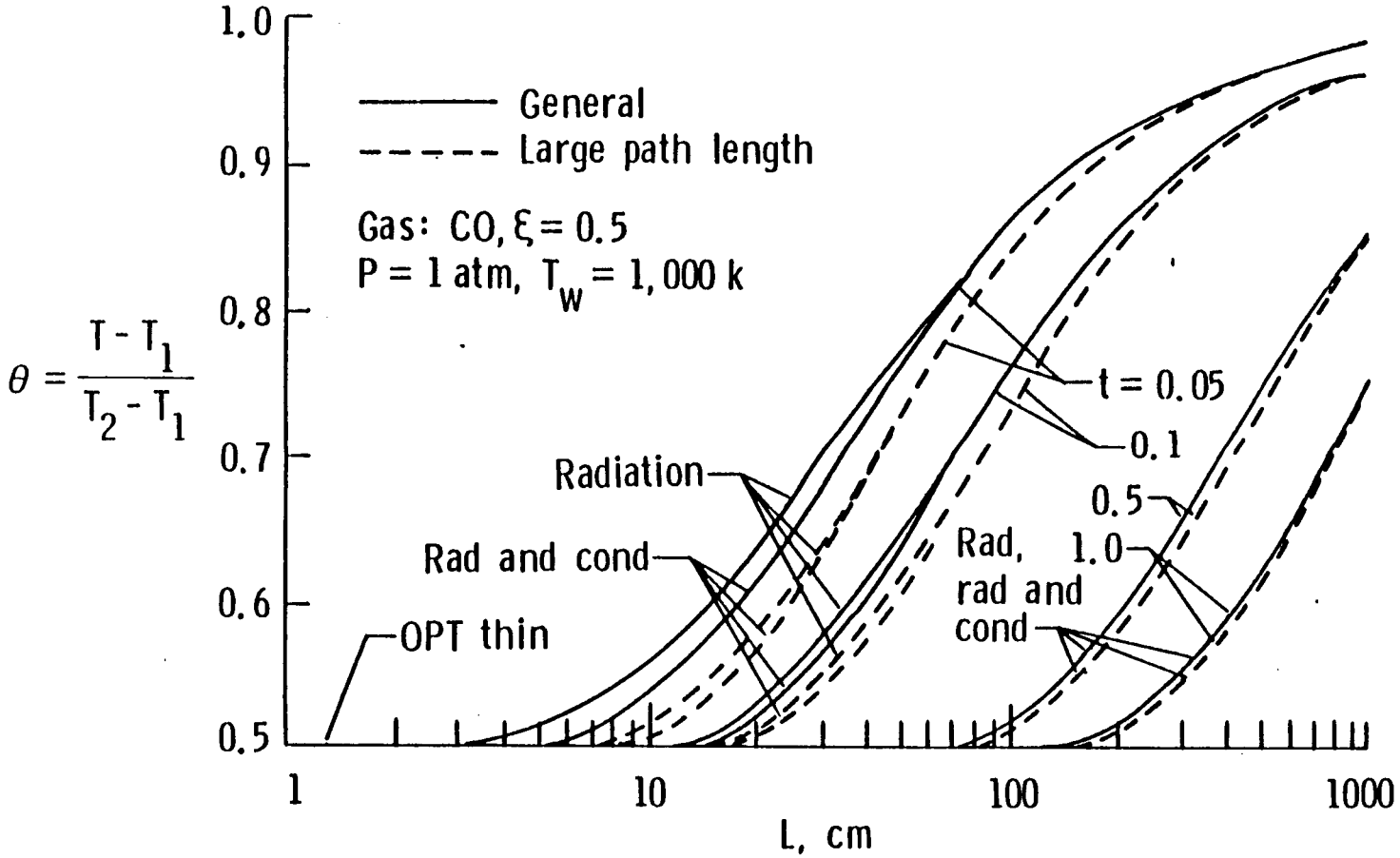

Fig. 5.12b Centerline temperature variation with L for CO (P = 1 atm and T_w = 1000 K).

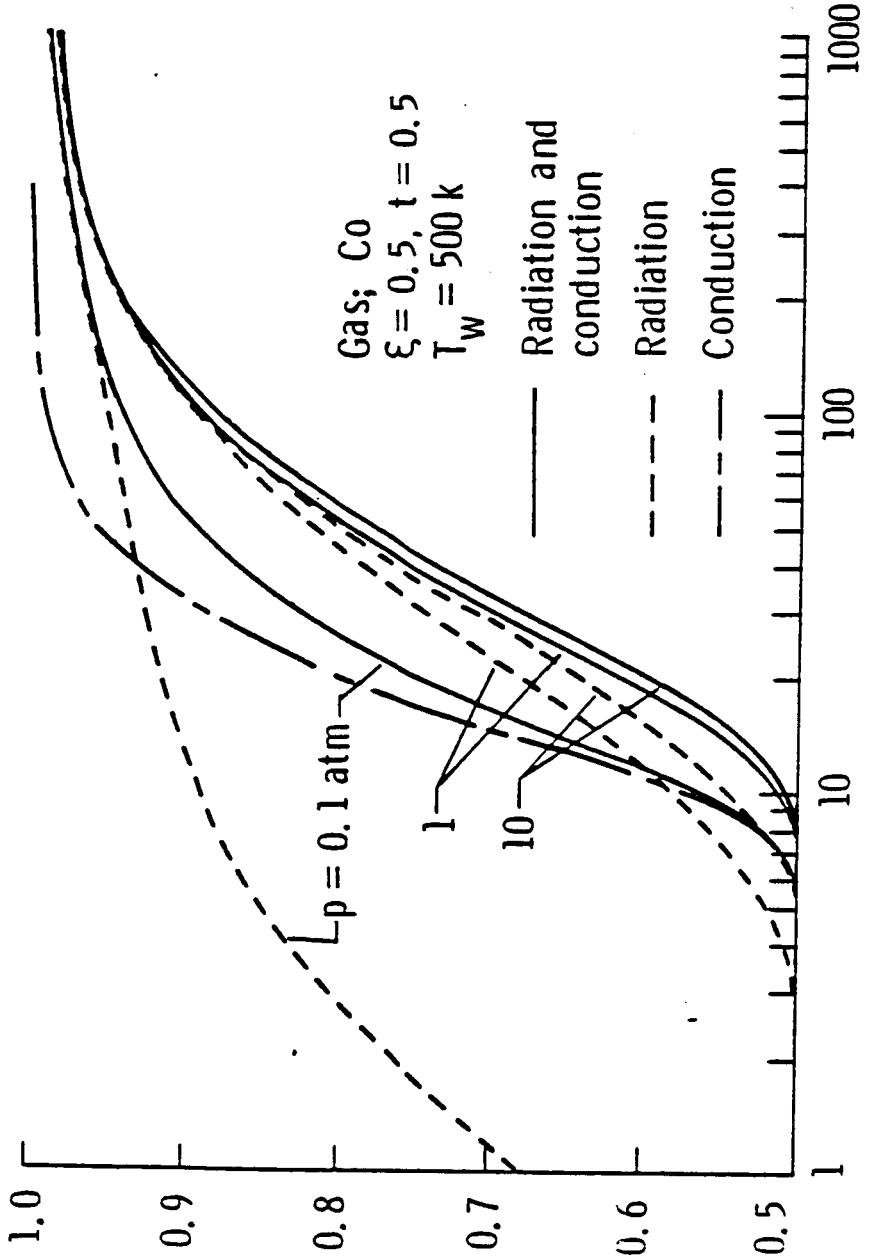

Fig. 5.12c Centerline temperature variation with L for CO (T_w = 500 K and t = 0.5).

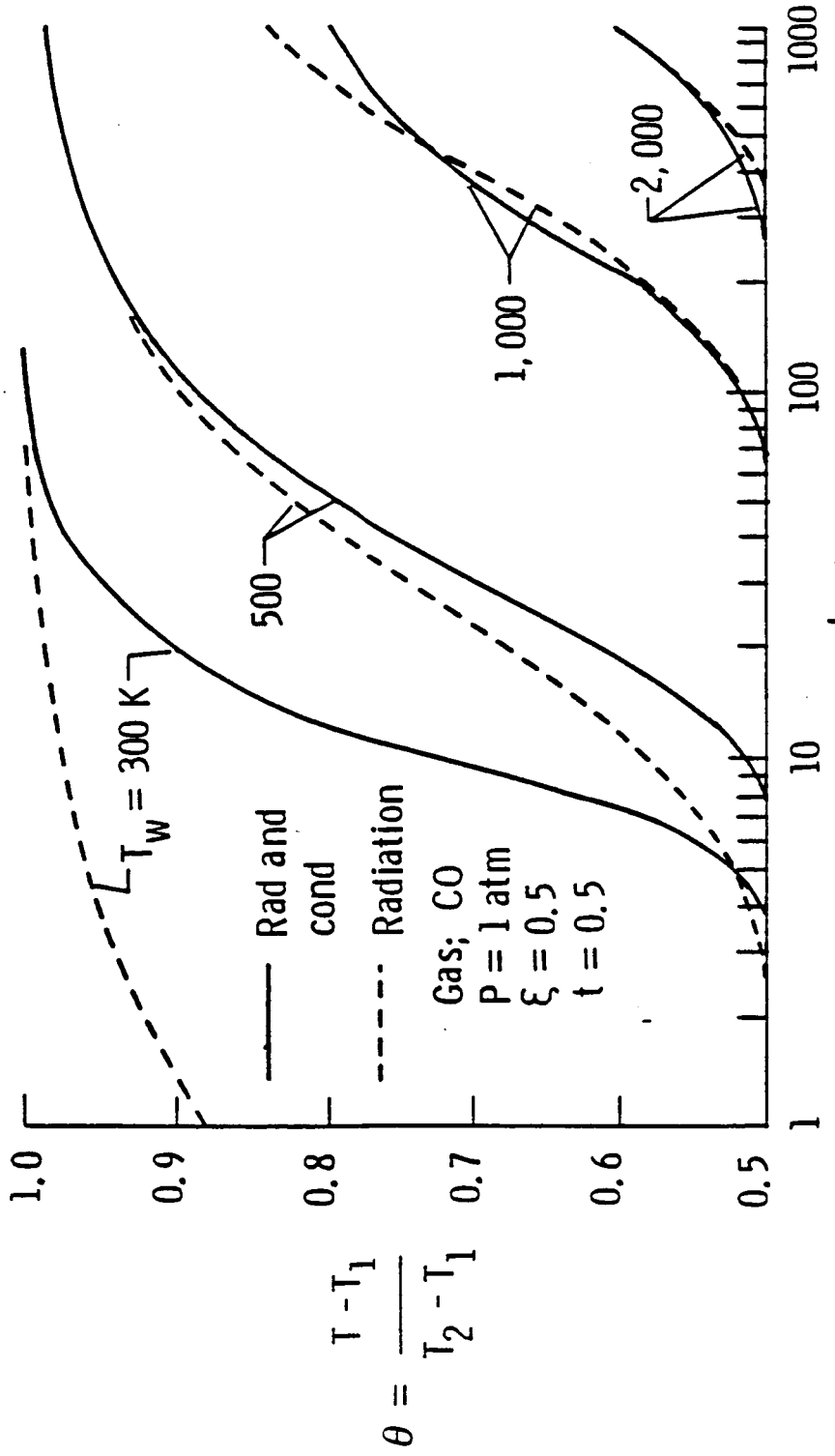

Fig. 5.12d Centerline temperature variation with L for CO (P = 1 atm and t = 0.5).

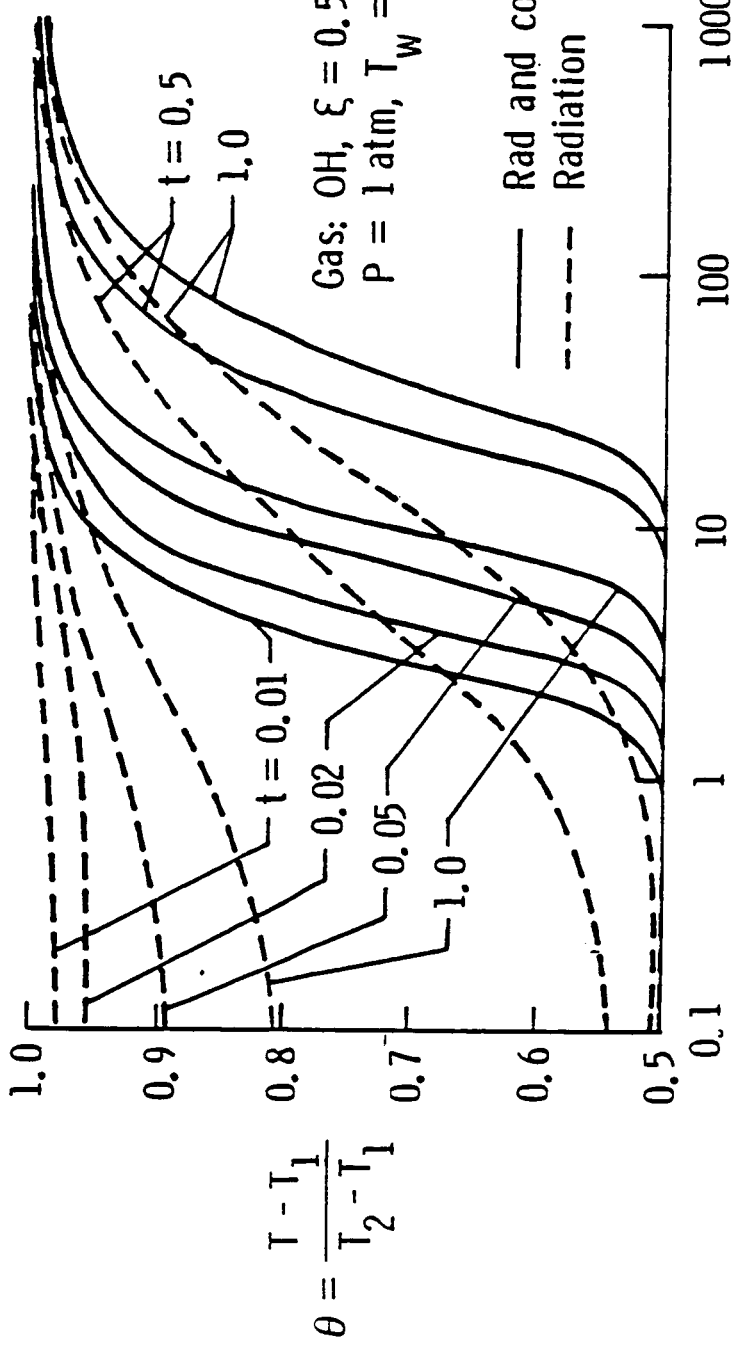

Fig. 5.13a Centerline temperature variation with L for OH (P = 1 atm and T_w = 500 K).

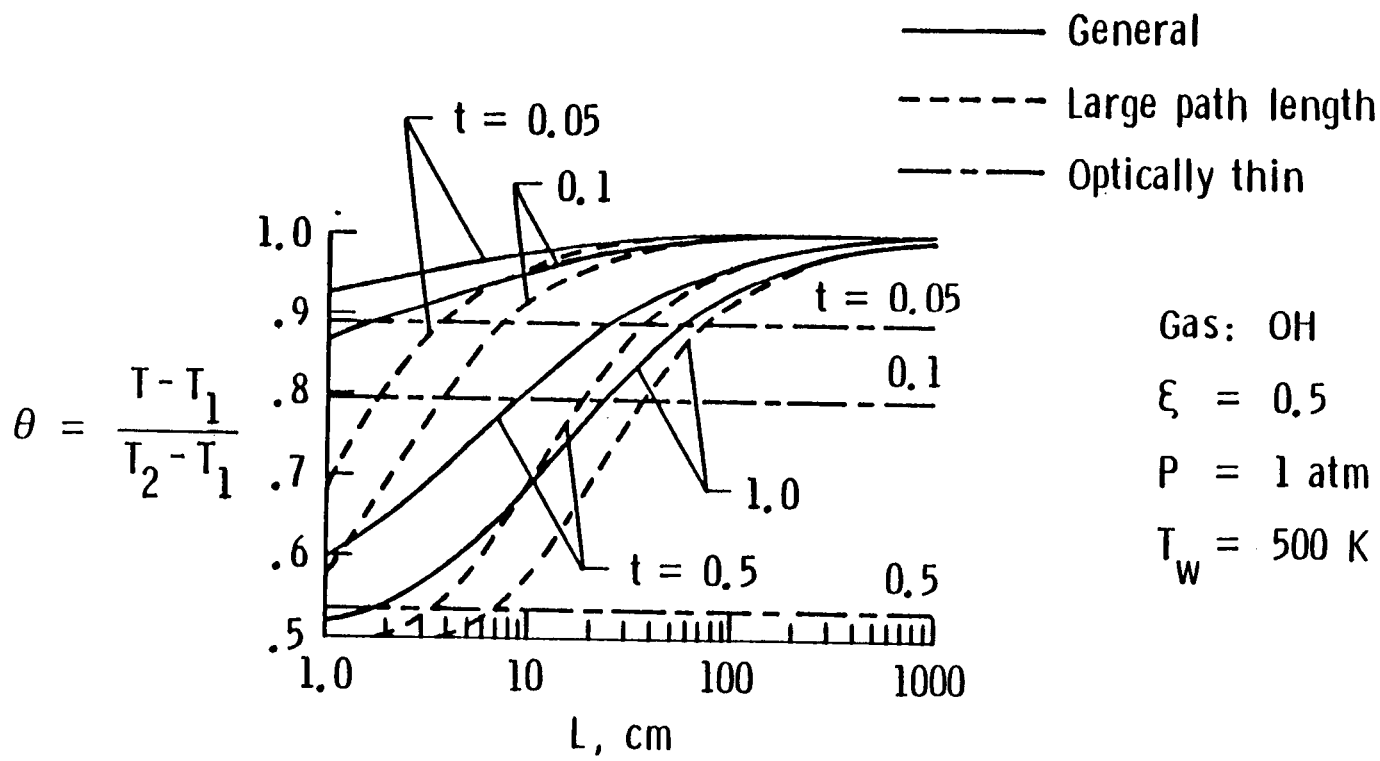

Fig. 5.13b Centerline temperature variation with L for pure radiation (OH, P = 1 atm, and T_w = 500 K).

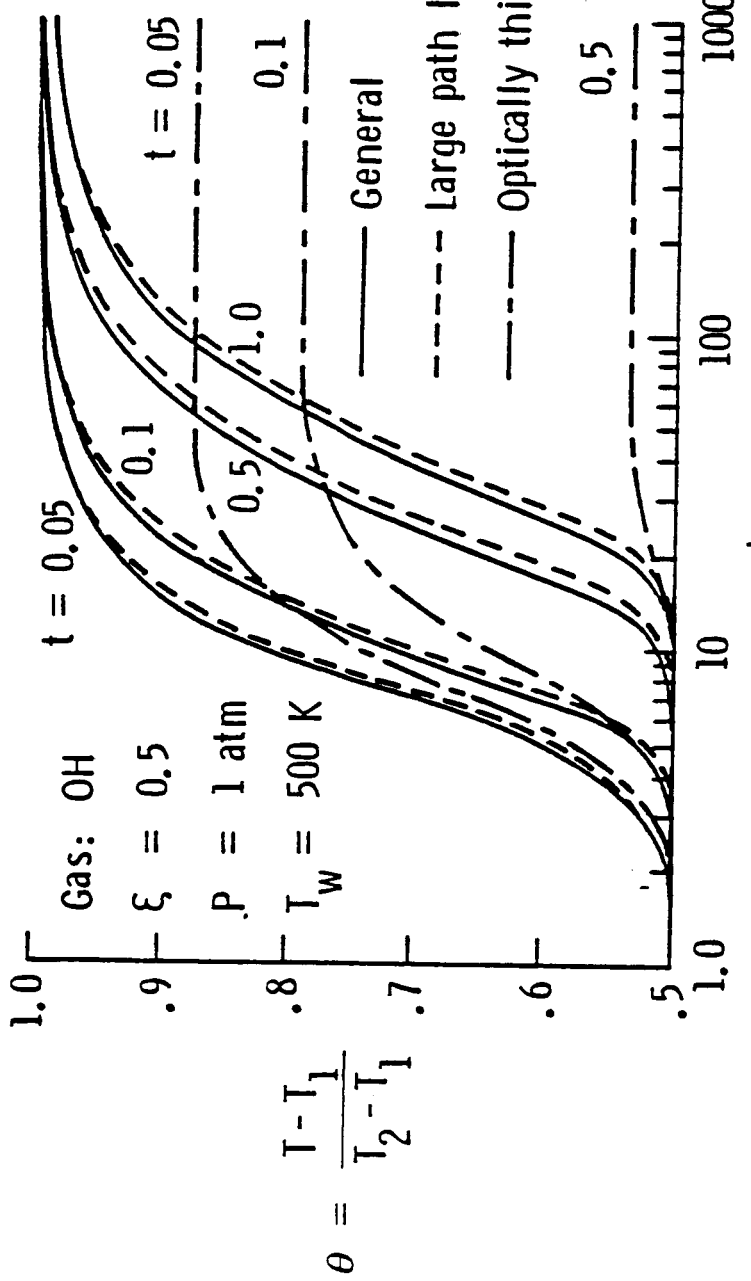

Fig. 5.13c Centerline temperature variation with L for combined radiation and conduction (OH, P = 1 atm, and T_w = 500 K).

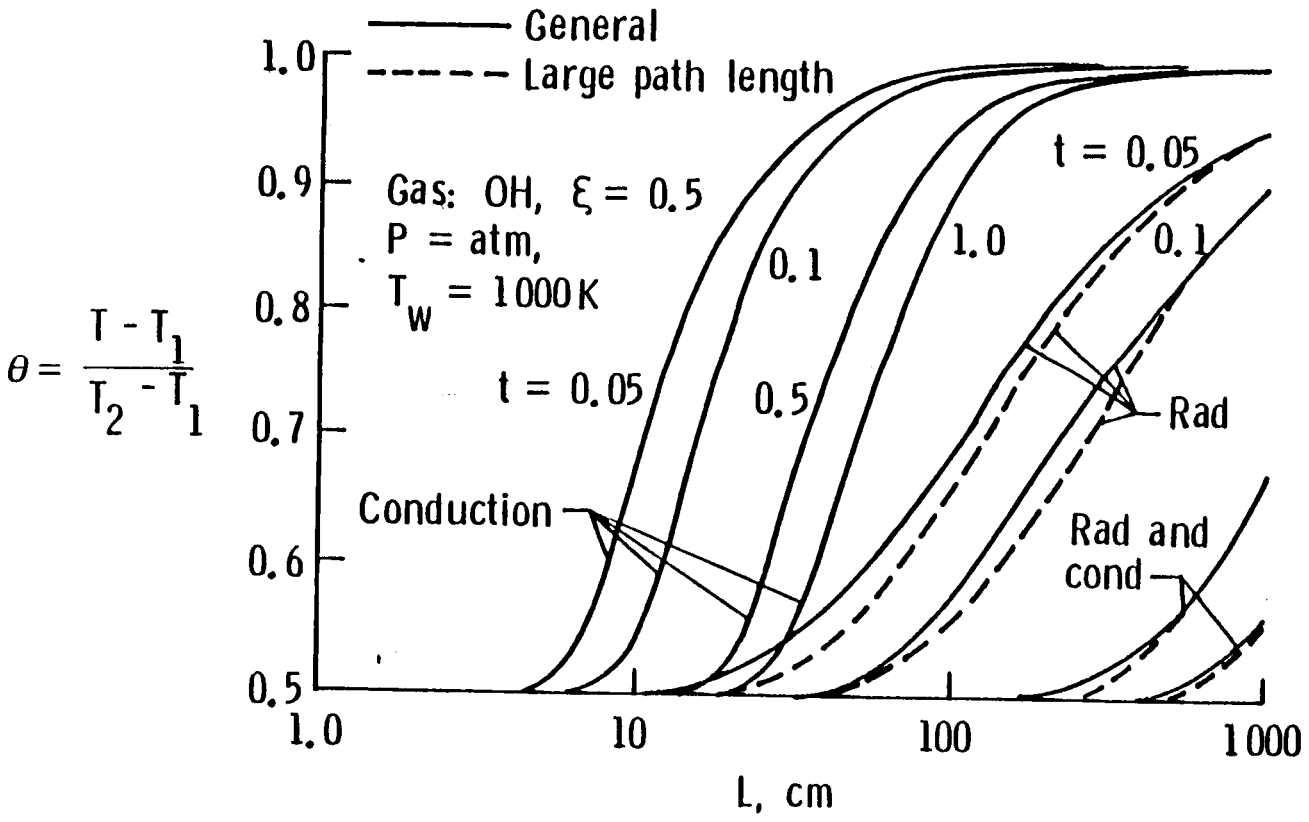

Fig. 5.13d Centerline temperature variation with L for OH (P = 1 atm, and T_w = 1000 K).

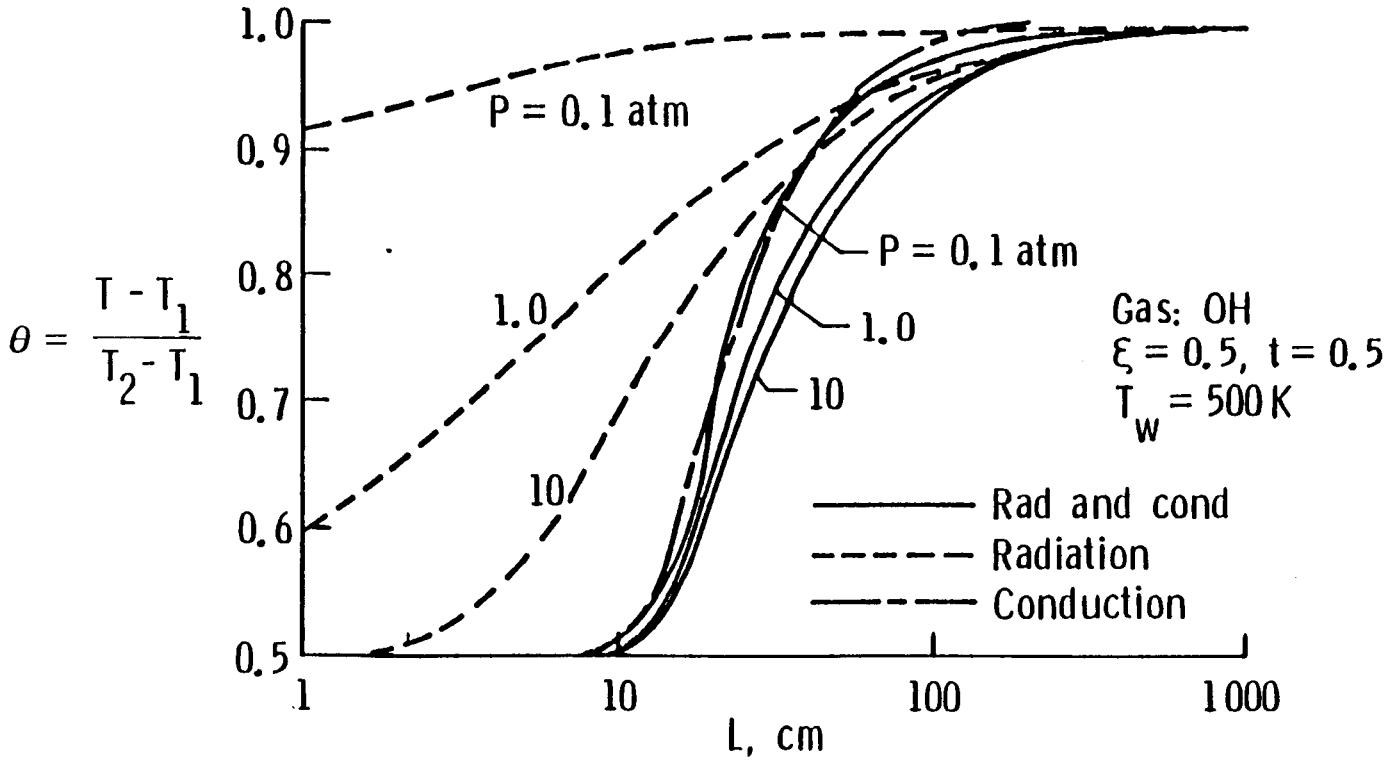

Fig. 5.13e Centerline temperature variation with L for OH at different pressures and T_w = 500 K.

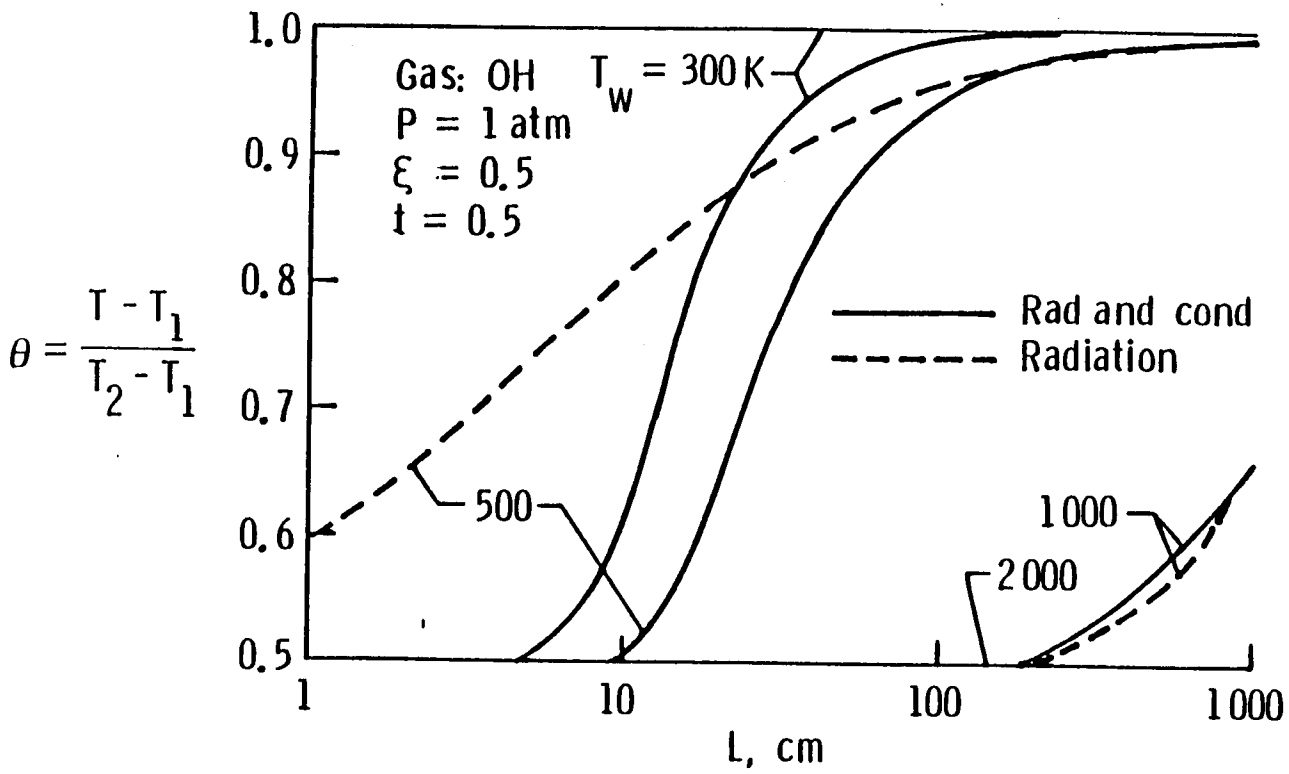

Fig. 5.13f Centerline temperature variation with L for OH at different T_w and P = 1 atm.

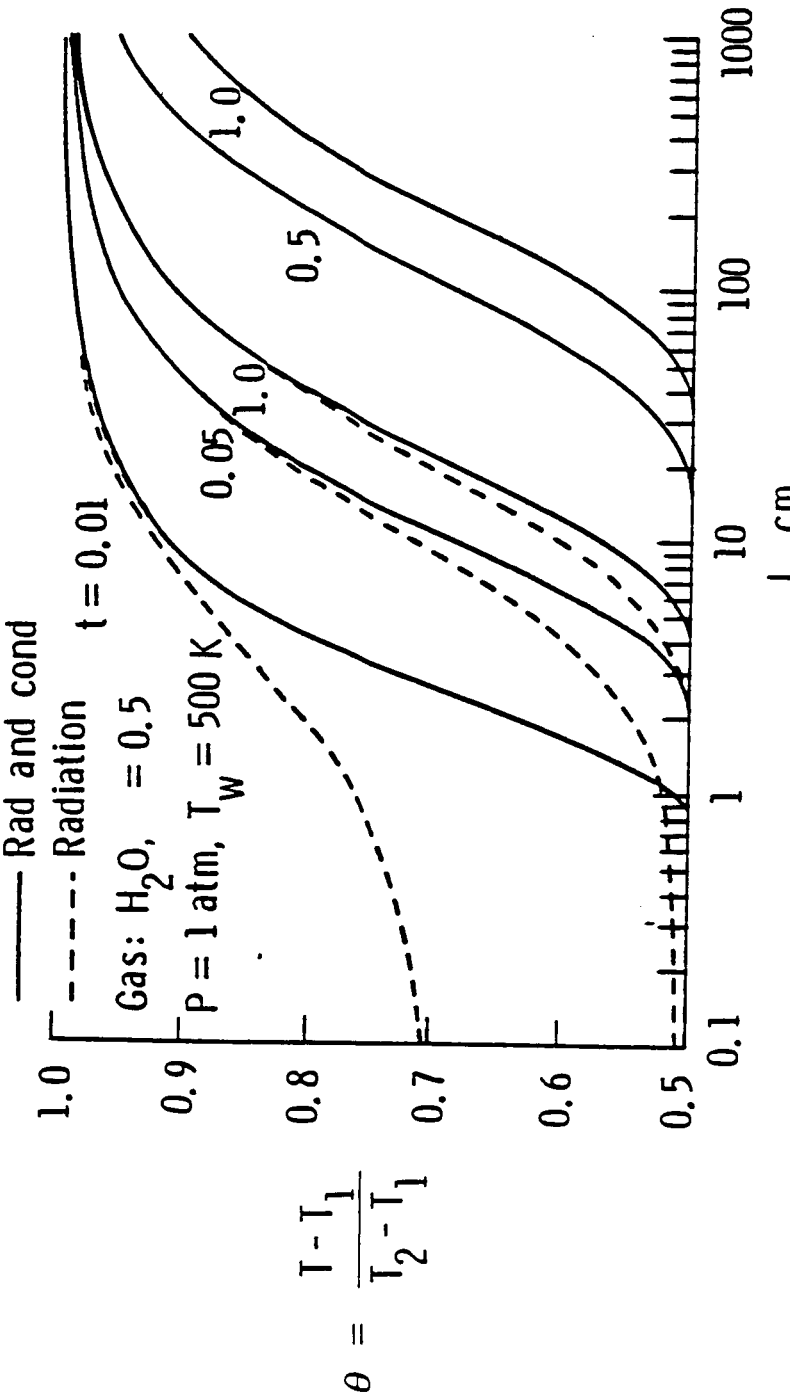

Fig. 5.14a Centerline temperature variation with L for H_2O (P = 1 atm and T_w = 500 K).

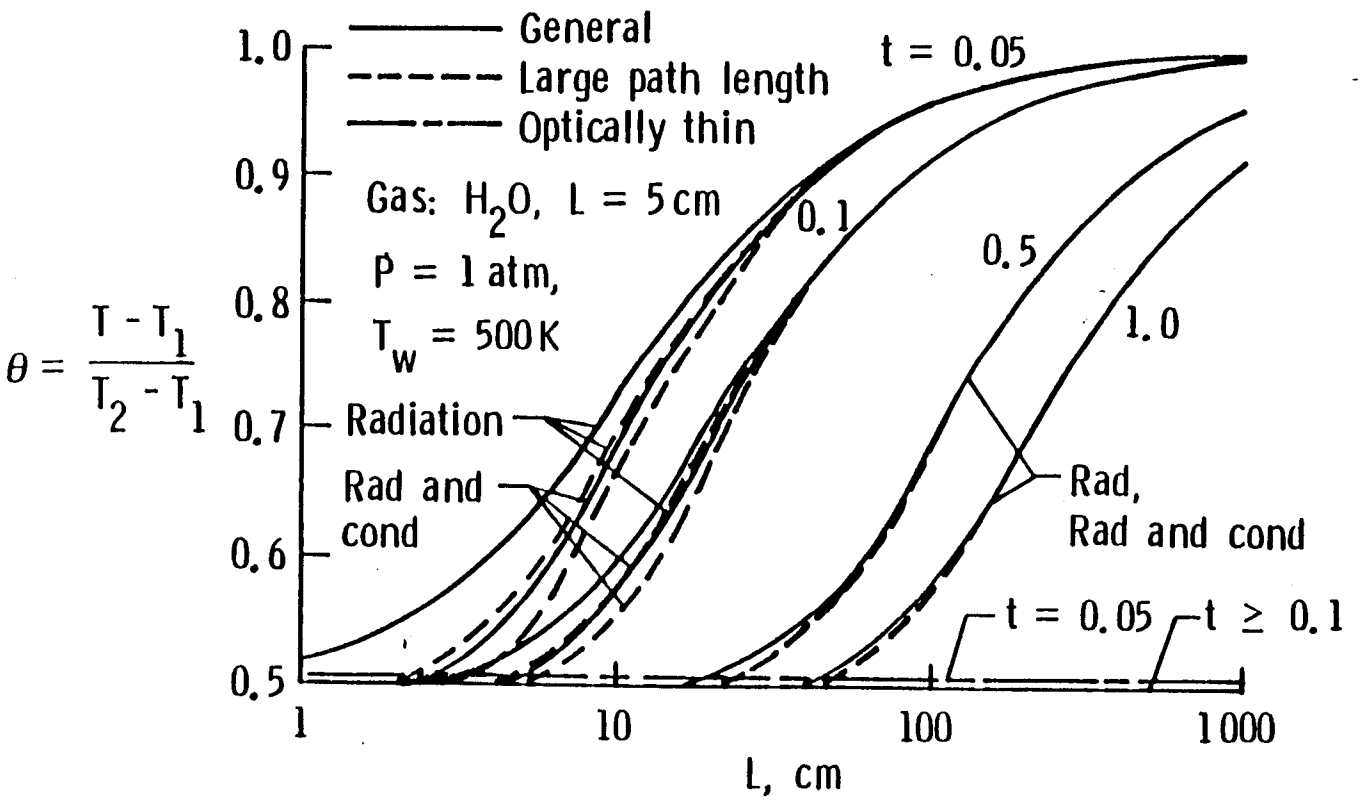

Fig. 5.14b Centerline temperature variation with L for H_2O (general and limiting solutions, P = 1 atm and T_w = 500 K).

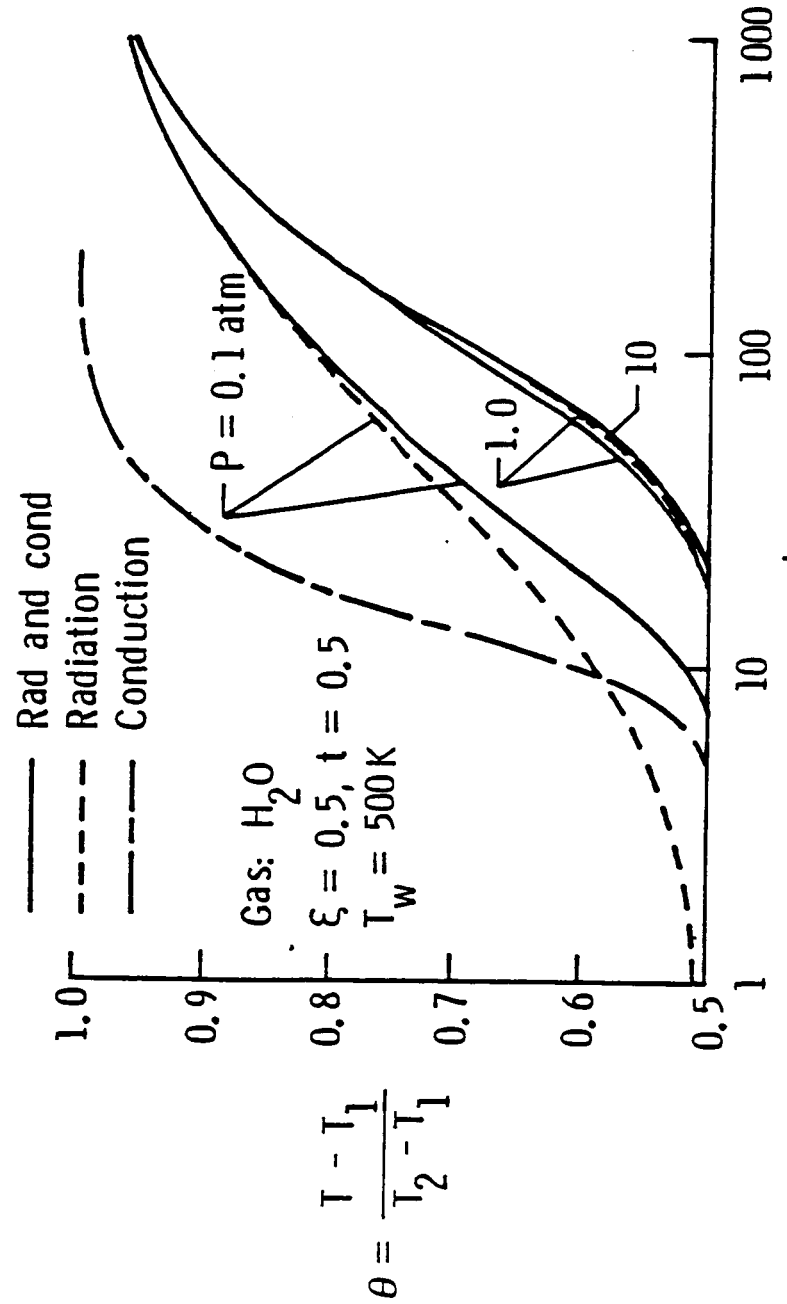

Fig 5.14c Centerline temperature variation with L for H_2O at different pressures and T_w = 500 K.

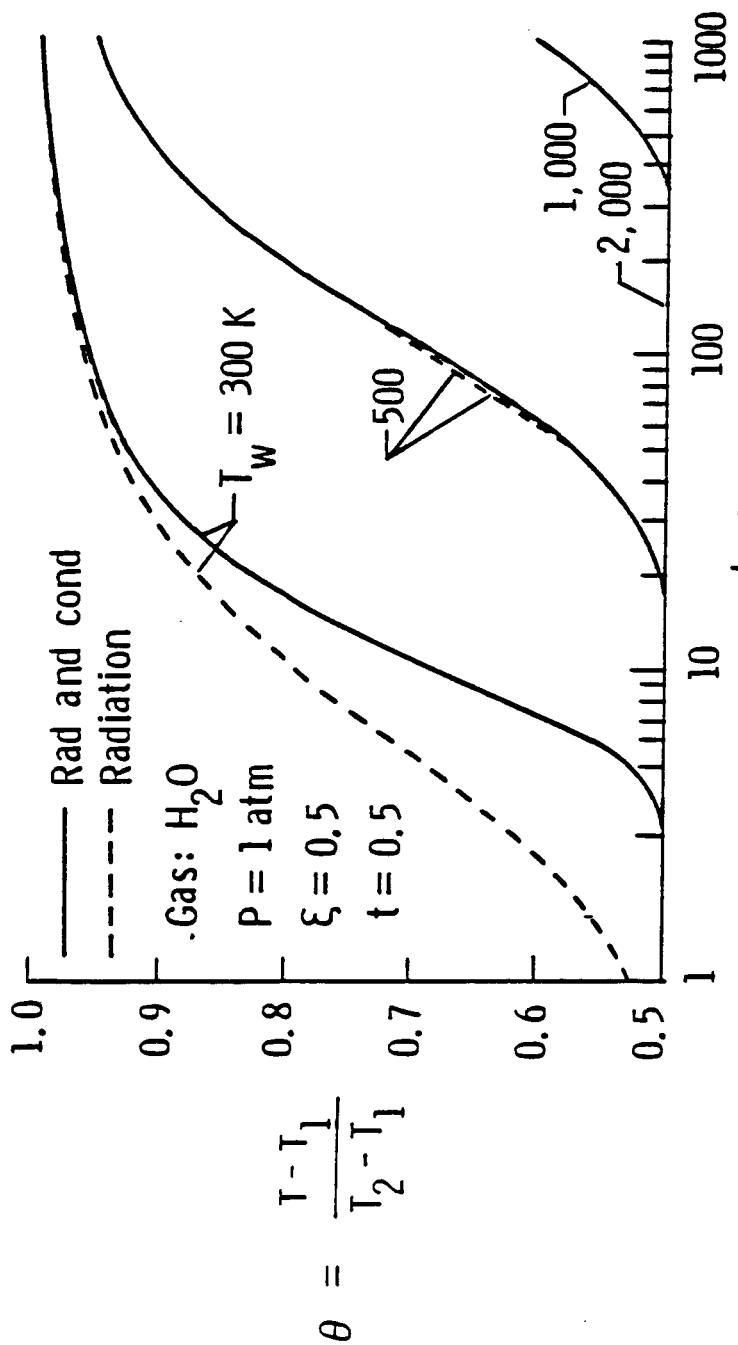

Fig. 5.14d Centerline temperature variation with L for H_2O at different T_w and P = 1 atm.

The centerline temperature variations are compared for different gases in Fig. 5.15 for P = 1 atm, T_w = 500 K, and t = 0.05. For the case of radiative equilibrium, it is noted that OH is the least effective and H_2O is the most effective gas in transferring the radiative energy for plate spacings greater than two centimeters. When molecular conduction is included, OH becomes more effective because of its relatively higher conductive ability. These points were noted also in earlier discussions. The story, however, can be entirely different for other physical conditions because of the radiative/conductive nature of participating species (Ref. 8 and Appendix C). This fact is partially evident from the steady-state results, for the case of combined radiation and conduction, presented in Fig. 5.16 for two different temperatures, T_w = 300 K and 500 K. For example, for T_w = 300 K and L = 10 cm, the temperature values for CO and CO_2 are about the same, for H_2O it is lower, and for OH it is the lowest; however, for plate spacing greater than L = 20 cm, the trend is entirely different. Also, it should be noted that the steady-state (t = 0.5) results for T_w = 500 K in Fig. 5.16 show different trend than the results for the same temperature in Fig. 5.15 for t = 0.05. Thus, in order to predict the relative ability of a gas for radiative interactions, it is very important to consider the exact physical conditions for all species. These predictions may not be applicable if physical conditions of the problem are changed.

Extensive results for the variation in heat transfer can be presented analogous to the variation of temperature for different conditions. However, this should not be necessary because the heat transfer variation follows the trend of the temperature variation in a reverse manner. If the temperature differences are higher, the rate of heat transfer will be higher and the steady-state conditions will be reached at earlier times. The results for

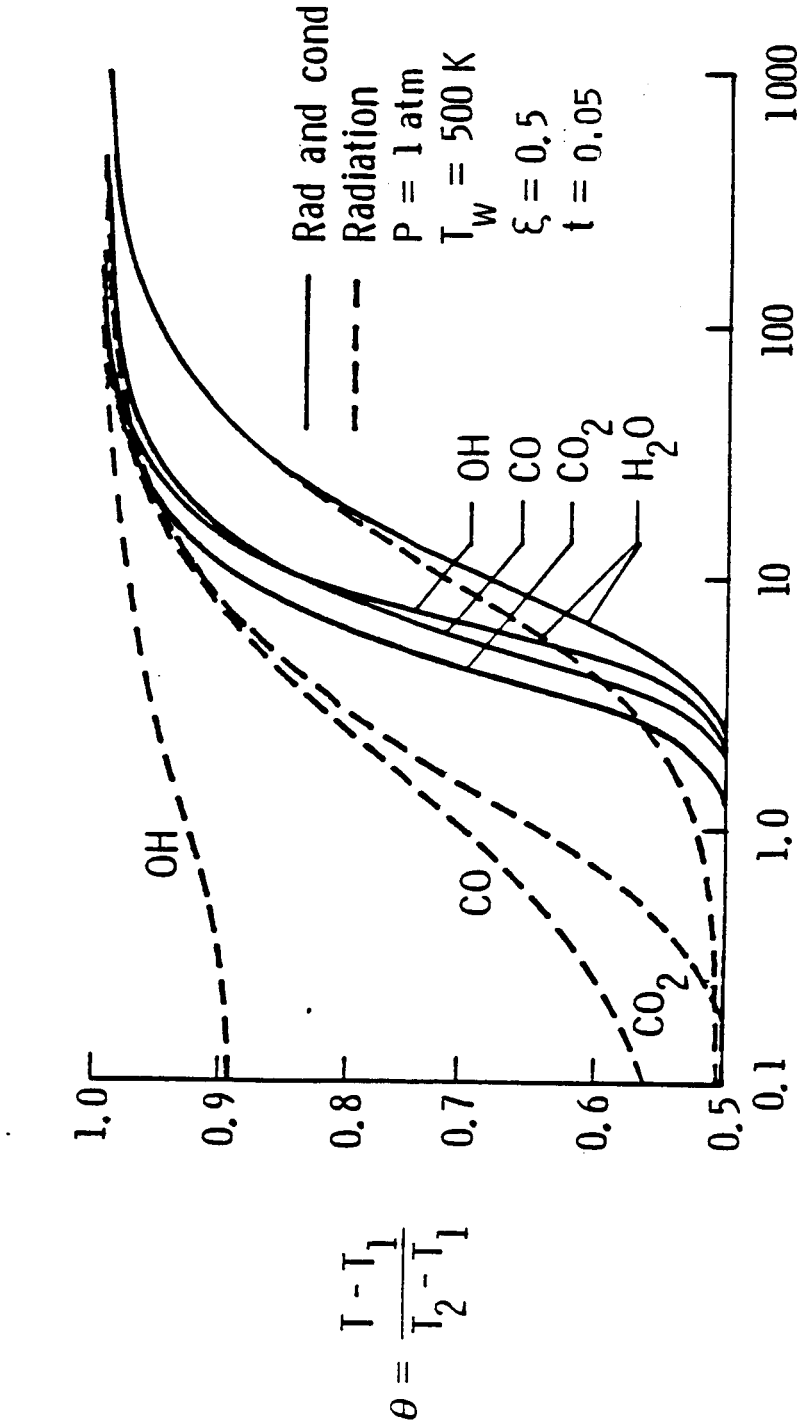

Fig 5.15 Comparison of centerline temperature variation with L for P = 1 atm, T_w = 500 K and t = 0.05.

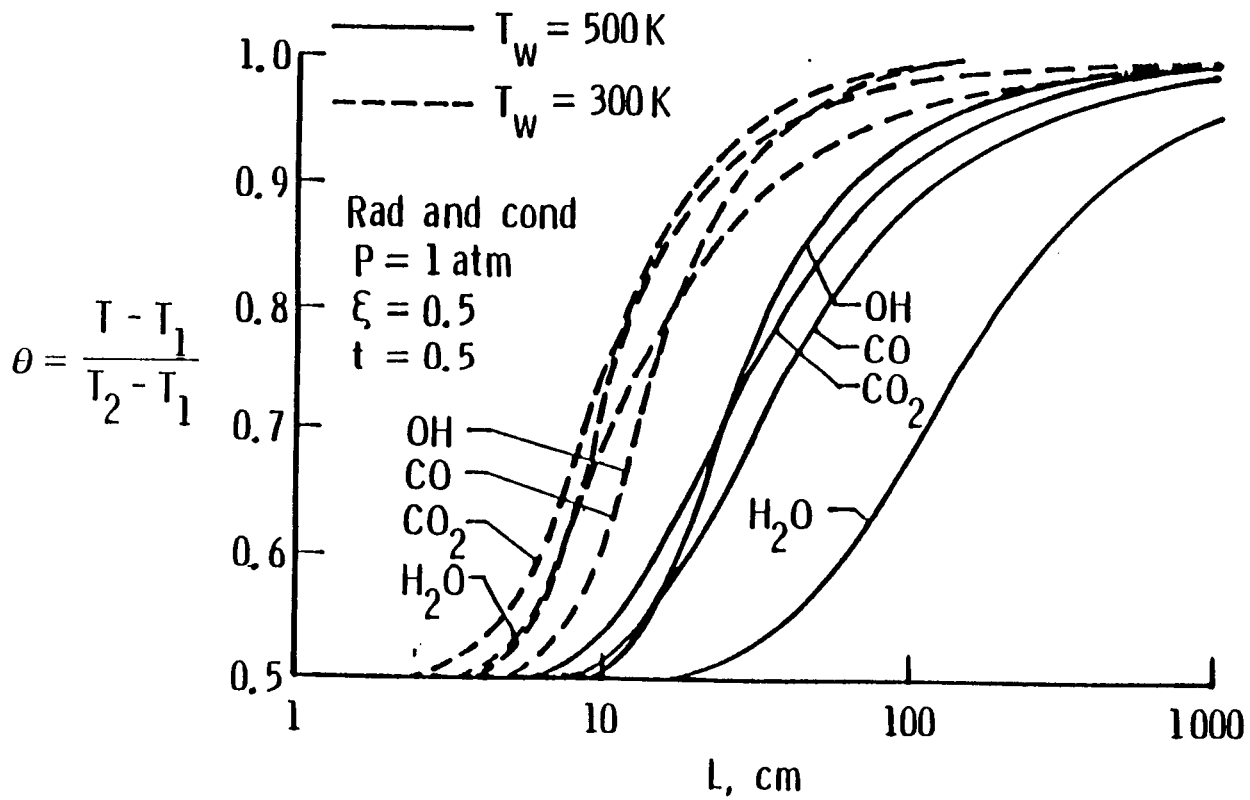

Fig 5.16 Comparison of centerline temperature variation with L for combined radiation and conduction (P = 1 atm and t = 0.5).

heat transfer variations have been obtained for selected conditions and these are discussed here briefly.

For P = 1 atm, the results for Q and $\bar{Q}$ are illustrated, as a function of t^*, in Figs. 5.17-5.20 for different species. The results for t^* = 0.0 - 1.0 are shown in Fig. 5.17a for H_2O. However, it is found that for the t_m value selected in this study, the steady-state conditions are reached in most cases at about t^* = 0.2. Consequently, other results (Figs. 5.17b, 5.17c, 5.18-5.20) are presented only in the range of t^* = 0.0 - 0.2 to demonstrate the rate of cooling at different temperatures. As would be expected, the results show that for a given plate spacing the gas layer reaches the steady-state condition faster at higher values of T_w because of stronger radiative interactions. It should be noted that the rate of energy transfer increases with time for a gas layer closer to the upper wall (ξ = 0.75) and decreases with time for a gas layer closer to the lower wall (ξ = 0.25) until the steady-state conditions are reached. The rate of cooling is entirely different if the plate spacing is changed (Fig. 5.17c). From a comparison of results of Figs. 5.17-5.20, it is noted that the trend and rate of energy transfer are different for different species. This, however, would be expected because of the relative ability of different species to participate in the radiation-conduction interaction process (Appendix C).

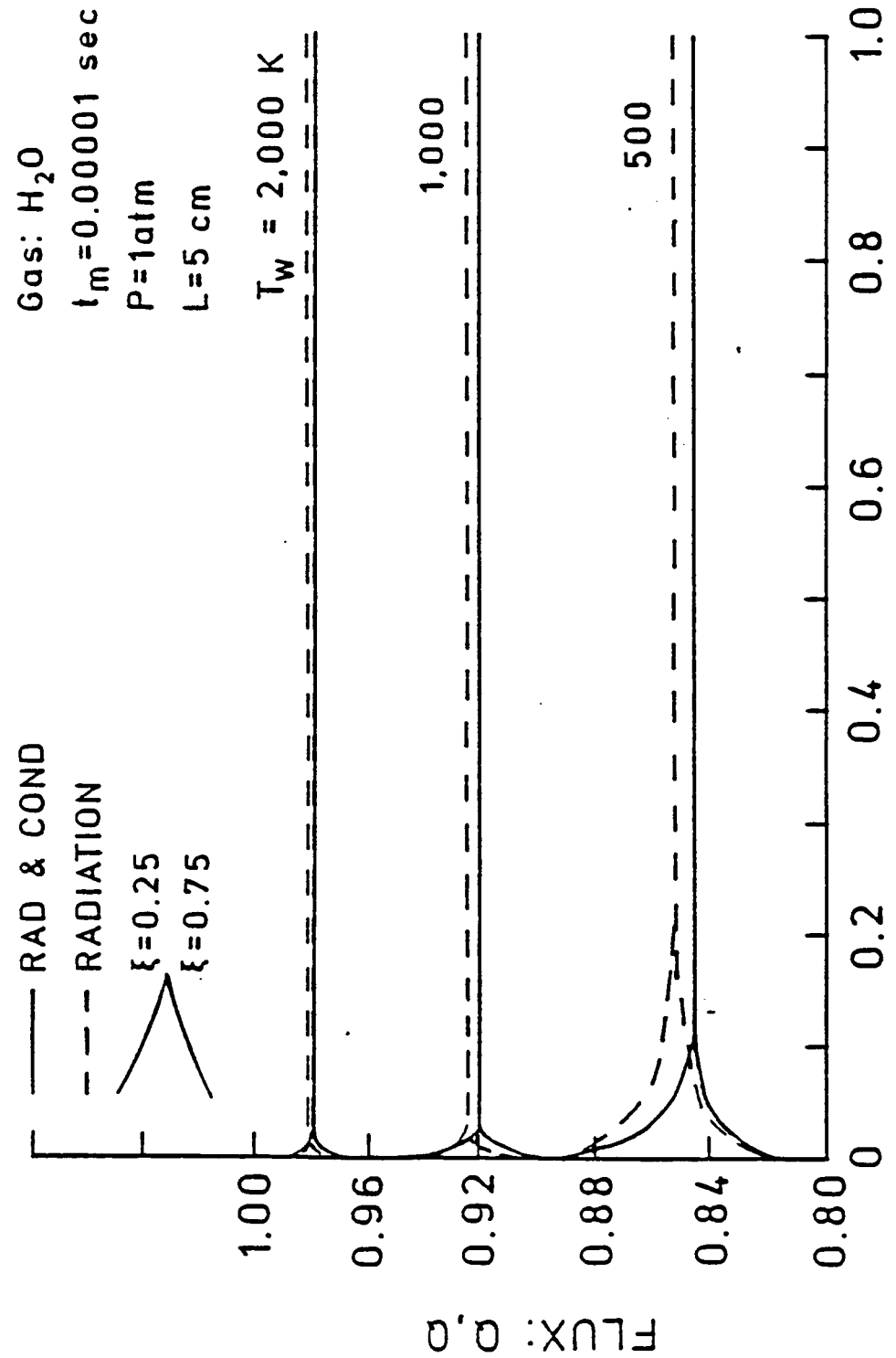

Fig. 5.17a Variation in heat flux with time for H_2O (P = 1 atm, L = 5 cm, and t^* = 0.0 - 1.0).

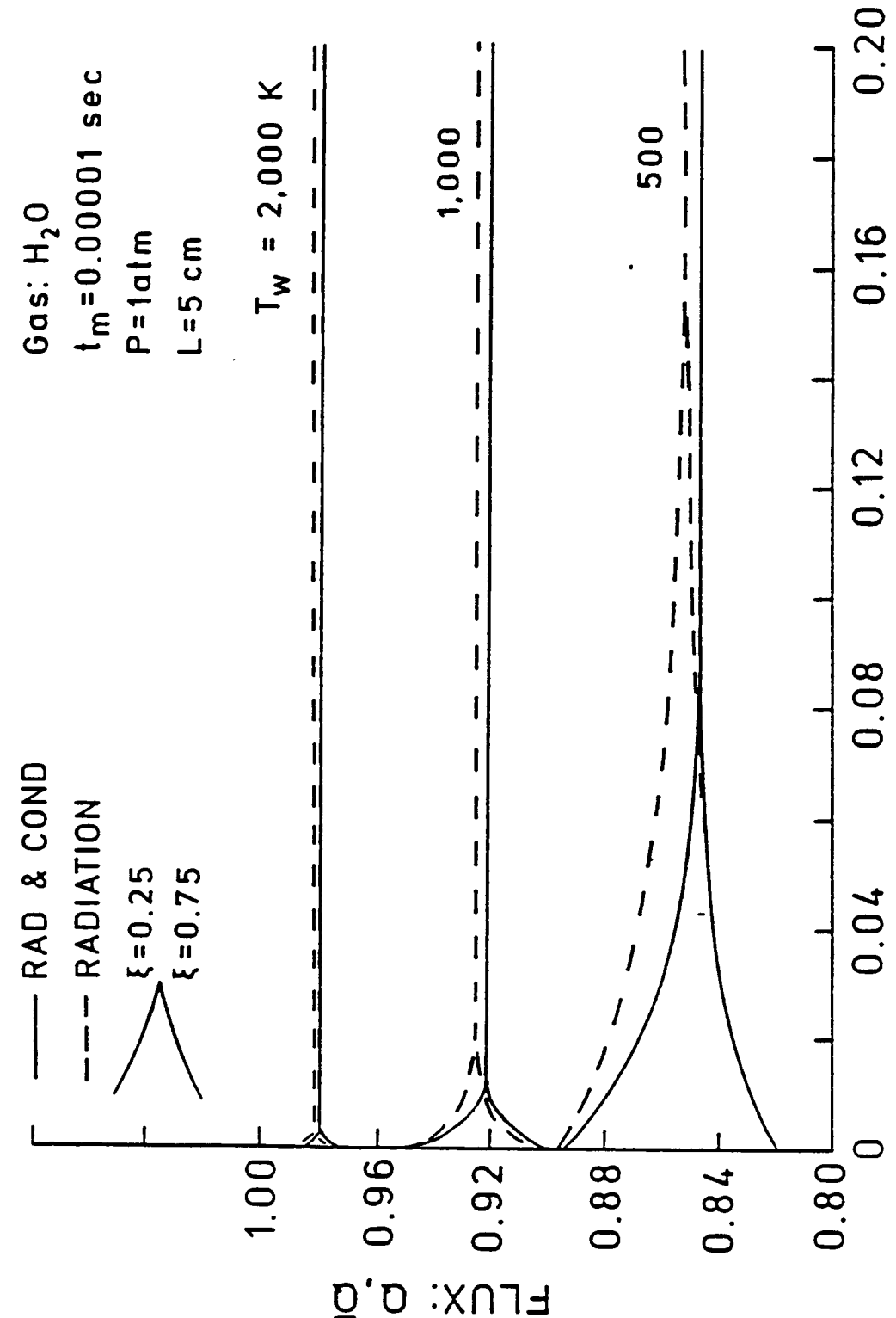

Fig 5.17b Variation in heat flux with time for H_2O (P = 1 atm, L = 5 cm, and t^* = 0.0 - 0.2).

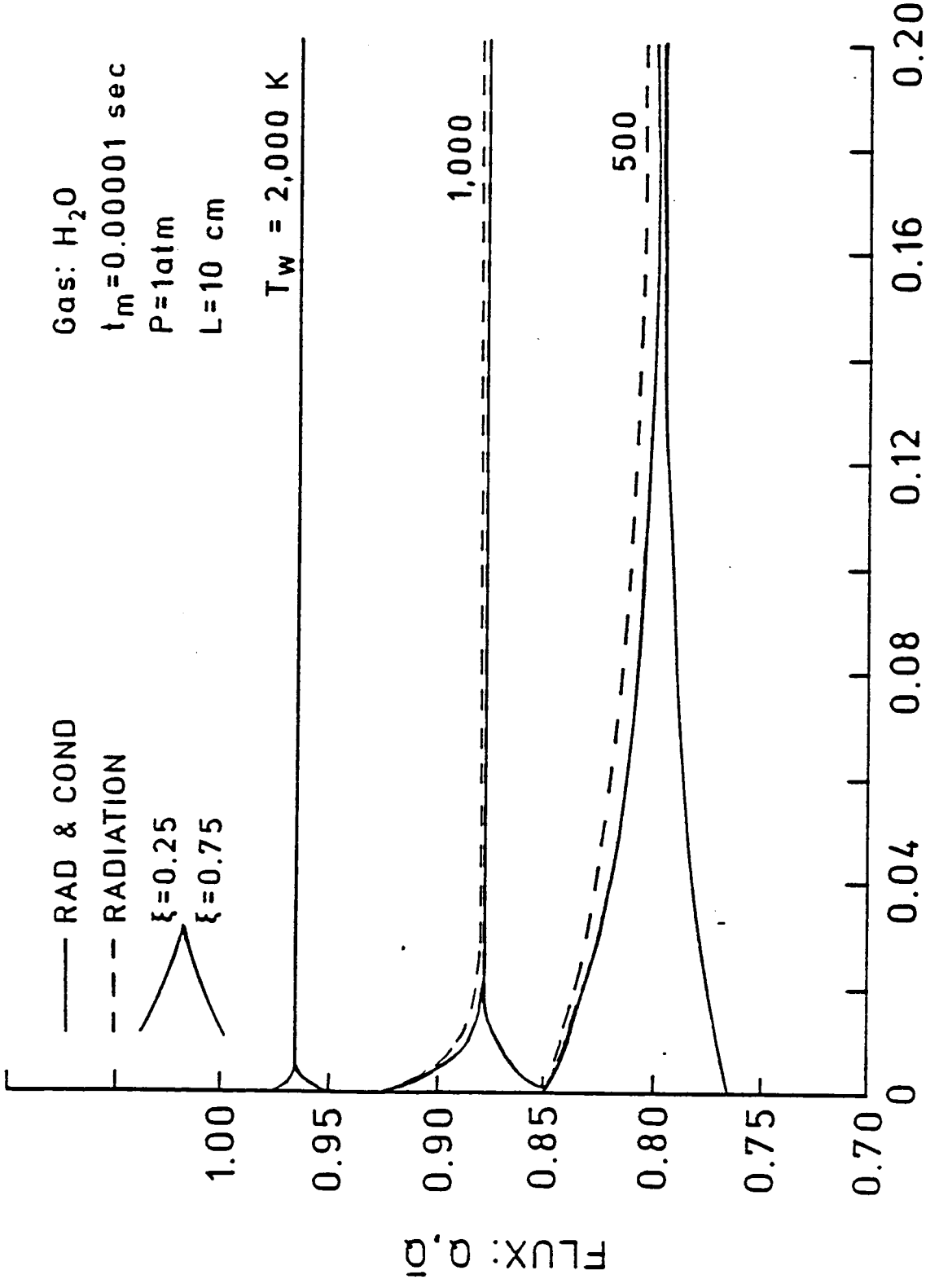

Fig. 5.17c Variation in heat flux with time for H_2O (P = 1 atm, L = 10 cm, and t* = 0.0 = 0.2).

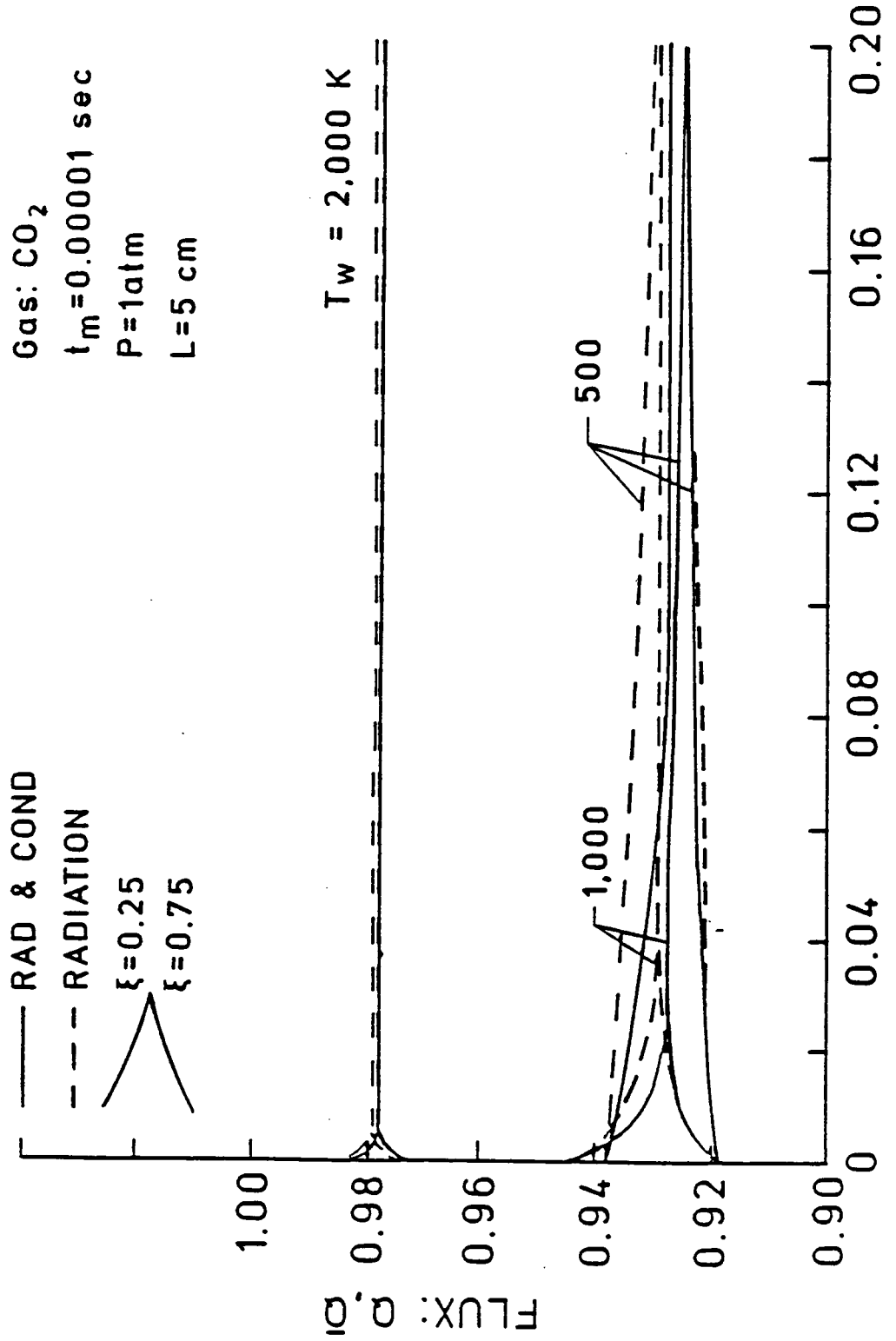

Fig 5.18 Variation in heat flux with time for CO_2 (P = 1 atm, L = 5 cm, and t* = 0.0 - 0.2).

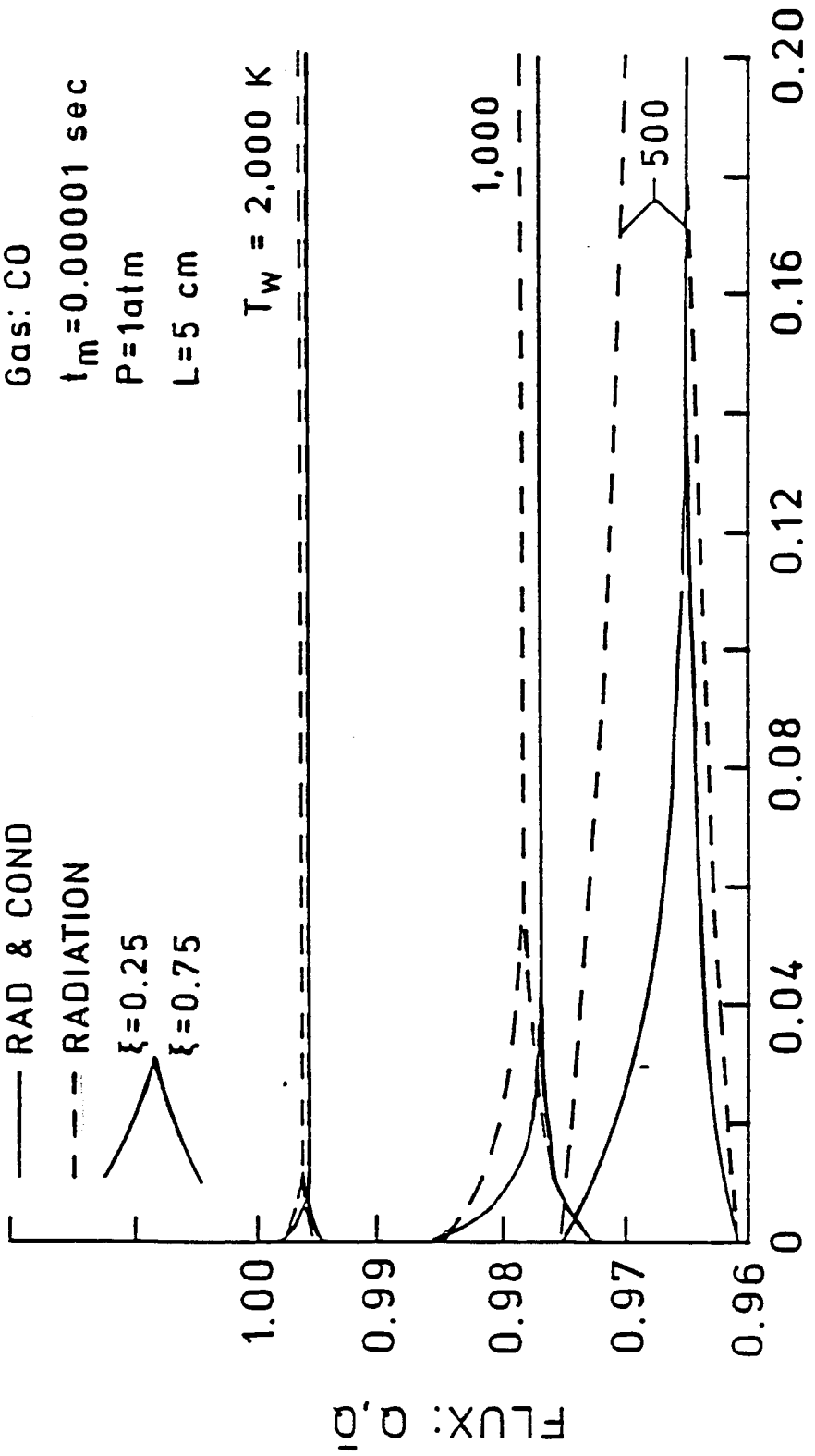

Fig. 5.19 Variation in heat flux with time for CO (P = 1 atm, L = 5 cm, and t* = 0.0 - 0.2).

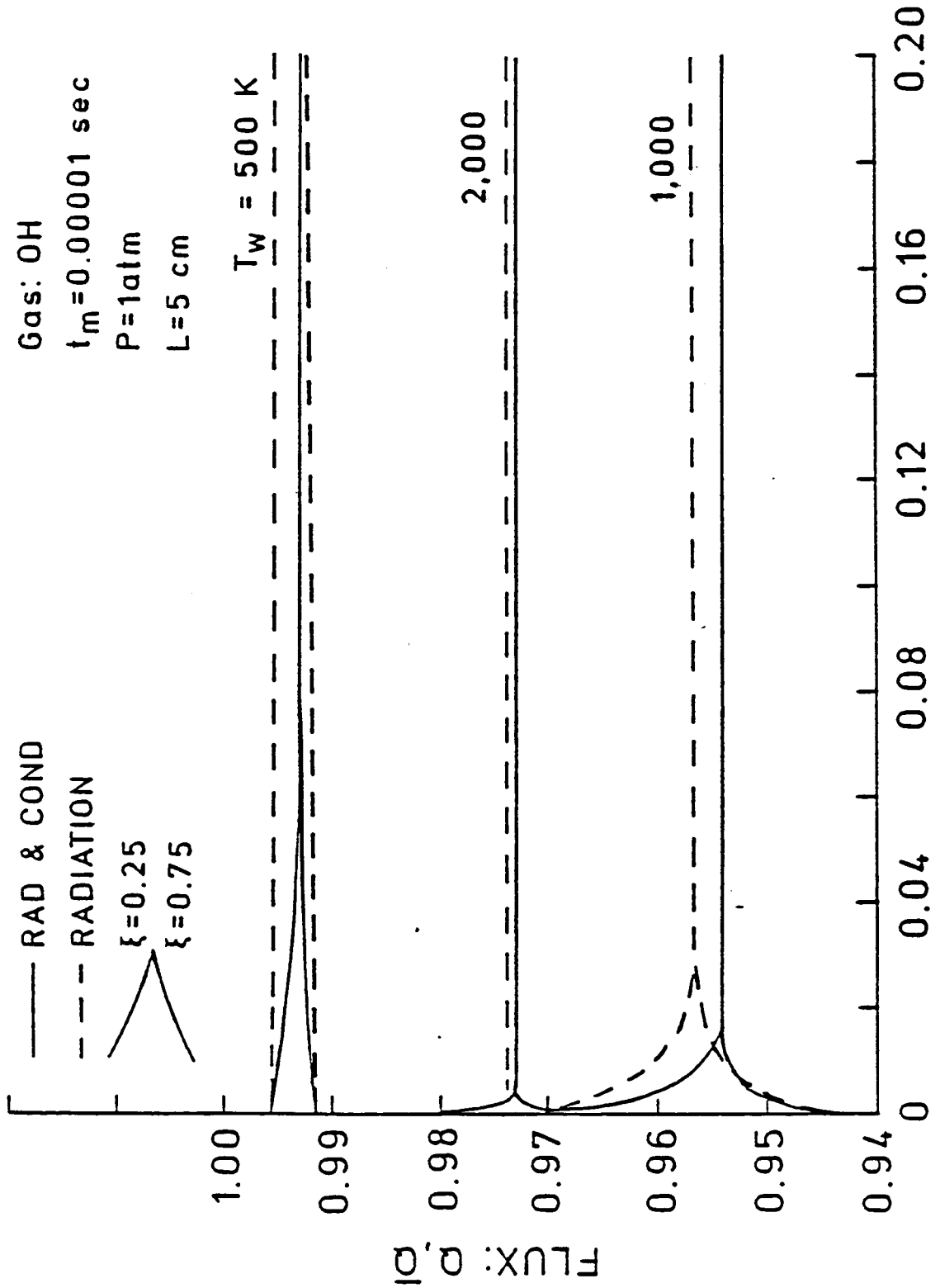

Fig. 5.20 Variation in heat flux with time for OH (P = 1 atm, L = 5 cm, and t* = 0.0 - 0.2).

6. CONCLUSIONS

The problem of transient radiative interaction in nongray absorbing-emitting species has been formulated in a general sense such that sophisticated absorption models can be used to obtain accurate results if desired. Results have been obtained for the special case of radiative interactions in a plane gas layer bounded by two parallel plates when the temperature of the bottom plate is suddenly reduced to a lower but constant temperature. The energy transfer by pure radiation, and by simultaneous radiation and conduction were considered and specific results have been obtained for CO, CO_2, H_2O, and OH by employing the Tien an Lowder's correlation for band absorption. It is noted that the extent of radiative interaction is dependent on the nature of the participating species and parameters T_1, T_2/T_1, P, L, and t_m. The steady-state conditions are reached at relatively longer times for radiative equilibrium than for radiation with conduction. For a particular value of P and T_1, the time required to reach the steady-state condition increases with increasing plate spacing. For a fixed plate spacing, the energy is transferred quickly for higher T_1 values because of large temperature differences between the plates. The rate of radiative interaction increases with increasing pressure until the large path length limit is reached. The radiative equilibrium solutions are found to be independent of the plate spacing in the optically thin limit. In the case of simultaneous radiation and conduction, both optically thin and large path length solutions depend on the y-location between the plates. At moderate temperatures, OH is a poor radiating but better heat conducting gas. For most conditions, H_2O is found to be highly radiation participating species, and the steady-state conditions are reached quickly for H_2O than for other species. The information on radiative interactions for OH and H_2O is useful in the analysis of the flow field in the scramjet engine.

REFERENCES

1. Sparrow, E. M. and Cess, R. D., Radiation Heat Transfer, Brooks/Cole, Belmont, Calif., 1966 and 1970. New Augmented Edition, Hemisphere Publishing Corp., Washington, D.C., 1978.

2. Hottel, H. C. and Sarofim, A. F., Radiative Transfer, McGraw-Hill Book Co., New York, 1967.

3. Siegel, R. and Howell, J. R., Thermal Radiation Heat Transfer, McGraw-Hill Book Co., New York, 1971; Second Edition, 1981.

4. Cess, R. D., "The Interaction of Thermal Radiation with Conduction and Convection Heat Transfer," Advances in Heat Transfer, Vol. 3, Academic Press, New York, 1966.

5. Sparrow, E. M., "Radiation Heat Transfer between Surfaces," Advances in Heat Transfer, Vol. 2, Academic Press, New York, 1965.

6. Viskanta, R., "Radiation Transfer and Interaction of Convection with Radiatin Heat Transfer," Advances in Heat Transfer, Vol. 3, Academic Press, New York, 1966.

7. Tien, C. L., "Thermal Radiation Properties of Gases," Advances in Heat Transfer, Vol. 5, Academic Press, New York, 1968.

8. Cess, R. D. and Tiwari, S. N., "Infrared Radiative Energy Transfer in Gases," Advances in Heat Transfer, Vol. 8, Academic Press, New York, 1972.

9. Edwards, D. K., "Molecular Gas Band Radiation," Advances in Heat Transfer, Vol. 12, Academic Press, New York, 1976; also, Radiation Heat Transfer Notes, Hemisphere Publishing Corporation, Washington, D.C., 1981.

10. Tiwari, S. N. "Band Models and Correlations for Infrared Radiation," Radiative Transfer and Thermal Control (Progress in Astronautics and Aeronautics), Vol. 49, American Institute of Aeronautics and Astronautics, New York, 1976.

11. Tiwari, S. N., "Models for Infrared Atmospheric Radiation," Advances in Geophysics, Vol. 20, Academic Press, New York, 1978.

12. Lick, W., "Transient Energy Transfer by Radiation and Conduction," International Journal of Heat and Mass Transfer, Vol. 8, 1965, pp. 119-127.

13. Chang, Y. P. and Kang, C. S., "Transient and Steady Heat Transfer in a Conducting and Radiating Medium," AIAA Journal, Vol. 8, No. 4, April 1970, pp. 609-614.

14. Chang, Y. P. and Smith, R. C., Jr., "Steady and Transient Heat Transfer by Radiative and Conduction in a Medium Bounded by Two Coaxial Cylindrical Surfaces," International Journal of Heat and Mass Transfer, Vol. 13, 1970, pp. 69-80.

15. Doornink, D. G. and Hering, R. G., "Transient Radiative Heat Transfer in a Nongray Medium," Journal of the Quantitative Spectroscopy and Radiative Transfer, Vol. 12, 1972, pp. 1161-1174.

16. Larson, D. W. and Vikanta, R., "Transient Combined Laminar Free Convection and Radiation in a Rectangular Enclosure," Journal of Fluid Mechanics, Vol. 78, Part 1, 1976, pp. 65-85.

17. Melnikov, V. I. and Sukhovich, E. P., "Transient Heat Exchange Between a Radiating Plate and a High-Temperature Gas Flow," Heat Transfer-Soviet Research, Vol. 10, No. 3, May-June 1978, pp. 11-20 (Translation).

18. Heinisch, R. P. and Viskanta, R., "Transient Combined Conduction-Radiation in an Optically Thick Semi-Infinite Medium, AIAA Journal, Vol. 6, 1968, pp. 1409-1411.

19. Hazzah, A. S. and Beck, J. V., "Unsteady Combined Conduction-Radiation Energy Transfer Using a Rigorous Differential Method," International Journal of Heat and Mass Transfer, Vol. 13, March 1970, pp. 517-522.

20. Lii, C. C. and Özisik , M. N., "Transient Radiation and Conduction in an Absorbing, Emitting and Scattering Slab with Reflecting Boundaries," International Journal of Heat and Mass Transfer, Vol. 15, May 1972, pp. 1175-1179.

21. Weston, K. C. and Hauth, J. L., "Unsteady, Combined Radiation and Conduction in an Absorbing, Scattering and Emitting Medium," Journal of Heat Transfer, Vol. 95, August 1973, pp. 357-364.

22. Sutton, W. H., "A Short Time Solution for Coupled Conduction and Radiation in a Participating Slab Geometry," ASME Paper No. 84-HT-34, 1984.

23. Tiwari, S. N., "Radiative Interactions in Transient Energy Transfer in Gaseous Systems," Progress Report NAG-1-423, Dept. of Mechanical Engineering and Mechanics, Old Dominion University, Norfolk, VA, December 1985.

24. Herzberg, G., Molecular Spectra and Molecular Structure, D. van Nostrand Company, Inc., 1950.

25. Goulard, R. and Thomson, J. A. L. (Editors), Handbook of Infrared Radiation from Combustion Gases, NASA SP-3090, 1973.

26. Svehla, R. A., "Estimated Viscosity and Thermal Conductivities of Gases at High Temperature," NASA TR-132, 1962.

27. Tsederberg, N. V., Thermal Conductivity of Gases and Liquids, M.I.T. Press, Cambridge, Mass., 1965.

28. Van Wylen, G. J. and Sonntag, R. E., Fundamentals of Classical Thermodynamics, John Wiley and Sons, 1978.

APPENDIX A

SPECTRAL INFORMATION AND CORRELATION QUANTITIES FOR IMPORTANT INFRARED BANDS

Spectral information and correlation quantities for important infrared bands are available in [7-9]. The exponential band model correlation quantities for important bands of CO, CO_2, H_2O, and CH_4 are given in Table A.1. For some species, revised data are now available in [9].

In developing correlation quantities for different bands, it is important to have information on the integrated band intensity $S(T_0)$ and the band width parameter $A_0(T)$. The band intensities of many molecular bands are available in the literature [7-9, 24, 25] but this is not the case with the band width parameter. Different relations for $A_0(T)$ are proposed by Edwards et al. in references cited in [9]. From a critical evaluation of different relations available in the literature for $A_0(T)$ and after personal communications with Dr. D.K. Edwards, it was decided to adopt the following two relations:

$$A_0(T) = \frac{1}{2}\,\Gamma^2\,\left(\frac{3}{4}\right)\,\left(\frac{4kTB}{hc}\right)^{1/2} \qquad (A.1)$$

$$A_0(T) = 0.9\,\Gamma^2\,\left(\frac{3}{4}\right)\,\left(\frac{2kTB}{hc}\right)^{1/2} \qquad (A.2)$$

where B is the rotational constant of lower level, c is the speed of light, h is the Planck's constant and k is the Boltzmann's constant. The value of B is different for different molecules. Equations (A.1) and (A.2) are

essentially the same except Eq. (A.1) will result in a coefficient of 0.707 instead of 0.9. It is suggested to use Eq. (A.2) in determining approximate relations for $A_o(T)$ for all molecules whose values are not available in the literature. Information on the rotational constants for different molecules is available in the literature (for example, see Ref. 24). It is suggested to use the equivalent value for the rotational constant of polyatomic molecules.

It should be noted that in Eqs. (A.1) and (A.2), B, c, h, and k are constants and do not depend on the temperature. Thus, Eq. (A.2) may be expressed as:

$$A_o(T) = \text{CONST } (T)^{1/2} \tag{A.3a}$$

where

$$\text{CONST} = 0.9\, \Gamma^2 \left(\frac{3}{4}\right) \left(\frac{2kB_e}{hc}\right)^{1/2} \tag{A.3b}$$

and B_e represents the equivalent rotational constant. By evaluating Eq. (A.3a) at a reference temperature T_{ref}, the value of $A_o(T_{ref})$ can be determined and, therefore, Eq. (A.3a) may be expressed alternately as:

$$A_o(T) = A_o(T_{ref})\ (T/T_{ref})1/2. \tag{A.4}$$

Equation (A.4) is a convenient form to compare its results with experimental values.

By noting that $\Gamma^2 \left(\frac{3}{4}\right) = [\Gamma\ (3/4)]^2$ and substituting values for c, h, and k, Eq. (A.3) can be expressed as:

$$A_o(T) = 1.59313\ (B_eT)^{1/2} \tag{A.5}$$

where A_o and B_e have units of cm^{-1} and T is in degrees Kelvin. For a particular gas, $A_o\ (T_{ref})$ can be obtained from Eq. (A.5) and then Eq. (A.4) can be used to determine $A_o(T)$ at other temperatures. For example, for CO the rotational constant is 1.931 cm^{-1} and at a reference temperature of 300 K, $A_o(T_{ref} = 300\ K) = 38.344\ cm^{-1}$. This compares very well with the experimental value of 38.1 given if Refs. 7 and 9 and presented in Table A.1. Similarly, for the 4.3 μ band of CO_2, the equivalent rotational constant is 0.3906 cm^{-1} and, therefore, $A_o(T_{ref} = 300\ K) = 17.246\ cm^{-1}$; the experimental value of 19.9 cm^{-1} given in Table A.1 for this band is slightly higher.

Spectral Information for OH

For the fundamental band of OH, the following information is obtained from Ref. 25:

$$\text{Band center, } \omega_c = 3570\ cm^{-1},$$

$$\text{Band strength at STP, } S(T_o) = 110\ cm^{-2}\ atm^{-1}$$

Also, from Ref. 24 the information on equilibrium rotational constant for OH is obtained as:

$$A\ ^2\Sigma^+ \rightarrow 17.355\ cm^{-1}$$

$$X\ ^2\Pi_i \rightarrow 18.871\ cm^{-1}$$

Thus, it is suggested to use a value for the equilibrium rotational constant for OH as $B_e = 18\ cm^{-1}$. Using this, a value of A_o (T_{ref}= 300 K) is found as

$$A_o\ (T_{ref} = 300) = 1.59313\ (B_e T_{ref})^{1/2} = 117.0707. \qquad (A.6)$$

Considering the value of $A_o(T_{ref}) = 117\ cm^{-1}$, the relation for $A_o(T)$ for OH is given as:

$$A_o(T) = 117\ (T/300)^{1/2}. \qquad (A.7)$$

By knowing ω_c, S (T_o), and $A_o(T)$, other required spectral information for OH can be evaluated.

Table A.1 Exponential Band Model Correlation Quantities**

Molecule	Band μ	Band Center cm^{-1}	Pressure Parameters		$A_o(T)$ cm^{-1}	$C_o^2(T)$ $atm^{-1}\ cm^{-1}$	B^2 (T) dimensionless
			b	n			
CO	4.7	2143	1.1	0.8	38.1 $K_1(T)$	6.24 $K_2(T)$	0.314 $\delta_1(T)$
	2.35	4260	1.0	0.8	38.1 $K_1(T)$	0.042 $K_2(T)$	0.300 $\delta_1(T)$
CO_2	15	667	1.3	0.7	22.3 $K_1(T)$	15.2 $K_2(T)$	0.084 K_1 (T)
	4.3*	2350	1.3	0.8	19.9 $K_1(T)$	98.7 $K_2(T)$	0.329 $K_1(T)$
	2.7	3715	1.3	0.65	41.6 $K_1(T)$	1.72 $K_2T)\phi_2(T)$	0.111$\delta_2(T)$
H_2O	I.R	500	5.0	1.0	49.4 $K_1(T)$	771 $K_2(T)\phi_7(T)$	0.073/$K_1(T)$
	6.3	1600	5.0	1.0	90.1 $K_1(T)$	3.35 $K_2(T)$	0.130/$K_1(T)$
	2.7	3750	5.0	1.0	112.6 $K_1(T)$	1.52 $K_2(T)$	0.145/K_1 (T)
	1.87	5350	5.0	1.0	79.7 $K_1(T)$	0.276 $K_2(T)\phi_{101}(T)$	0.118/$K_1(T)$
	1.38	7250	5.0	1.0	79.7 $K_1(T)$	0.230 $K_2(T)\phi_{101}(T)$	0.201/$K_1(T)$
CH_4	7.6	1310	1.3	0.8	39.8 $K_1(T)$	4.58 $K_2(T)$	0.067 $K_1(T)$
	3.3	3020	1.3	0.8	95.3 $K_1(T)$	3.15 $K_2(T)$	0.036 $K_1(T)$

**Notes on Table A.1. (See next page)

1. Correlation quantities are based on the results of reference [9]. The intensity of the band marked with * was taken from the reference [7].

2. Notations: $K_1(T) = (T/300)^{1/2}$, $K_2(T) = (300/T)^{3/2}$,

$\delta_1 = [\phi_1{}^2(T)/K_1(T)] \times 10^{-3}$, $\delta_2 = \phi_3{}^2(T)/[\phi_2(T)K_1(T)]$

$h = 6.625 \times 10^{-27}$ erg-sec, $C = 2.998 \times 10^{10}$ cm/sec,

$k = 1.380 \times 10^{-16}$ erg/K , $hC/k \simeq 1.44$ cm - K

3. Temperature range: $300\ K \leq T \leq T_{max}$. For CO, $T_{max} = 1800$ K.

For CO_2, $T_{max} = 1400$ K. For H_2O, $T_{max} = 1100$ K. For CH_4,

$T_{max} = 830$ K.

4. For CO, $\omega = 2143\ cm^{-1}$ and

$\phi_1(T) = [15.15 + 0.22\ (T/T_o)^{3/2}]\ [1-\exp\ (-hC\omega/kT)]$, $T_o = 100$ K

5. For CO_2, $\omega_1 = 1351\ cm^{-1}$, $\omega_2 = 667\ cm^{-1}$, $\omega_3 = 2396\ cm^{-1}$

$\phi_2(T) = \{1 - \exp\ [(\ -\ hC/KT\ )\ (\omega_1 + \omega_3)]\}x$

$\{[1 - \exp\ (\ -\ hC\omega_1/kT)]\ [1 - \exp\ (-hC\omega_3/kT)]\}^{-1}$, $\phi_3(T) = 1 +$

$0.053\ (T/100)^{3/2}$

6. For H_2O, $\omega_1 = 3652\ cm^{-1}$, $\omega_2 = 1595\ cm^{-1}$, $\omega_3 = 3756\ cm^{-1}$

$$\phi_{v_1\ v_2\ v_3}(T) = \{1 - \exp[-hC(v_1\ \omega_1 + v_2\ \omega_2 + v_3\ \omega_3)/kT]\} \times$$

$$\{[1-\exp(-hC\omega_1/kT)]\ [1-\exp(-hC\omega_2/kT]\ [1-\exp(-hC\omega_3/kT]\}^{-1}$$

$$\phi_7(T) = \exp[-17.6\ (T/100)^{-1/2}]$$

APPENDIX B

THERMODYNAMIC AND TRANSPORT PROPERTIES OF SELECTED SPECIES

It is important to consider the variation of thermodynamic and transport properties of various species with temperature and pressure. Quite often, the variation in properties with the pressure is not as crucial as with the temperature. The information on variation of different properties is provided here.

The information on variation of the thermal conductivity with temperature is obtained from Ref. 27 and this is expressed as:

$$\lambda = \lambda_o \, (T/T_o)^n \qquad (B.1)$$

where

T = Temperature, K

λ_o = thermal conductivity at T_o = 273 K, k cal/m-hr-K

n = constant as given in Table B1

In order to be consistent with the units used in the present work, Eq. (B.1) is expressed as:

$$\lambda = \frac{10^4 \lambda_o}{(36)\ (23.889)} \, (T/273)^n \ , \ \text{erg/sec-cm-K} \qquad (B.2)$$

For Eq. (B.2) the value of λ_o is obtained from Table B.1; the units for λ_o are shown in the table. For example, thermal conductivities of CO and CO_2 are expressed as:

$$CO: \quad \lambda = (11.627865289 \times 200)\ (T/273)^{0.8} \qquad (B.3)$$

$$= 2325.570579^* ((TW/273.0)^{**}0.8)$$

$$CO_2: \quad \lambda = (11.627865289 \times 128)\ (T/273)^{1.23} \qquad (B.4)$$

$$= 1488.365171^* ((TW/273.0)^{**}1.23)$$

Thus, for Eq. (B.2), the tabulated values for λ_o should be used without dividing by the factor 10^4.

Thermal conductivities of other species can be calculated in a similar manner. For species not listed in the Table B.1, values should be obtained from Ref. 27 or other sources such as Ref. 26. For higher tmperatures, values available in Ref. 26 should be used. Some of the values used in the present study are listed in Table B.2.

The relations for the constant-pressure specific heat for different ideal gases are available in Ref. 28 and these are given in Table B.3 for CO, OH, CO_2, and H_2O.

Table B.1 Constants for Calculation of Thermal Conductivity.

Molecule	$\lambda_o \cdot 10^4$ kcal/m-hr-°C	n	Maximum Temperature, °C
CO	200	0.80	1,000
CO_2	128	1.23	1,000
CH_4	264	1.33	600
H_2O	130	1.48	1,000
NH_3	181	1.53	1,000
N_2O	130	1.23	1,000

Table B.2 Thermal Conductivity of Selected Species*, erg/(cm-sec-K).

Temp., K	Molecule			
	OH	CO	CO_2	H_2O
300	(4879.71)	2507.82 (2674.22)	1671.43 (1820.47)	1738.04 (2925.31)
500	(6993.13)	3773.77 (3938.09)	3133.02 (3339.63)	3703.67 (4980.15)
1,000	(11504.56)	6570.51 (6888.51)	7349.02 (6716.93)	10325.76 (11588.26)
2,000	(20276.33)	11439.93 (11730.56)	17238.37 (11822.63)	28803.58 (26302.73)

* Values in parenthesis are from Ref. 26.

Table B.3 Constant-pressure specific heat for selected ideal gases (Ref. 28).

Gas	C_p = kJ/kmole-K, θ = T (Kelvin)/100
CO	$C_p = 69.145 - 0.70463\ \theta^{0.75} - 200.77\ \theta^{-0.5} + 176.76\ \theta^{-0.75}$
OH	$C_p = 81.546 - 59.350\ \theta^{0.25} + 17.329\ \theta^{0.75} - 4.266\ \theta$
CO_2	$C_p = 3.7357 + 30.529\ \theta^{0.5} - 4.1034\ \theta + 0.024198\ \theta^{2}$
H_2O	$C_p = 143.05 - 183.54\ \theta^{0.25} + 82.751\ \theta^{0.5} - 3.6989\ \theta$

APPENDIX C

RADIATIVE ABILITY OF SELECTED SPECIES IN OPTICALLY THIN AND LARGE PATH LENGTH LIMITS

The quantities, M_1 and N_1 defined in Eqs. (2.10) represent the interaction parameters for radiation versus conduction heat transfer. As pointed out in Secs. 2.3 and 4, the dimensional gas property N_1/k represents the relative importance of radiation versus conduction in the optically thin limit. Similarly, the gas property $M_1/(RL) = H_1/k$ represents the relative importance of radiation versus conduction in the large path length limit. The radiative properties K_1 and H_1 are defined, respectively, by Eqs. (2.10c) and (2.10e).

The quantities K_1 and K_1/k were calculated for a number of gases and the results are illustrated in Figs. C.1. The results presented in Fig. C.1a show the radiative ability of different species in the optically thin limit. The results presented in Fig. C.1b demonstrate the relative importance of radiation versus conduction in the optically thin limit. Similarly, the results for H_1 and H_1/k were calculated to investigate the interaction in the large path length limit and these are illustrated in Figs. C.2a and C.2b. A comparison of results presented in Figs. C.1 and C.2 shows a considerable difference in the radiation-conduction interaction for the optically thin limit as opposed to the large path length limit. For example, in the optically thin limit CO_2 possesses a large radiation interaction relative to the other gases, while the reverse is true in the large path length limit. On the other hand, just the opposite trend is observed for H_2O.

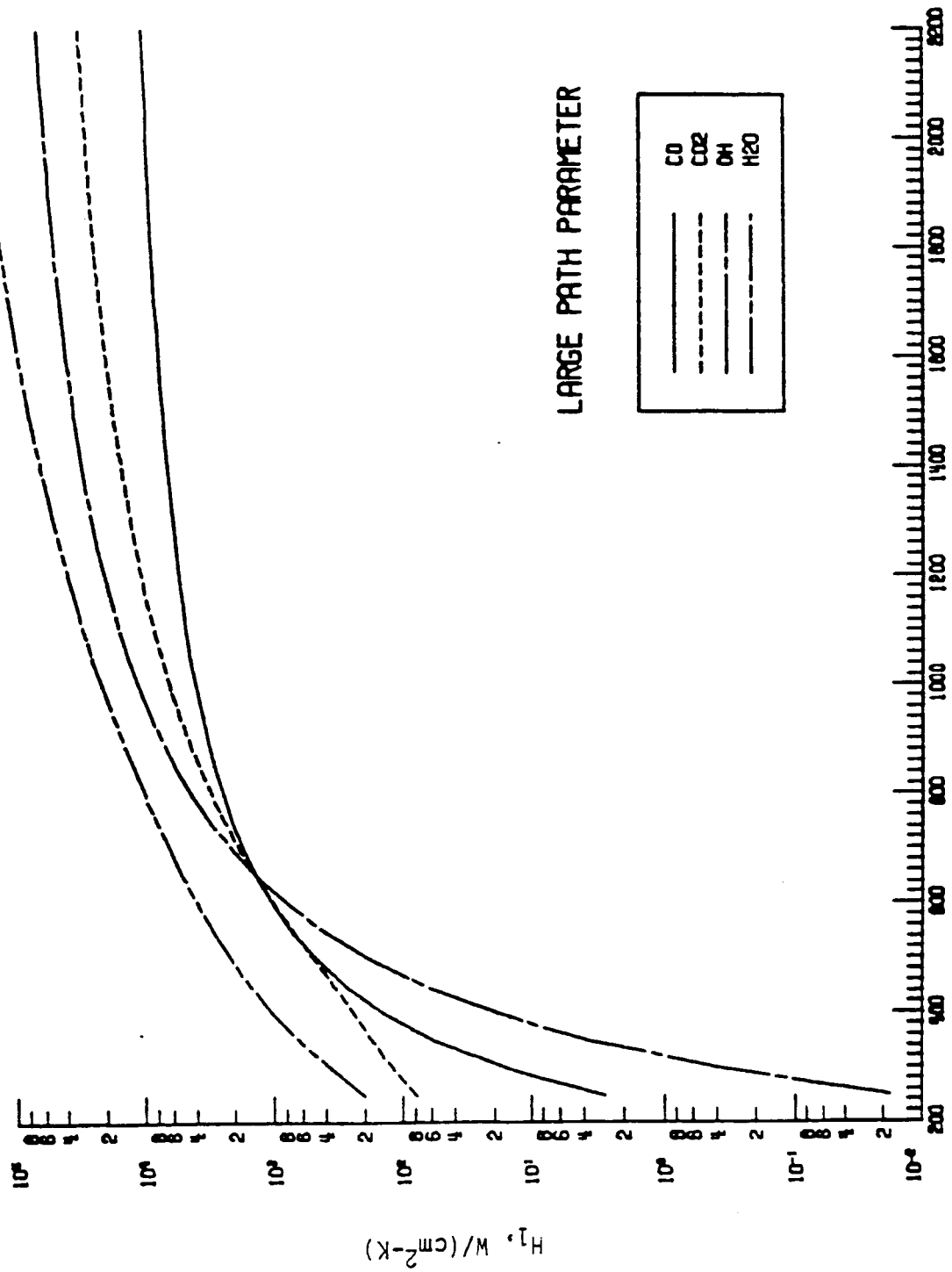

Fig. C.1a Radiative ability of different species in the optically thin limit.

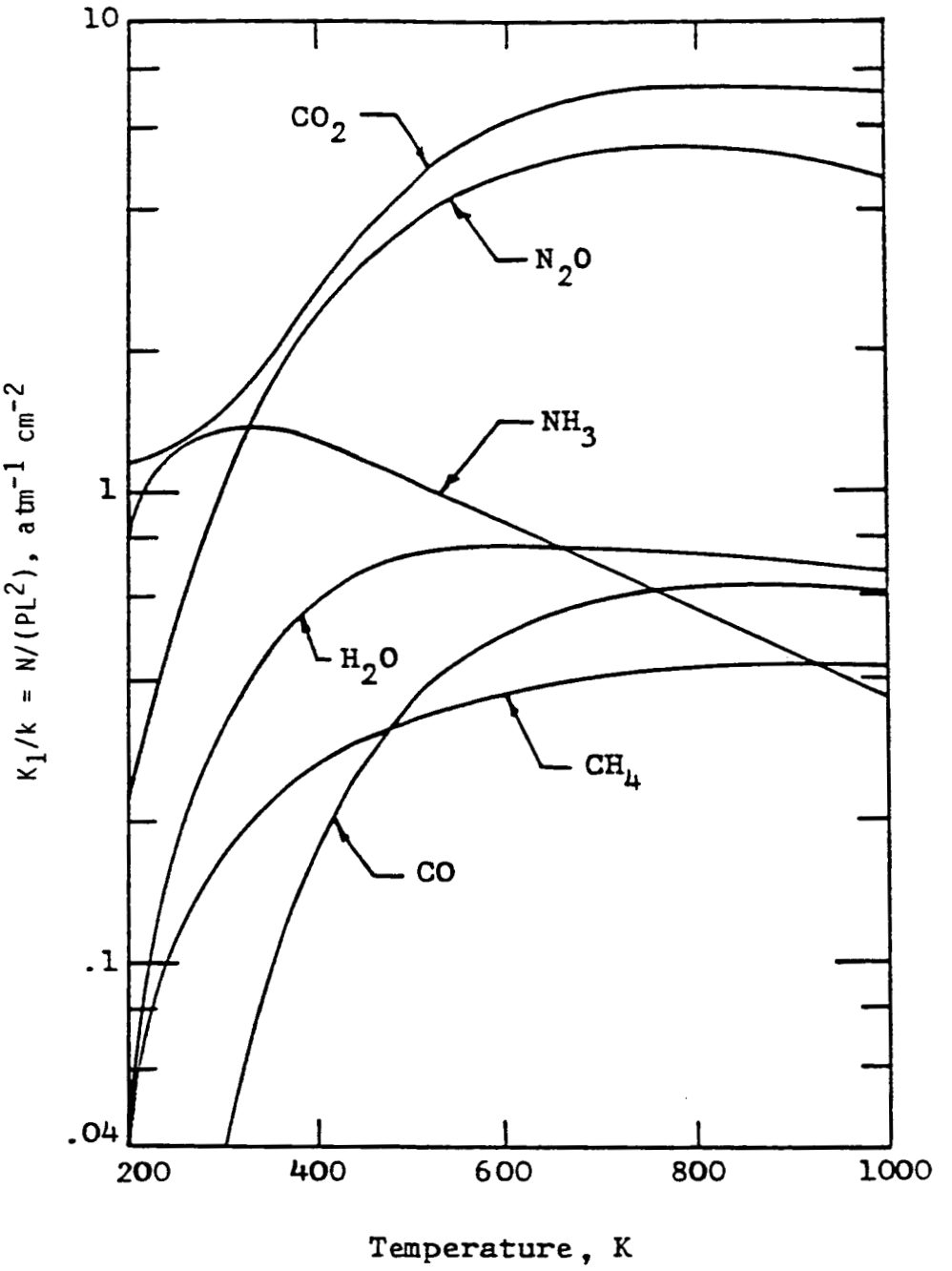

Fig. C.1b Interaction parameter for optically thin radiation.

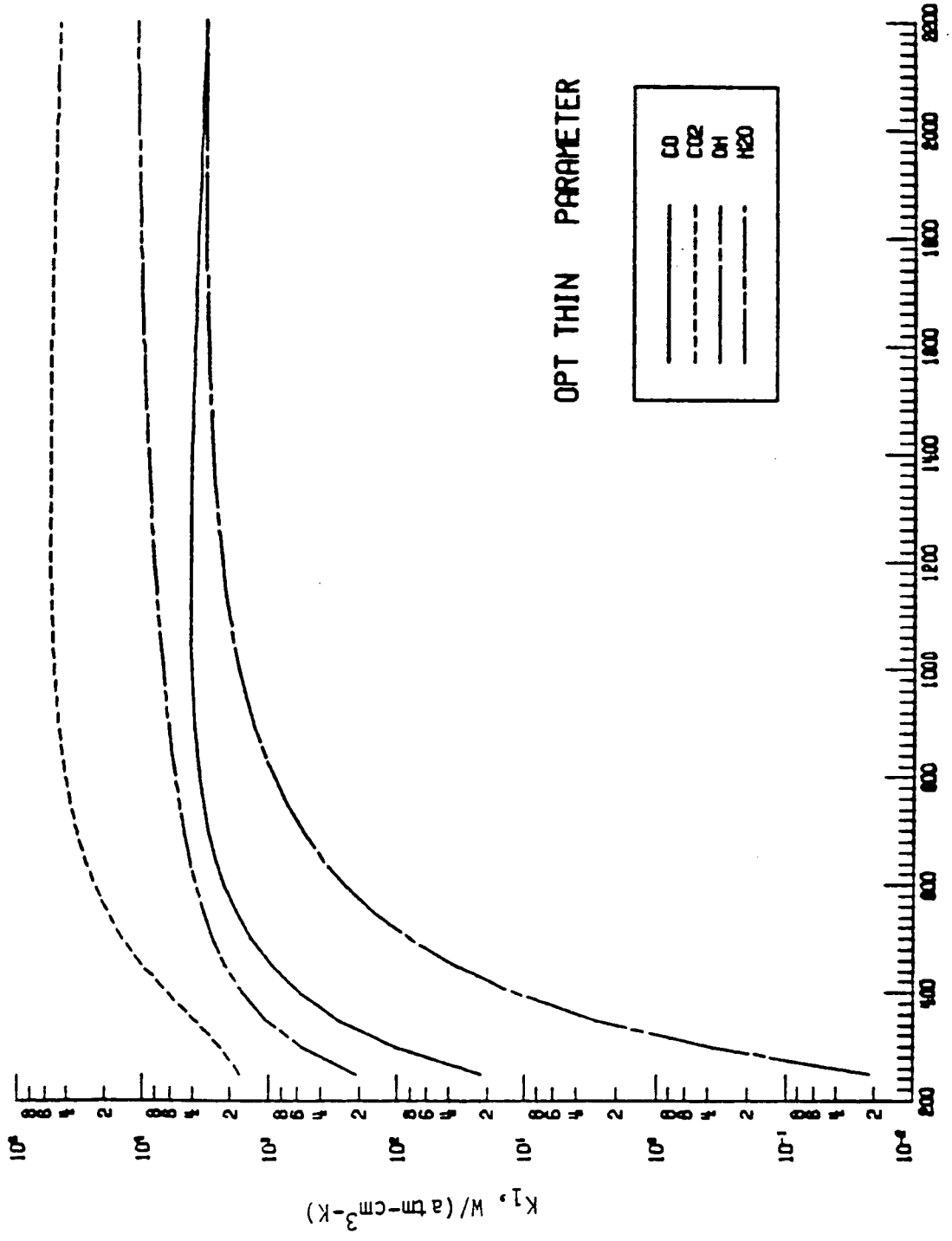

Fig. C.2a Radiative ability of different species in the large path limit.

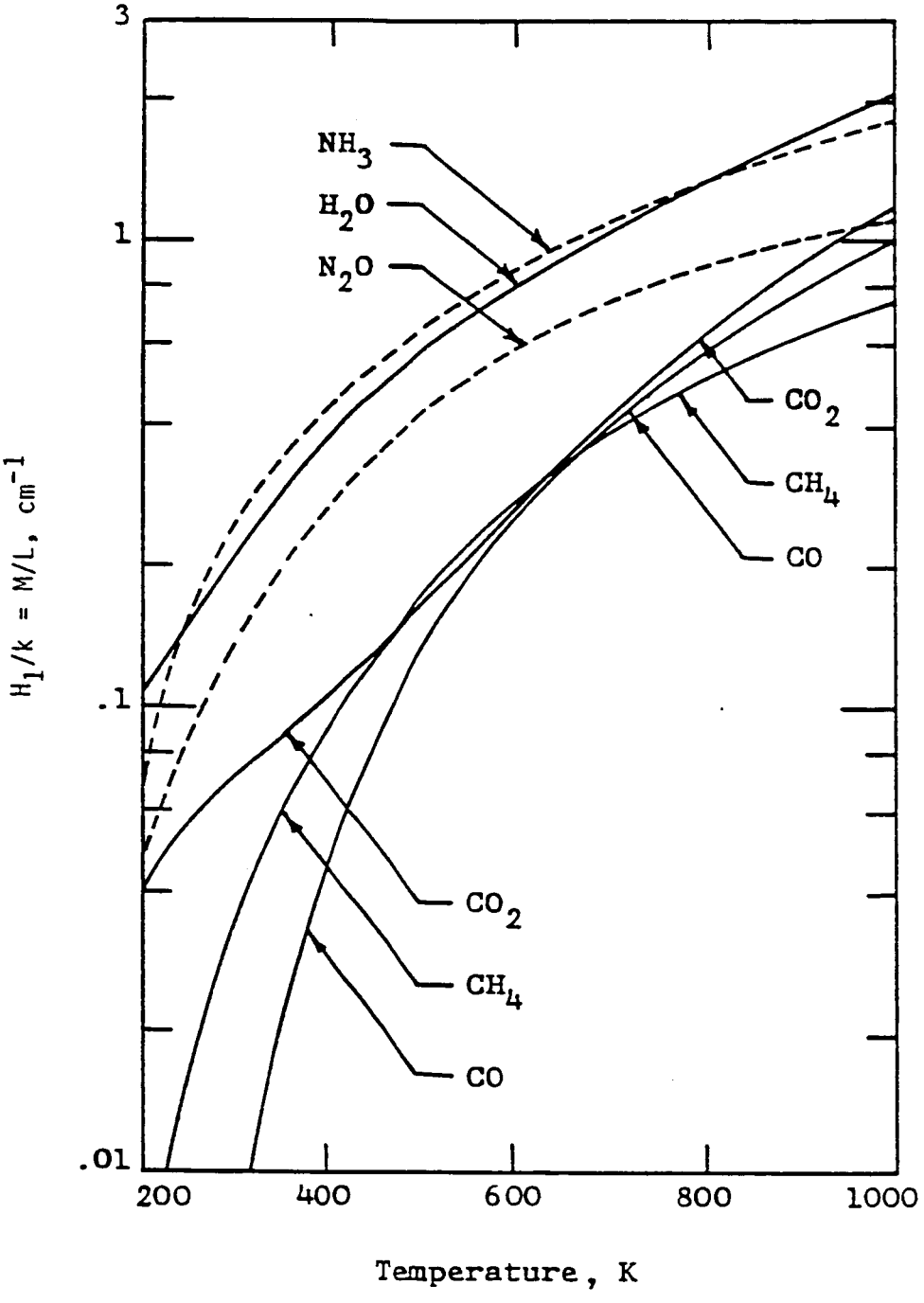

Fig. C.2b Interaction parameter for large path length limit.

APPENDIX D

COMPUTER PROGRAM FOR TRANSIENT RADIATIVE TRANSFER IN NONGRAY GASES

Following the numerical procedure of Sec. 3, a general computer program is developed to calculate the transient radiative transfer in nongray gases between two parallel plates having constant wall temperature. The program can be used to calculate the conduction and radiation heat transfer separately as well as heat transfer due to the combined process of conduction and radiation. The program provides the general solution as well as the limiting (optically thin and large path length) solutions. The program is written for the five-band H_2O gas, but can be used for any gas by employing appropriate thermophysical and radiative properties.

```
1       PROGRAM TRAN(OUTPUT=65,TAPE6,TAPE10,TAPE15)
 C**********************************************************************
 C
 C      THIS PROGRAM CALCULATES THE TRANSIENT RADIATIVE
 C      INTERACTION IN H2O BETWEEN TWO PARALLEL PLATES
 C      FOR CONSTANT WALL TEMPRATURE.
 C
 C**********************************************************************
 C                 T-----NONDIMENSIONAL TIME
 C                 P-----PRESSURE (ATM)
 C                 TW----TEMPERATURE OF LOWER PLATE (K)
 C                 L-----DISTANCE BETWEEN TWO PLATES (CM)
 C                 Z-----NONDIMENSIONAL Y COORDINATE
 C                 TM----CHARACTERSITIC TIME (SEC)
 C                 IR=1      ONLY RADIATION
 C                 IR=2      RADIATION & CONDUCTION
 C                 IR=3      ONLY CONDUCTION
       EXTERNAL F311,F312,F313,F314,F315,F321,F322,F323,F324,F325,F411
      &,F412,F413,F414,F415,F421,F422,F423,F424,F425,FQ11,FQ12,FQ13,FQ14
      & ,FQ15,FQ21,FQ22,FQ23,FQ24,FQ25
       DIMENSION U(20),EPS(3),PRES(10),TEMP(8),TT(20)
       REAL KFB,L,M1,M2,M3,M4,M5,R
       COMMON F1,F2,F3,F4,F5,B1,B2,B3,B4,B5,THETA,Z
       DATA U/0.1,0.2,0.5,1.0,2.,5.,10.,20.,50.,100.,
      & 200.,500.,1000./
       DATA PRES/0.01,0.1,1.0,10.0/
       DATA TEMP/300.0,500.0,1000.0,2000.0,3000.0/
       DATA TT/0.01,0.02,0.05,0.1,0.5,1.0/
       DO 11 IR=1,3
       IF(IR.EQ.1) WRITE(6,111)
       IF(IR.EQ.1) WRITE(10,114)
       IF(IR.EQ.1) WRITE(15,115)
       IF(IR.EQ.2) WRITE(6,112)
       IF(IR.EQ.2) WRITE(10,113)
       IF(IR.EQ.2) WRITE(15,116)
       IF(IR.EQ.3) WRITE(6,561)
       IF(IR.EQ.3) WRITE(10,564)
       IF(IR.EQ.3) WRITE(15,565)
       TM=0.00001
       WRITE(6,886) TM
       WRITE(10,886)TM
       WRITE(15,886)TM
 C
 C      TIME MARCHING
 C
       DO 22 ITT=1,5
       T=TT(ITT)
       WRITE(6,888)T
       WRITE(10,888)T
       WRITE(15,888) T
       WRITE(6,666)
       WRITE(10,666)
       WRITE(15,666)
       DO 33 IT=1,4
       TW=TEMP(IT)
```

```
      T2=2*TW
      DZ=0.1
      Z=0.1
      DO 44 IZ=1,5
      DO 55 KK=2,4
      P=PRES(KK)
      DO 66 I=1,13
      L=U(I)
      IF(IR.EQ.3) GOTO 360
C
C     CALCULATION OF PLANCK FUNCTION AND ITS DERIVATIVE
C
C     WNB----  BAND CENTER (1/CM)
C     HCK----  CONSTANT (K CM)
C     CCC----  C1*C2 (ERG-K-CM**3/SEC)
C     PFDBI--  PLANCK FUNCTION DERIVATIVE FOR I BAND
C
      CESS=TW**2.0
      STU=TW**0.5
      SNT=TW/273.0
      HCK=1.439257246
      BT3=5.668*10**(-5.)*TW**3.
      WN1=500.0
      WN2=1600.0
      WN3=3750.0
      WN4=5350.0
      WN5=7250.0
      C2C1=HCK*WN1
      C2C2=HCK*WN2
      C2C3=HCK*WN3
      C2C4=HCK*WN4
      C2C5=HCK*WN5
      CCC=0.000053847734
C
C     SPECTROSCOPIC PROPERTIES OF H2O
C     WNBI---- BAND CENTER (1/CM)
C     HERE WE HAVE CONSIDERED ONLY FIVE BANDS(20,6.3,2.7,1.87, &1.38 MICRONS)
C
      CCC1=CCC*(WN1**4)
      CCC2=CCC*(WN2**4)
      CCC3=CCC*(WN3**4)
      CCC4=CCC*(WN4**4)
      CCC5=CCC*(WN5**4)
      TB1=C2C1/TW
      TB2=C2C2/TW
      TB3=C2C3/TW
      TB4=C2C4/TW
      TB5=C2C5/TW
      TEB1=EXP(TB1)
      TEB2=EXP(TB2)
      TEB3=EXP(TB3)
      TEB4=EXP(TB4)
      TEB5=EXP(TB5)
      SNTB1=CESS*((TEB1-1.0)**2.0)
      SNTB2=CESS*((TEB2-1.0)**2.0)
```

```
      SNTB3=CESS*((TEB3-1.0)**2.0)
      SNTB4=CESS*((TEB4-1.0)**2.0)
      SNTB5=CESS*((TEB5-1.0)**2.0)
      PFDB1=(CCC1*TEB1)/SNTB1
      PFDB2=(CCC2*TEB2)/SNTB2
      PFDB3=(CCC3*TEB3)/SNTB3
      PFDB4=(CCC4*TEB4)/SNTB4
      PFDB5=(CCC5*TEB5)/SNTB5
C
C     BAND MODEL CORRELATIONS (TIEN & LOWDER WIDE BAND MODEL)
C     AZI  ----AOI/(1/CM)
C     CZSI ----COI**2 (1/(ATM-CM))
C     BSI  ----B**2 (NON DIMENSIONAL)
C     OMGI ----WAVE NUMBER(1/CM)
C
      AK1=(TW/300.0)**0.5
      AK2=(300.0/TW)**1.5
      AZ1=49.4*AK1
      AZ2=90.1*AK1
      AZ3=112.6*AK1
      AZ4=79.7*AK1
      AZ5=79.7*AK1
      OMG1=3652.0
      OMG2=1595.0
      OMG3=3756.0
      TX=-(HCK/TW)
      TX1=TX*OMG1
      TX2=TX*OMG2
      TX3=TX*OMG3
      ETX1=EXP(TX1)
      ETX2=EXP(TX2)
      ETX3=EXP(TX3)
      C1=1.0-ETX1
      C2=1.0-ETX2
      C3=1.0-ETX3
      BRKT=TX*(OMG1+OMG3)
      PHI1Z1=(1.0-EXP(BRKT))/(C1*C2*C3)
      DJ=17.6/(TW/100.0)**0.5
      PHI7=EXP(-DJ)
      TS=300.0/TW
      CZS1=771*AK2*PHI7
      CZS2=3.35*AK2
      CZS3=1.52*AK2
      CZS4=0.276*AK2*PHI1Z1
      CZS5=0.23*AK2*PHI1Z1
C
C     SI  ---- INTEGRATED BAND INTENSITY (1/(ATM CM**2))
C
      S1=CZS1*AZ1
      S2=CZS2*AZ2
      S3=CZS3*AZ3
      S4=CZS4*AZ4
      S5=CZS5*AZ5
C
C      PL ---- PRESSURE PATH LENGTH (ATM-CM)
```

```
C
      PL=P*L
      UZ1=CZS1*PL
      UZ2=CZS2*PL
      UZ3=CZS3*PL
      UZ4=CZS4*PL
      UZ5=CZS5*PL
      B1=1.5*UZ1
      B2=1.5*UZ2
      B3=1.5*UZ3
      B4=1.5*UZ4
      B5=1.5*UZ5
      BS1=0.073/AK1
      BS2=0.13/AK1
      BS3=0.145/AK1
      BS4=0.118/AK1
      BS5=0.201/AK1
C
C     PEI ----EFFECTIVE PRESSURE FOR EACH BAND (NON DIMENSIONAL)
C
      PE1=(5.0*P)
      PE2=(5.0*P)
      PE3=(5.0*P)
      PE4=(5.0*P)
      PE5=(5.0*P)
C
C     BETAI ---- LINE STRUCTURE PARAMETER
C
      BETA1=BS1*PE1
      BETA2=BS2*PE2
      BETA3=BS3*PE3
      BETA4=BS4*PE4
      BETA5=BS5*PE5
C
C     CORRELATION FOR EACH BAND
C
      F1=2.94*(1.0-EXP(-(2.60*BETA1)))
      F2=2.94*(1.0-EXP(-(2.60*BETA2)))
      F3=2.94*(1.0-EXP(-(2.60*BETA3)))
      F4=2.94*(1.0-EXP(-(2.60*BETA4)))
      F5=2.94*(1.0-EXP(-(2.60*BETA5)))
C
C     NUMERICAL INTEGRATION
C     FOR DETAILS OF INTEGRATION REFER MATHEMATICAL LIBRARY
C     AT NASA LANGLEY (DOCUMENT N-3)
C
      EPS(1)=1.0E-12
      EPS(2)=1.0E-12
      X=0.0
      CALL CADRE(X,Z,F311,EPS,ITEXT,G311,IERR)
      CALL CADRE(X,Z,F312,EPS,ITEXT,G312,IERR)
      CALL CADRE(X,Z,F313,EPS,ITEXT,G313,IERR)
      CALL CADRE(X,Z,F314,EPS,ITEXT,G314,IERR)
      CALL CADRE(X,Z,F315,EPS,ITEXT,G315,IERR)
      CALL CADRE(Z,1.,F321,EPS,ITEXT,G321,IERR)
```

```
      CALL CADRE(Z,1.,F322,EPS,ITEXT,G322,IERR)
      CALL CADRE(Z,1.,F323,EPS,ITEXT,G323,IERR)
      CALL CADRE(Z,1.,F324,EPS,ITEXT,G324,IERR)
      CALL CADRE(Z,1.,F325,EPS,ITEXT,G325,IERR)
      CALL CADRE(X,Z,F411,EPS,ITEXT,G411,IERR)
      CALL CADRE(X,Z,F412,EPS,ITEXT,G412,IERR)
      CALL CADRE(X,Z,F413,EPS,ITEXT,G413,IERR)
      CALL CADRE(X,Z,F414,EPS,ITEXT,G414,IERR)
      CALL CADRE(X,Z,F415,EPS,ITEXT,G415,IERR)
      CALL CADRE(Z,1.0,F421,EPS,ITEXT,G421,IERR)
      CALL CADRE(Z,1.0,F422,EPS,ITEXT,G422,IERR)
      CALL CADRE(Z,1.0,F423,EPS,ITEXT,G423,IERR)
      CALL CADRE(Z,1.0,F424,EPS,ITEXT,G424,IERR)
      CALL CADRE(Z,1.0,F425,EPS,ITEXT,G425,IERR)
      H1=AZ1*PFDB1
      H2=AZ2*PFDB2
      H3=AZ3*PFDB3
      H4=AZ4*PFDB4
      H5=AZ5*PFDB5
360   CONTINUE
C
C     RHO-----DENSITY
C     CP------SPECIFIC HEAT AT CONSTANT PRESSURE
C     KFB-----THERMAL CONDUCTIVITY
C
      RHO=0.0128677*18./TW
      TC=TW/100.
      CP=(143.05-183.54*TC**0.25+82.751*TC**0.5-3.6989*TC)/18.
      CON=TM/(L*RHO*CP)
      KFB=(1511.620876)*(SNT**1.48)
      R=(KFB*TM)/(L*L*RHO*CP)
      Z2=Z*Z
      CZ=1./(Z-Z2)
      IF(IR.EQ.3) GOTO 362
      M1=CON*H1
      M2=CON*H2
      M3=CON*H3
      M4=CON*H4
      M5=CON*H5
      AN1=M1*UZ1
      AN2=M2*UZ2
      AN3=M3*UZ3
      AN4=M4*UZ4
      AN5=M5*UZ5
      SUM31=AN1*1.5*(G311-G321)
      SUM32=AN2*1.5*(G312-G322)
      SUM33=AN3*1.5*(G313-G323)
      SUM34=AN4*1.5*(G314-G324)
      SUM35=AN5*1.5*(G315-G325)
      G3=CZ*(SUM31+SUM32+SUM33+SUM34+SUM35)
      IF(IR.EQ.1) R=0.0
      AJ3=G3+CZ*2.*R
      SUM41=AN1*(G411-G421)
      SUM42=AN2*(G412-G422)
      SUM43=AN3*(G413-G423)
```

```
      SUM44=AN4*(G414-G424)
      SUM45=AN5*(G415-G425)
      G4=-3*CZ*(SUM41+SUM42+SUM43+SUM44+SUM45)
      AJ4=G4+2.*CZ*R
      GZ=(1-Z2)*CZ
      EAJ3T=EXP(-(AJ3*T))
      GT=(GZ-(AJ4/AJ3))*EAJ3T+AJ4/AJ3
362   CONTINUE
      IF(IR.EQ.3) GT=(EXP(2*R*T/(Z2-Z))+Z)/Z
      THETA=Z2+GT*(Z-Z2)
      IF(IR.EQ.3) DFLUX=-KFB*(T2-TW)*(2*Z+GT*(1-2*Z))/L
      TW4=TW**4
      T24=T2**4
      IF(IR.EQ.3) FLUX=DFLUX/(5.668*10**(-5.)*(TW4-T24))
      IF(IR.EQ.3) GOTO 364
      CALL CADRE(0.0,Z,FQ11,EPS,ITEXT,GQ11,IERR)
      CALL CADRE(0.0,Z,FQ12,EPS,ITEXT,GQ12,IERR)
      CALL CADRE(0.0,Z,FQ13,EPS,ITEXT,GQ13,IERR)
      CALL CADRE(0.0,Z,FQ14,EPS,ITEXT,GQ14,IERR)
      CALL CADRE(0.0,Z,FQ15,EPS,ITEXT,GQ15,IERR)
      CALL CADRE(Z,1.0,FQ21,EPS,ITEXT,GQ21,IERR)
      CALL CADRE(Z,1.0,FQ22,EPS,ITEXT,GQ22,IERR)
      CALL CADRE(Z,1.0,FQ23,EPS,ITEXT,GQ23,IERR)
      CALL CADRE(Z,1.0,FQ24,EPS,ITEXT,GQ24,IERR)
      CALL CADRE(Z,1.0,FQ25,EPS,ITEXT,GQ25,IERR)
      FLUX=1-3.*(UZ1*H1*(GQ11+GQ21)+UZ2*H2*(GQ12+GQ22)+UZ3*H3*(GQ13+GQ23
     &)+UZ4*H4*(GQ14+GQ24)+UZ5*H5*(GQ15+GQ25))/(8*BT3)
      DFLUX=5.668*10**(-5.)*FLUX*(TW4-T24)
364   CONTINUE
      WRITE(6,222) TW,P,L,THETA,Z,FLUX,DFLUX
      IF(IR.EQ.3) GOTO 366
C
C      LARGE PATH LENGTH
C
      DS=ABS((Z-1)/Z)
      G15=(2-(2*Z-1)*ALOG(DS))*CZ*(M1+M2+M3+M4+M5)
      G16=(1-Z*ALOG(DS))*CZ*(M1+M2+M3+M4+M5)*2.
      AJ15=G15+2.*R*CZ
      AJ16=G16+2.*R*CZ
      EAJ15=EXP(-AJ15*T)
      G4T=(GZ-(AJ16/AJ15))*EAJ15+AJ16/AJ15
      Z2=Z*Z
      THEL=Z2+G4T*(Z-Z2)
      GQ3=THEL*(ALOG(Z)+13.81551055)
      GQ4=(1-THEL)*(ALOG(1-Z)+13.81551055)
      FLUXL=1-(H1+H2+H3+H4+H5)*(GQ3+GQ4)/(4*BT3)
      WRITE(10,222) TW,P,L,THEL,Z  ,FLUXL
C
C      OPTICALLY THIN --H2O
C
      AJ25=3*(AN1+AN2+AN3+AN4+AN5)+2*R/(Z-Z2)
      AJ26=(-3*(AN1+AN2+AN3+AN4+AN5)*(Z2-0.5)+2*R)/(Z-Z2)
      EAJ25=EXP(-(AJ25*T))
      G6T=(GZ-(AJ26/AJ25))*EAJ25+AJ26/AJ25
      THET=Z2+G6T*(Z-Z2)
```

```
      SPFD=S1*PFDB1+S2*PFDB2+S3*PFDB3+S4*PFDB4+S5*PFDB5
      FLUXO=1-(3./(8*BT3))*P*L*SPFD*((1-Z)+(2*Z-1)*THET)
      WRITE(15,222) TW,P,L,THET,Z,FLUXO
366   CONTINUE
66    CONTINUE
55    CONTINUE
      Z=Z+DZ
44    CONTINUE
33    CONTINUE
22    CONTINUE
11    CONTINUE
111   FORMAT(5X,*GENERAL --H2O----ONLY RADIATION*)
112   FORMAT(5X,*GENERAL --H2O----RADIATION AND CONDUCTION*)
113   FORMAT(5X,*LARGE PATH LENGTH --H2O----RADIATION AND CONDUCTION*)
114   FORMAT(5X,*LARGE PATH LENGTH --H2O----ONLY RADIATION*)
115   FORMAT(5X,* OPTICALLY THIN --H2O----ONLY RADIATION*)
116   FORMAT(5X,* OPTICALLY THIN --H2O----RADIATION AND CONDUCTION*)
561   FORMAT(5X,*GENERAL --H2O----ONLY CONDUCTION*)
564   FORMAT(5X,*LARGE PATH LENGTH --H2O----ONLY CONDUCTION*)
565   FORMAT(5X,* OPTICALLY THIN --H2O----ONLY CONDUCTION*)
886   FORMAT(10X,*CHARACTERSITIC TIME (TM)=*,F12.9)
888   FORMAT(10X,*TIME=*,F8.3)
666   FORMAT(4X,*TW*,T18,*P*,T28,*L*,T38,*THETA*,T48,*Z*,T56,*FLUX*
     &,T65,*DFLUX*)
222   FORMAT(6(1X, F9.4),1X,E12.6)
      STOP
      END
      FUNCTION F311(ZB)
      COMMON F1,F2,F3,F4,F5,B1,B2,B3,B4,B5,THETA,Z
      XX=B1*(Z-ZB)
      DEN1=(F1*((XX**2.0)+(2.0*XX)+2.0)+XX)*(XX+2.0*F1)
      AUD1=(F1*((XX**2.0)+(4.0*XX*F1)+(4.0*F1)))/DEN1
      F311=(1-2*ZB)*AUD1
      RETURN
      END
      FUNCTION F312(ZB)
      COMMON F1,F2,F3,F4,F5,B1,B2,B3,B4,B5,THETA,Z
      XX=B2*(Z-ZB)
      DEN2=(F2*((XX**2.0)+(2.0*XX)+2.0)+XX)*(XX+2.0*F2)
      AUD2=(F2*((XX**2.0)+(4.0*XX*F2)+(4.0*F2)))/DEN2
      F312=(1-2*ZB)*AUD2
      RETURN
      END
      FUNCTION F313(ZB)
      COMMON F1,F2,F3,F4,F5,B1,B2,B3,B4,B5,THETA,Z
      XX=B3*(Z-ZB)
      DEN3=(F3*((XX**2.0)+(2.0*XX)+2.0)+XX)*(XX+2.0*F3)
      AUD3=(F3*((XX**2.0)+(4.0*XX*F3)+(4.0*F3)))/DEN3
      F313=(1-2*ZB)*AUD3
      RETURN
      END
      FUNCTION F314(ZB)
      COMMON F1,F2,F3,F4,F5,B1,B2,B3,B4,B5,THETA,Z
      XX=B4*(Z-ZB)
      DEN4=(F4*((XX**2.0)+(2.0*XX)+2.0)+XX)*(XX+2.0*F4)
```

```
AUD4=(F4*((XX**2.0)+(4.0*XX*F4)+(4.0*F4)))/DEN4
F314=(1-2*ZB)*AUD4
RETURN
END
FUNCTION F315(ZB)
COMMON F1,F2,F3,F4,F5,B1,B2,B3,B4,B5,THETA,Z
XX=B5*(Z-ZB)
DEN5=(F5*((XX**2.0)+(2.0*XX)+2.0)+XX)*(XX+2.0*F5)
AUD5=(F5*((XX**2.0)+(4.0*XX*F5)+(4.0*F5)))/DEN5
F315=(1-2*ZB)*AUD5
RETURN
END
FUNCTION F321(ZB)
COMMON F1,F2,F3,F4,F5,B1,B2,B3,B4,B5,THETA,Z
XX=B1*(ZB-Z)
DEN1=(F1*((XX**2.0)+(2.0*XX)+2.0)+XX)*(XX+2.0*F1)
AUD1=(F1*((XX**2.0)+(4.0*XX*F1)+(4.0*F1)))/DEN1
F321=(1-2*ZB)*AUD1
RETURN
END
FUNCTION F322(ZB)
COMMON F1,F2,F3,F4,F5,B1,B2,B3,B4,B5,THETA,Z
XX=B2*(ZB-Z)
DEN2=(F2*((XX**2.0)+(2.0*XX)+2.0)+XX)*(XX+2.0*F2)
AUD2=(F2*((XX**2.0)+(4.0*XX*F2)+(4.0*F2)))/DEN2
F322=(1-2*ZB)*AUD2
RETURN
END
FUNCTION F323(ZB)
COMMON F1,F2,F3,F4,F5,B1,B2,B3,B4,B5,THETA,Z
XX=B3*(ZB-Z)
DEN3=(F3*((XX**2.0)+(2.0*XX)+2.0)+XX)*(XX+2.0*F3)
AUD3=(F3*((XX**2.0)+(4.0*XX*F3)+(4.0*F3)))/DEN3
F323=(1-2*ZB)*AUD3
RETURN
END
FUNCTION F324(ZB)
COMMON F1,F2,F3,F4,F5,B1,B2,B3,B4,B5,THETA,Z
XX=B4*(ZB-Z)
DEN4=(F4*((XX**2.0)+(2.0*XX)+2.0)+XX)*(XX+2.0*F4)
AUD4=(F4*((XX**2.0)+(4.0*XX*F4)+(4.0*F4)))/DEN4
F324=(1-2*ZB)*AUD4
RETURN
END
FUNCTION F325(ZB)
COMMON F1,F2,F3,F4,F5,B1,B2,B3,B4,B5,THETA,Z
XX=B5*(ZB-Z)
DEN5=(F5*((XX**2.0)+(2.0*XX)+2.0)+XX)*(XX+2.0*F5)
AUD5=(F5*((XX**2.0)+(4.0*XX*F5)+(4.0*F5)))/DEN5
F325=(1-2*ZB)*AUD5
RETURN
END
FUNCTION F411(ZB)
COMMON F1,F2,F3,F4,F5,B1,B2,B3,B4,B5,THETA,Z
XX=B1*(Z-ZB)
```

```
DEN1=(F1*((XX**2.0)+(2.0*XX)+2.0)+XX)*(XX+2.0*F1)
AUD1=(F1*((XX**2.0)+(4.0*XX*F1)+(4.0*F1)))/DEN1
F411=ZB*AUD1
RETURN
END
FUNCTION F412(ZB)
COMMON F1,F2,F3,F4,F5,B1,B2,B3,B4,B5,THETA,Z
XX=B2*(Z-ZB)
DEN2=(F2*((XX**2.0)+(2.0*XX)+2.0)+XX)*(XX+2.0*F2)
AUD2=(F2*((XX**2.0)+(4.0*XX*F2)+(4.0*F2)))/DEN2
F412=ZB*AUD2
RETURN
END
FUNCTION F413(ZB)
COMMON F1,F2,F3,F4,F5,B1,B2,B3,B4,B5,THETA,Z
XX=B3*(Z-ZB)
DEN3=(F3*((XX**2.0)+(2.0*XX)+2.0)+XX)*(XX+2.0*F3)
AUD3=(F3*((XX**2.0)+(4.0*XX*F3)+(4.0*F3)))/DEN3
F413=ZB*AUD3
RETURN
END
FUNCTION F414(ZB)
COMMON F1,F2,F3,F4,F5,B1,B2,B3,B4,B5,THETA,Z
XX=B4*(Z-ZB)
DEN4=(F4*((XX**2.0)+(2.0*XX)+2.0)+XX)*(XX+2.0*F4)
AUD4=(F4*((XX**2.0)+(4.0*XX*F4)+(4.0*F4)))/DEN4
F414=ZB*AUD4
RETURN
END
FUNCTION F415(ZB)
COMMON F1,F2,F3,F4,F5,B1,B2,B3,B4,B5,THETA,Z
XX=B5*(Z-ZB)
DEN5=(F5*((XX**2.0)+(2.0*XX)+2.0)+XX)*(XX+2.0*F5)
AUD5=(F5*((XX**2.0)+(4.0*XX*F5)+(4.0*F5)))/DEN5
F415=ZB*AUD5
RETURN
END
FUNCTION F421(ZB)
COMMON F1,F2,F3,F4,F5,B1,B2,B3,B4,B5,THETA,Z
XX=B1*(ZB-Z)
DEN1=(F1*((XX**2.0)+(2.0*XX)+2.0)+XX)*(XX+2.0*F1)
AUD1=(F1*((XX**2.0)+(4.0*XX*F1)+(4.0*F1)))/DEN1
F421=ZB*AUD1
RETURN
END
FUNCTION F422(ZB)
COMMON F1,F2,F3,F4,F5,B1,B2,B3,B4,B5,THETA,Z
XX=B2*(ZB-Z)
DEN2=(F2*((XX**2.0)+(2.0*XX)+2.0)+XX)*(XX+2.0*F2)
AUD2=(F2*((XX**2.0)+(4.0*XX*F2)+(4.0*F2)))/DEN2
F422=ZB*AUD2
RETURN
END
FUNCTION F423(ZB)
COMMON F1,F2,F3,F4,F5,B1,B2,B3,B4,B5,THETA,Z
```

```
      XX=B3*(ZB-Z)
      DEN3=(F3*((XX**2.0)+(2.0*XX)+2.0)+XX)*(XX+2.0*F3)
      AUD3=(F3*((XX**2.0)+(4.0*XX*F3)+(4.0*F3)))/DEN3
      F423=ZB*AUD3
      RETURN
      END
      FUNCTION F424(ZB)
      COMMON F1,F2,F3,F4,F5,B1,B2,B3,B4,B5,THETA,Z
      XX=B4*(ZB-Z)
      DEN4=(F4*((XX**2.0)+(2.0*XX)+2.0)+XX)*(XX+2.0*F4)
      AUD4=(F4*((XX**2.0)+(4.0*XX*F4)+(4.0*F4)))/DEN4
      F424=ZB*AUD4
      RETURN
      END
      FUNCTION F425(ZB)
      COMMON F1,F2,F3,F4,F5,B1,B2,B3,B4,B5,THETA,Z
      XX=B5*(ZB-Z)
      DEN5=(F5*((XX**2.0)+(2.0*XX)+2.0)+XX)*(XX+2.0*F5)
      AUD5=(F5*((XX**2.0)+(4.0*XX*F5)+(4.0*F5)))/DEN5
      F425=ZB*AUD5
      RETURN
      END
      FUNCTION FQ11(ZB)
      COMMON F1,F2,F3,F4,F5,B1,B2,B3,B4,B5,THETA,Z
      XX=B1*(Z-ZB)
      DEN1=(F1*((XX**2.0)+(2.0*XX)+2.0)+XX)*(XX+2.0*F1)
      AUD1=(F1*((XX**2.0)+(4.0*XX*F1)+(4.0*F1)))/DEN1
      FQ11=(THETA)*AUD1
      RETURN
      END
      FUNCTION FQ12(ZB)
      COMMON F1,F2,F3,F4,F5,B1,B2,B3,B4,B5,THETA,Z
      XX=B2*(Z-ZB)
      DEN2=(F2*((XX**2.0)+(2.0*XX)+2.0)+XX)*(XX+2.0*F2)
      AUD2=(F2*((XX**2.0)+(4.0*XX*F2)+(4.0*F2)))/DEN2
      FQ12=(THETA)*AUD2
      RETURN
      END
      FUNCTION FQ13(ZB)
      COMMON F1,F2,F3,F4,F5,B1,B2,B3,B4,B5,THETA,Z
      XX=B3*(Z-ZB)
      DEN3=(F3*((XX**2.0)+(2.0*XX)+2.0)+XX)*(XX+2.0*F3)
      AUD3=(F3*((XX**2.0)+(4.0*XX*F3)+(4.0*F3)))/DEN3
      FQ13=(THETA)*AUD3
      RETURN
      END
      FUNCTION FQ14(ZB)
      COMMON F1,F2,F3,F4,F5,B1,B2,B3,B4,B5,THETA,Z
      XX=B4*(Z-ZB)
      DEN4=(F4*((XX**2.0)+(2.0*XX)+2.0)+XX)*(XX+2.0*F4)
      AUD4=(F4*((XX**2.0)+(4.0*XX*F4)+(4.0*F4)))/DEN4
      FQ14=(THETA)*AUD4
      RETURN
      END
      FUNCTION FQ15(ZB)
```

```
      COMMON F1,F2,F3,F4,F5,B1,B2,B3,B4,B5,THETA,Z
      XX=B5*(Z-ZB)
      DEN5=(F5*((XX**2.0)+(2.0*XX)+2.0)+XX)*(XX+2.0*F5)
      AUD5=(F5*((XX**2.0)+(4.0*XX*F5)+(4.0*F5)))/DEN5
      FQ15=(THETA)*AUD5
      RETURN
      END
      FUNCTION FQ21(ZB)
      COMMON F1,F2,F3,F4,F5,B1,B2,B3,B4,B5,THETA,Z
      XX=B1*(ZB-Z)
      DEN1=(F1*((XX**2.0)+(2.0*XX)+2.0)+XX)*(XX+2.0*F1)
      AUD1=(F1*((XX**2.0)+(4.0*XX*F1)+(4.0*F1)))/DEN1
      FQ21=(1-THETA)*AUD1
      RETURN
      END
      FUNCTION FQ22(ZB)
      COMMON F1,F2,F3,F4,F5,B1,B2,B3,B4,B5,THETA,Z
      XX=B2*(ZB-Z)
      DEN2=(F2*((XX**2.0)+(2.0*XX)+2.0)+XX)*(XX+2.0*F2)
      AUD2=(F2*((XX**2.0)+(4.0*XX*F2)+(4.0*F2)))/DEN2
      FQ22=(1-THETA)*AUD2
      RETURN
      END
      FUNCTION FQ23(ZB)
      COMMON F1,F2,F3,F4,F5,B1,B2,B3,B4,B5,THETA,Z
      XX=B3*(ZB-Z)
      DEN3=(F3*((XX**2.0)+(2.0*XX)+2.0)+XX)*(XX+2.0*F3)
      AUD3=(F3*((XX**2.0)+(4.0*XX*F3)+(4.0*F3)))/DEN3
      FQ23=(1-THETA)*AUD3
      RETURN
      END
      FUNCTION FQ24(ZB)
      COMMON F1,F2,F3,F4,F5,B1,B2,B3,B4,B5,THETA,Z
      XX=B4*(ZB-Z)
      DEN4=(F4*((XX**2.0)+(2.0*XX)+2.0)+XX)*(XX+2.0*F4)
      AUD4=(F4*((XX**2.0)+(4.0*XX*F4)+(4.0*F4)))/DEN4
      FQ24=(1-THETA)*AUD4
      RETURN
      END
      FUNCTION FQ25(ZB)
      COMMON F1,F2,F3,F4,F5,B1,B2,B3,B4,B5,THETA,Z
      XX=B5*(ZB-Z)
      DEN5=(F5*((XX**2.0)+(2.0*XX)+2.0)+XX)*(XX+2.0*F5)
      AUD5=(F5*((XX**2.0)+(4.0*XX*F5)+(4.0*F5)))/DEN5
      FQ25=(1-THETA)*AUD5
      RETURN
      END
```